Computers and Mathematics with Applications 91 (2021) 122–149

Contents lists available at ScienceDirect

Computers and Mathematics with Applications

journal homepage: www.elsevier.com/locate/camwa

Guaranteed and computable error bounds for approximations constructed by an iterative decoupling of the Biot problem

Kundan Kumar [a], Svetlana Kyas [b], Jan Martin Nordbotten [a,*], Sergey Repin [c,d,e]

[a] Department of Mathematics, University of Bergen, Norway
[b] Geothermal Energy and Geofluids, Institute of Geophysics, ETH Zürich, Switzerland
[c] University of Jyvaskyla, Finland
[d] Steklov Inst. Math. of the RAS at St. Petersburg, Russia
[e] Peter the Great Polytechnic University, St. Petersburg, Russia

ARTICLE INFO

Article history:
Available online 11 June 2020

Keywords:
Biot problem
Fixed-stress split iterative scheme
a posteriori error estimates
Contraction mappings

ABSTRACT

The paper is concerned with guaranteed a posteriori error estimates for a class of evolutionary problems related to poroelastic media governed by the quasi-static linear Biot equations. The system is decoupled by employing the fixed-stress split scheme, which leads to an iteratively solved semi-discrete system. The error bounds are derived by combining a posteriori estimates for contractive mappings with functional type error control for elliptic partial differential equations. The estimates are applicable to any approximation in the admissible functional space and are independent of the discretization method. They are fully computable, do not contain mesh-dependent constants, and provide reliable global estimates of the error measured in the energy norm. Moreover, they suggest efficient error indicators for the distribution of local errors and can be used in adaptive procedures.

1. Introduction

The problems defined in a poroelastic medium contribute to a wide range of application areas, including simulation of oil reservoirs, prediction of environmental changes, soil subsidence and liquefaction in earthquake engineering, well stability, sand production, waste deposition, hydraulic fracturing, CO_2 sequestration, and understanding of the biological tissues in biomechanics. In recent years, mathematical modeling of poroelastic problems has become a highly important topic because it helps engineers to understand and predict complicated phenomena arising in such media. However, numerical schemes designed for any of the existing models provide approximations that contain errors of different nature, and these errors must be controlled. Therefore, a reliable quantitative analysis of poroelasticity problems requires efficient and computable error estimates that can be applied for various approximations and computation methods.

Mathematical modeling of poroelasticity is usually based on the Biot model that consists of the quasi-static elasticity problem coupled with an equation governing slow fluid motion. Computational errors in one part of the model may seriously affect the accuracy of the other part. Therefore, getting reliable and efficient a posteriori error estimates is generally much more complicated for coupled problems than for a single equation.

The Biot model is a system describing the flow and displacement in a porous medium by the momentum and mass conservation equations. Initially, it was derived at a macroscopic scale (with inertia effects negligible) in the works by

* Corresponding author.
E-mail addresses: kundan.kumar@uib.no (K. Kumar), svetlana.kyas@erdw.ethz.ch (S. Kyas), jan.nordbotten@math.uib.no (J.M. Nordbotten), sergey.s.repin@jyu.fi (S. Repin).

https://doi.org/10.1016/j.camwa.2020.05.005

Terzaghi [1] and Biot [2]. Settlement of different types of soils was predicted in [1], which was later extended to the generalized concept of consolidation [2,3]. A comprehensive discussion of the theory of poromechanics can be found in [4]. Thus, to model the *solid displacement* $\boldsymbol{u}$ and the *fluid pressure* p, we consider the system that governs the coupling of an *elastic isotropic porous medium* saturated with *slightly compressible viscous single-phase fluid*

$$\begin{aligned} -\mathrm{div}\big(\lambda\,(\mathrm{div}\boldsymbol{u})\,\mathbb{I} + 2\,\mu\,\boldsymbol{\varepsilon}(\boldsymbol{u}) - \alpha\,p\,\mathbb{I}\big) &= \boldsymbol{f} \quad \text{in} \quad Q := \Omega \times (0,T), \\ \partial_t\big(\beta\,p + \alpha\mathrm{div}\boldsymbol{u}\big) - \mathrm{div}\mathbb{K}\nabla p &= g \quad \text{in} \quad Q, \end{aligned} \tag{1.1}$$

where Q denotes a space–time cylinder (with bounded domain $\Omega \subset \mathbb{R}^d$, $d = \{2,3\}$ having a Lipschitz continuous boundary $\partial\Omega$ and a given time-interval $(0,T)$, $0 < T < +\infty$), $\boldsymbol{f} \in H^1(0,T;[L^2(\Omega)]^d)$ and $g \in L^2(0,T;L^2(\Omega))$ are the body force and the volumetric fluid source, respectively.[1] The first equation in (1.1) follows from the balance of linear momentum for the *total Cauchy stress tensor*

$$\boldsymbol{\sigma}_{\mathrm{por}} := \boldsymbol{\sigma}(\boldsymbol{u}) - \alpha\,p\,\mathbb{I}$$

that accounts not only for $\boldsymbol{u}$ but also for the pressure p scaled by the dimensionless Biot–Willis coefficient $\alpha > 0$. The stress tensor for the material is governed by Hooke's law

$$\boldsymbol{\sigma}(\boldsymbol{u}) := 2\,\mu\,\boldsymbol{\varepsilon}(\boldsymbol{u}) + \lambda\,\mathrm{tr}\boldsymbol{\varepsilon}(\boldsymbol{u})\,\mathbb{I} = 2\,\mu\,\boldsymbol{\varepsilon}(\boldsymbol{u}) + \lambda\,(\mathrm{div}\boldsymbol{u})\,\mathbb{I},$$

where $\boldsymbol{\varepsilon}(\boldsymbol{u}) := \frac{1}{2}\big(\nabla\boldsymbol{u} + (\nabla\boldsymbol{u})^{\mathrm{T}}\big)$ is the *tensor of small strains*. Here, $\lambda, \mu > 0$ are the *Lamé constants* proportional to Young's modulus E and Poisson's ratio ν via relations $\mu = \frac{E}{2(1+\nu)}$ and $\lambda = \frac{E\,\nu}{(1+\nu)(1-2\nu)}$. The second equation is the fluid mass conservation (continuity) equation in Q. Here, β stands for the *storage coefficient* and $\mathbb{K}$ is the *permeability tensor* assumed to be symmetric, uniformly bounded, anisotropic, heterogeneous in space, and constant in time, i.e.,

$$\lambda_{\mathbb{K}}|\boldsymbol{\tau}|^2 \le \mathbb{K}(x)\boldsymbol{\tau}\cdot\boldsymbol{\tau} \le \mu_{\mathbb{K}}|\boldsymbol{\tau}|^2, \quad \lambda_{\mathbb{K}}, \mu_{\mathbb{K}} > 0, \quad \text{for all } \boldsymbol{\tau} \in \mathbb{R}^d. \tag{1.2}$$

Let $\Sigma = \partial\Omega \times (0,T)$ be a lateral surface of Q, whereas $\Sigma_0 := \partial\Omega \times \{0\}$ and $\Sigma_T := \partial\Omega \times \{T\}$ define the bottom and the top parts of the mantel, such that $\partial Q = \Sigma \cup \Sigma_0 \cup \Sigma_T$. Initial conditions are assumed to be as follows:

$$p(x,0) = p^\circ \in H^1(\Omega) \quad \text{and} \quad \boldsymbol{u}(x,0) = \boldsymbol{u}^\circ \in [H^1(\Omega)]^d \quad \text{on} \quad \Sigma_0. \tag{1.3}$$

We introduce the following partitions of the boundary: $\partial\Omega = \Sigma_D^p \cup \Sigma_N^p = \Sigma_D^{\boldsymbol{u}} \cup \Sigma_N^{\boldsymbol{u}}$, where Σ_D^p and $\Sigma_D^{\boldsymbol{u}}$ must have positive measures, i.e., $|\Sigma_D^p|, |\Sigma_D^{\boldsymbol{u}}| > 0$, with the corresponding boundary conditions (BCs):

$$\begin{aligned} p &= p_D \quad \text{on} \quad \Sigma_D^p, \\ -\mathbb{K}\nabla p\cdot\boldsymbol{n} &= z_N \quad \text{on} \quad \Sigma_N^p, \\ \boldsymbol{u} &= \boldsymbol{u}_D \quad \text{on} \quad \Sigma_D^{\boldsymbol{u}}, \\ \boldsymbol{\sigma}_{\mathrm{por}}\cdot\boldsymbol{n} &= \boldsymbol{t}_N \quad \text{on} \quad \Sigma_N^{\boldsymbol{u}}. \end{aligned} \tag{1.4}$$

For the fluid content $\beta\,p + \alpha\,\mathrm{div}\boldsymbol{u}$, we prescribe the following initial condition

$$\eta(x,0) := \beta\,p(x,0) + \alpha\,\mathrm{div}\boldsymbol{u}(x,0) = \beta\,p^\circ + \alpha\,\mathrm{div}\boldsymbol{u}^\circ,$$

where p° and $\boldsymbol{u}^\circ$ are defined in (1.3). To simplify the exposition, we consider only homogeneous BCs, i.e., $p_D, z_N = 0$ and $\boldsymbol{u}_D, \boldsymbol{t}_N = \boldsymbol{0}$ for the time being, even though all results are valid for more general assumptions.

The work [5] provides the results on existence, uniqueness, and regularity theory for (1.1)–(1.4) in the Hilbert space setting, whereas [6] extends the recent results to a wider class of diffusion problems in poroelastic media with more general material deformation models. Corresponding a priori error estimates can be found in [7]. The considered system can be regarded as the singular limit of the fully dynamic Biot–Allard problem (see the details in [8]), where the acceleration of solid in the mechanics part of (1.1) is neglected.

Since the Biot model is a coupled system of partial differential equations (PDEs), both iterative and monolithic approaches can be used to solve the problem (see, e.g., [9]). For the first approach, the problem can be reformulated with a contractive operator, which naturally yields iterative methods for its solution (see [8]). At each step in time, the flow problem is considered first. Next, we solve the mechanics using the pressure from the first step. The procedure is repeated until the desired convergence is reached. Different alteration of iterative cycles in flow and mechanics, i.e., single- [10] and multi-rate schemes [11,12], can be considered. The second approach is fully coupled and considers the system (1.1)–(1.4) with two unknowns simultaneously.

The iterative coupling offers several advantages over the monolithic method in code design, in particular, in terms of availability of highly developed discretization methods (primal [13–15], mixed [7,16,17], Galerkin least-squares [18], finite volume (FV) [19], discontinuous Galerkin (dG) methods [20], Hybrid High-Order methods [21] isogeometric analysis [22], as well as combinations of above-mentioned ones) and algebraic solvers (e.g., general Schur complement based preconditioners [23–30] and the recently developed robust ones with respect to (w.r.t.) the model parameters

[1] For convenience of the reader, we collected the definitions related to the functional spaces in the Appendix.

[31–35]). In the fully-coupled methods, constructing efficient preconditioning techniques for the arising algebraic systems remains a matter of active ongoing scientific research (see, e.g., [30,36–39]).

The a posteriori error control for poroelastic models has been already addressed using different techniques. Application of residual-based error estimates to coupled elliptic–parabolic problems can be traced back to works [40,41]. Recently, similar error indicators were used in [42–46] for immiscible incompressible two- or multi-phase flows in porous media to address the questions of adaptive stopping criteria and mesh refinement. In [47], authors suggested an a posteriori error estimator based on a corresponding dual problem in space–time for a coupled consolidation problem that involves large deformations. In [48–51], adaptive space–time algorithms relying on the equilibrated fluxes technique were applied to the Biot's consolidation model (formulated as a system with four unknowns). In this work, however, we turn to the functional error estimates (majorants) that are fully computable and provide guaranteed bounds of errors arising in numerical approximations. The derivation of such estimates is based on functional arguments and variational formulation of the problem in question. Therefore, the method does not use specific properties of approximations (e.g., Galerkin orthogonality) and special properties of the exact solution (e.g., high regularity). The estimates do not contain mesh-dependent constants and are valid for any approximation in the natural energy class. Moreover, the majorants also yield an efficient error indicator that can be used to drive mesh adaptation. Since a concise mesh adaptation algorithm is still the matter of ongoing research, we postpone including a specific example with adaptivity discussions until the next paper on this matter.

Our main goal is to deduce efficient a posteriori error estimates for the approximation of the system (1.1) and demonstrate their suitability through the application to numerical problems. In [52], a posteriori error estimates of the functional type were derived for the stationary Barenblatt–Biot model of porous media. This paper deals with a more complicated Biot problem presented by an elliptic–parabolic system of partial differential equations. Our approach is based on the contraction property of the iterative method [53], which is rather general and not restricted only to the fixed-stress scheme, and functional type estimates of each equation in the Biot system (see, e.g., [54]). To the best knowledge of the authors, it is the first study targeting such a coupling between the elastic behavior of the medium and the fluid flow in the context of functional error estimates. The main result is presented in Theorem 2. Moreover, these estimates serve not only as reliable estimates of the global error measured in the energy norm, but also as efficient indicators of the local error distribution over the computational domain. The latter property makes functional majorants advantageous in automated adaptive mesh generation algorithms.

The paper has the following structure: Section 2 is dedicated to the generalized formulation of the Biot system and its semi-discrete counterpart derived after applying the explicit Euler scheme in time. In Section 3, we introduce an incremental approach, namely, the fixed-stress split scheme, for discretizing the considered coupled system. In particular, it clarifies the arguments for choosing the optimal parameters in the iterative scheme and proves that it is a contraction with an explicitly computable convergence rate. For the reader's convenience, Section 4 summarizes the main results of the work and the concepts that were used for their derivation, as well as highlights the most important properties of the error estimates. Sections 5 and 6 are dedicated to the derivation of auxiliary lemmas used in the proof of Theorem 2 (or Theorem 3) with general estimates for the approximations generated by the fully decoupled iterative approach. Finally, Section 7 contains a collection of examples that illustrate the application of derived error estimates to the Biot problem.

2. Variational formulation and discretization

We study approximations of the system (1.1), where $\widetilde{\boldsymbol{V}} \equiv H^1(0,T;[H^1(\Omega)]^d)$ denotes the space for u (field of displacements) and $\widetilde{W} \equiv H^1(0,T;H^1(\Omega))$ is the space for the variable p (pressure). The generalized setting of (1.1) is read as: find a pair $(\boldsymbol{u},p) \in \widetilde{\boldsymbol{V}}_0 \times \widetilde{W}_0$ such that

$$2\mu\,(\boldsymbol{\varepsilon}(\boldsymbol{u}),\boldsymbol{\varepsilon}(\boldsymbol{v}))_Q + \lambda\,(\mathrm{div}\boldsymbol{u},\mathrm{div}\boldsymbol{v})_Q + \alpha\,(\nabla p,\boldsymbol{v})_Q = (\boldsymbol{f},\boldsymbol{v})_Q, \qquad \forall \boldsymbol{v} \in \widetilde{\boldsymbol{V}}_0, \tag{2.1}$$

$$(\mathbb{K}\nabla p,\nabla w)_Q + (\partial_t(\beta\,p + \alpha\,\mathrm{div}\boldsymbol{u}),w)_Q = (g,w)_Q, \qquad \forall\, w \in \widetilde{W}_0, \tag{2.2}$$

where

$$\widetilde{\boldsymbol{V}}_0 := \left\{ v \in H^1(0,T;[H^1(\Omega)]^d) \;\middle|\; \boldsymbol{v}(t)|_{\Sigma_D^u} = \boldsymbol{0} \quad \text{a.e. } t \in (0,T) \right\},$$

$$\widetilde{W}_0 := \left\{ w \in H^1(0,T;H^1(\Omega)) \;\middle|\; w(t)|_{\Sigma_D^p} = 0 \quad \text{a.e. } t \in (0,T) \right\}.$$

The Biot system of type (2.1)–(2.2) was analyzed by several authors to establish the existence, uniqueness, and regularity of its solution. First theoretical results on the existence and uniqueness of a (weak) solution are presented in [55] for the case of $\beta = 0$. Further work in this direction can be found in [5,56]. The well-posedness of the quasi-static Biot system is ensured under the above-mentioned assumptions. In fact, [57,58] established contractive results in suitable norms for the iterative coupling of (2.1)–(2.2). For an overview of the stability of existing iterative algorithms, we refer the reader to [59,60].

The system (2.1)–(2.2) can be viewed as a two-field formulation of the poroelasticity problem. In numerical analysis, there are alternative approaches that treat such a system as *three- and four-field formulations*. In the three-field model, an additional variable is introduced to represent the flux in the flow equations, whereas the four-field approach considers stress as yet another unknown. The three-field formulation is rather flexible since it allows different combinations of

discretizations. The scientific community agrees that it provides more physical approximations of the unknowns than the two-field case. Recently, the four-field formulation, where both equations were treated with mixed methods, drew much attention from the research community. The advantages of the latter representation are local conservation of mass and momentum balance and a more accurate representation of fluxes and stresses. The choice of the formulation (from the above-mentioned list) is usually motivated by the considered application as well as the limits of the computational resources. For instance, the mixed formulation of (2.2) not only provides the flux that satisfies the local mass conservation property but also generates an effective approximation of this function, which is advantageous for the functional type error control. It minimizes the majorant related to the pressure variable (see (5.2)). The same principle works for the stress field reconstruction in mechanics part.

The system (2.1)–(2.2) is considered in the time-interval $[0, T]$ divided by N sub-intervals, such that it forms the corresponding set $\mathcal{T}_N = \cup_{n=1}^{N} \overline{I^n}$, $I^n = (t^{n-1}, t^n)$. Let $\boldsymbol{u}^n(x) \in \boldsymbol{V_0}$ and $p^n(x) \in W_0$, where

$$\boldsymbol{V_0} := \left\{ \boldsymbol{v} \in \boldsymbol{V} \equiv [H^1(\Omega)]^d \,|\, \boldsymbol{v}\big|_{\Sigma_D^{\boldsymbol{u}}} = 0 \right\} \quad \text{and} \quad W_0 := \left\{ w \in W \equiv H^1(\Omega) \,|\, w\big|_{\Sigma_D^{p}} = 0 \right\}, \tag{2.3}$$

respectively, are spatial parts of the solution at $t = t^n$. Then, the semi-discrete approximation of (2.1)–(2.2) reads as

$$\begin{aligned} &(2\,\mu\,\boldsymbol{\varepsilon}(\boldsymbol{u}^n), \boldsymbol{\varepsilon}(\boldsymbol{v}))_\Omega + (\lambda\,\mathrm{div}\boldsymbol{u}^n, \mathrm{div}\boldsymbol{v})_\Omega + \alpha\,(\nabla p^n, \boldsymbol{v})_\Omega = (\boldsymbol{f}^n, \boldsymbol{v})_\Omega, \quad \forall\, \boldsymbol{v} \in \boldsymbol{V_0}, \\ &(\mathbb{K}\nabla p^n, \nabla w)_\Omega + \tfrac{1}{\tau^n}\,(\beta(p^n - p^{n-1})_\Omega + \alpha\,\mathrm{div}(\boldsymbol{u}^n - \boldsymbol{u}^{n-1}), w)_\Omega = (g^n, w)_\Omega, \quad \forall\, w \in W_0, \end{aligned}$$

where $\tau^n = t^n - t^{n-1}$. This system generates the following problem to be solved on each step of the time-incremental method: find the pair $(\boldsymbol{u}, p)^n \in \boldsymbol{V_0} \times W_0$

$$(2\,\mu\,\boldsymbol{\varepsilon}(\boldsymbol{u}^n), \boldsymbol{\varepsilon}(\boldsymbol{v}))_\Omega + (\lambda\,\mathrm{div}\boldsymbol{u}^n, \mathrm{div}\boldsymbol{v})_\Omega + \alpha\,(\nabla p^n, \boldsymbol{v})_\Omega = (\boldsymbol{f}^n, \boldsymbol{v})_\Omega, \quad \forall\, \boldsymbol{v} \in \boldsymbol{V_0}, \tag{2.4}$$

$$(\mathbb{K}_{\tau^n}\nabla p^n, \nabla w)_\Omega + \beta\,(p^n, w)_\Omega + \alpha\,(\mathrm{div}\,\boldsymbol{u}^n, w)_\Omega = (\widetilde{g}^n, w)_\Omega, \quad \forall\, w_0 \in W_0, \tag{2.5}$$

where $\mathbb{K}_{\tau^n} := \tau^n\,\mathbb{K}$, the right-hand side of (2.5) is defined as

$$\widetilde{g}^n = \tau^n\,g^n + \beta\,p^{n-1} + \alpha\,\mathrm{div}\boldsymbol{u}^{n-1}, \tag{2.6}$$

and the pair $(\boldsymbol{u}, p)^{n-1} \in \boldsymbol{V_0} \times W_0$ is given by the previous time step. The initial values are chosen as $(\boldsymbol{u}, p)^0 = (p^\circ, \boldsymbol{u}^\circ)$. Since, from now on, we deal only with the semi-discrete counterpart of the Biot problem, we omit the subscript Ω in the scalar product. Moreover, we always consider (2.4)–(2.5) on nth time step, which allows us to also neglect the superscript n for the rest of the paper and consider the system

$$(2\,\mu\,\boldsymbol{\varepsilon}(\boldsymbol{u}), \boldsymbol{\varepsilon}(\boldsymbol{v})) + (\lambda\,\mathrm{div}\boldsymbol{u}, \mathrm{div}\boldsymbol{v}) + \alpha\,(\nabla p, \boldsymbol{v}) = (\boldsymbol{f}, \boldsymbol{v}), \quad \forall\, \boldsymbol{v} \in \boldsymbol{V_0}, \tag{2.7}$$

$$(\mathbb{K}_\tau\nabla p, \nabla w) + \beta\,(p, w) + \alpha\,(\mathrm{div}\,\boldsymbol{u}, w) = (\widetilde{g}, w), \quad \forall\, w \in W_0. \tag{2.8}$$

This work aims to derive a fully guaranteed a posteriori estimates of the error between the obtained approximations $(\tilde{\boldsymbol{u}}, \tilde{p}) \in \boldsymbol{V_{0h}} \times W_{0h}$, where $\boldsymbol{V_{0h}}$ and W_{0h} are discretization spaces of conforming approximations of functional spaces $\boldsymbol{V_0}$ and W_0, respectively, and the pair of the exact solutions $(\boldsymbol{u}, p)$ of the Biot system, which is accumulated from the errors on all N time steps, i.e.,

$$e_{\boldsymbol{u}} := \boldsymbol{u} - \tilde{\boldsymbol{u}} \quad \text{and} \quad e_p := p - \tilde{p}.$$

On each sub-interval, these errors are measured in terms of the combined norm

$$\left|\left[(e_{\boldsymbol{u}}, e_p)\right]\right| := |\!|\!|\, e_{\boldsymbol{u}} \,|\!|\!|_{\boldsymbol{u}}^2 + |\!|\!|\, e_p \,|\!|\!|_p^2. \tag{2.9}$$

In turn, each contribution is defined as follows:

$$|\!|\!|\, e_{\boldsymbol{u}} \,|\!|\!|_{\boldsymbol{u}}^2 := \|\, \boldsymbol{\varepsilon}(e_{\boldsymbol{u}}) \,\|_{2\mu}^2 + \|\, \mathrm{div}(e_{\boldsymbol{u}}) \,\|_\lambda^2 \quad \text{and} \quad |\!|\!|\, e_p \,|\!|\!|_p^2 := \|\, \nabla e_p \,\|_{\mathbb{K}_\tau}^2 + \|\, e_p \,\|_\beta^2, \tag{2.10}$$

where $\|\, w \,\|_\lambda^2 := \int_\Omega \lambda\, w^2\, \mathrm{d}x$, $\|\, \boldsymbol{\varepsilon}(\boldsymbol{w}) \,\|_{2\mu}^2 := \int_\Omega 2\mu\, \boldsymbol{\varepsilon}(\boldsymbol{w}) : \boldsymbol{\varepsilon}(\boldsymbol{w})\, \mathrm{d}x$, and $\|\, \boldsymbol{w} \,\|_{\mathbb{K}_\tau}^2 := \int_\Omega \mathbb{K}_\tau\, \boldsymbol{w} \cdot \boldsymbol{w}\, \mathrm{d}x$ are L^2-norms respectively weighted with 2μ, λ, and the tensor $\mathbb{K}_\tau$ for any scalar- and vector-valued functions w and $\boldsymbol{w}$. The global bound of the errors $e_{\boldsymbol{u}}$ and e_p contains incremental contributions from each time-interval, i.e.,

$$\sum_{n=1,\dots,N} \left|\left[(e_{\boldsymbol{u}}^{(n)}, e_p^{(n)})\right]\right| =: \left|\left[(e_{\boldsymbol{u}}, e_p)\right]\right| \le \overline{\mathrm{M}}(\tilde{\boldsymbol{u}}, \tilde{p}) := \sum_{n=1,\dots,N} \overline{\mathrm{M}}^{(n)}(\tilde{\boldsymbol{u}}, \tilde{p}). \tag{2.11}$$

For the iterative approach, on each time-step I^n, the Biot system is decoupled into two sub-problems, where one is related to the linear elasticity, and the other — to the single-phase flow problem. Then, an iterative procedure is applied to obtain the pair $(\boldsymbol{u}^i, p^i) = (\boldsymbol{u}, p)^i$. Next, each equation is discretized and solved, such that, instead of $(\boldsymbol{u}, p)^i$, we use the pair $(\boldsymbol{u}, p)_h^i$, which contains the approximation error of the numerical method. In Section 5, we derive computable a posteriori estimates for this pair of the approximate solution.

The functional $\overline{\mathrm{M}}^{(n)}$ is derived by combining the estimates obtained for the contractive mapping [53] and the a posteriori error majorants for elliptic problems (initially introduced [61,62]). The validity of such estimates is based on the contraction property of a specifically constructed linear combination of displacement and pressure $\frac{\alpha}{\gamma}\,\mathrm{div}\boldsymbol{u}^i - \frac{L}{\gamma}\,p^i$, $L, \gamma > 0$, (the so-called *volumetric mean stress*). The selection of parameters L and γ is justified and explained in Section 3.

Remark 1. For the alternative monolithic approach, one solves (2.7)–(2.8) for pressure and displacement simultaneously, reconstructing the pair of approximations $(\tilde{\boldsymbol{u}}, \tilde{p}) = (\boldsymbol{u}_h, p_h) = (\boldsymbol{u}, p)_h$. For this case, we can derive the corresponding computable bound of the error between $(\tilde{\boldsymbol{u}}, \tilde{p})$ and the exact solution. Such a functional error bound is a combination of a posteriori error estimates for each of the unknowns in (2.7) and (2.8) (see, e.g., [54,63] and references therein).

Remark 2. We note that due to the Korn and Friedrichs inequalities, both $\| e_{\boldsymbol{u}} \|^2$ and $\| e_{\boldsymbol{u}} \|^2_{\boldsymbol{u}}$ are estimated by $\| \boldsymbol{\varepsilon}(e_{\boldsymbol{u}}) \|^2$. Moreover, the physical bound on the Lamé parameters is given as $d\,\lambda + 2\,\mu > 0$, in the most general case, allowing for the first parameter λ to be slightly negative for so-called auxetic materials. In this case, we use the fact that

$$\| e_{\boldsymbol{u}} \|^2_{\boldsymbol{u}} := \| \boldsymbol{\varepsilon}(e_{\boldsymbol{u}}) \|^2_{2\mu} + \| \operatorname{div}(e_{\boldsymbol{u}}) \|^2_{\lambda} \overset{(7.5)}{\leq} (2\,\mu + d\,\lambda) \| \boldsymbol{\varepsilon}(e_{\boldsymbol{u}}) \|^2$$

holds, and work with the positively-weighted norm $\| \boldsymbol{\varepsilon}(e_{\boldsymbol{u}}) \|^2$. However, as auxetic materials are rare, this paper will not consider such cases. Consequently, the proofs below are based on the non-negative Lamé parameters.

3. The fixed-stress splitting scheme

The formal application of the iterative method to (2.7)–(2.8) yields the problem to be solved at the ith iteration step:

$$(\mathbb{K}_\tau \nabla p^i, \nabla w) + \beta\,(p^i, w) + \alpha\,(\operatorname{div}\boldsymbol{u}^{i-1}, w) = (\widetilde{g}, w), \quad \forall\, w \in W_0, \tag{3.1}$$

$$(2\,\mu\,\boldsymbol{\varepsilon}(\boldsymbol{u}^i), \boldsymbol{\varepsilon}(\boldsymbol{v})) + (\lambda \operatorname{div}\boldsymbol{u}^i, \operatorname{div}\boldsymbol{v}) + \alpha\,(\nabla p^i, \boldsymbol{v}) = (\boldsymbol{f}, \boldsymbol{v}), \quad \forall\, \boldsymbol{v} \in \boldsymbol{V_0}, \tag{3.2}$$

where the flow equation (3.1) is solved for p^i, using $\boldsymbol{u}^{i-1}$, and the elasticity equation (3.2) is used to reconstruct $\boldsymbol{u}^i$ using p^i recovered on the previous step. To obtain the initial data for the iterative procedure, we first set the pressure equal to the hydrostatic pressure and then obtain $\boldsymbol{u}^0$ solving (3.2). The iterative procedure proposed in (3.1)–(3.2) is known as the *fixed strain*, and is only conditionally stable.

To stabilize the iterative scheme (3.1)–(3.2), we consider the 'fixed-stress splitting approach', whose properties were initially studied in [60] and [57]. This scheme operates with a special quantity: the *volumetric mean total stress*

$$\eta^i = \tfrac{\alpha}{\gamma} \operatorname{div}\boldsymbol{u}^i - \tfrac{L}{\gamma}\, p^i \in W, \tag{3.3}$$

where γ and L are certain positive tuning parameters. These parameters are usually kept constant on each half-time step. The optimal choice of γ and L proves that this iterative scheme is a contraction in the L^2-norm $\|\delta\eta^i\|^2$, where $\delta\eta^i := \eta^i - \eta^{i-1}$. Moreover, it reduces the number of iterations.

By adding $L\,(p^i - p^{i-1})$ to the right-hand side of (3.1), we rewrite the system (3.1)–(3.2) using the definition (3.3) as

$$(\mathbb{K}_\tau \nabla p^i, \nabla w) + (\beta + L)(p^i, w) = (\widetilde{g} - \gamma\,\eta^{i-1}, w), \quad \forall\, w \in W_0, \tag{3.4}$$

$$\big(2\,\mu\,\boldsymbol{\varepsilon}(\boldsymbol{u}^i), \boldsymbol{\varepsilon}(\boldsymbol{v})\big) + (\lambda \operatorname{div}\boldsymbol{u}^i, \operatorname{div}\boldsymbol{v}) = (\boldsymbol{f}^i - \alpha \nabla p^i, \boldsymbol{v}), \quad \forall\, \boldsymbol{v} \in \boldsymbol{V_0}, \tag{3.5}$$

with complemented mixed BCs $p^i = 0$ on Σ_D^p and $\mathbb{K}_\tau \nabla p^i \cdot \boldsymbol{n} = 0$ on Σ_N^p as well as $\boldsymbol{u}^i = \boldsymbol{0}$ on $\Sigma_D^{\boldsymbol{u}}$ and $\boldsymbol{\sigma}^i_{\text{por}} \cdot \boldsymbol{n} = \boldsymbol{0}$ on $\Sigma_N^{\boldsymbol{u}}$.

Let

$$\delta\nabla p^i := \nabla p^i - \nabla p^{i-1}, \quad \boldsymbol{\varepsilon}(\delta\boldsymbol{u}^i) := \boldsymbol{\varepsilon}(\boldsymbol{u}^i) - \boldsymbol{\varepsilon}(\boldsymbol{u}^{i-1}), \quad \delta\eta^i := \eta^i - \eta^{i-1}. \tag{3.6}$$

Theorem 1 establishes a contraction-type inequality for the norm $\|\delta\eta^i\|^2$.

Theorem 1 (*[57,58]*). *If $\gamma = \frac{\alpha}{\sqrt{\lambda}}$ and $L \geq \frac{\alpha^2}{2\lambda}$, then the scheme (3.4)–(3.5) is a contraction that satisfies the estimate*

$$\|\boldsymbol{\varepsilon}(\delta\boldsymbol{u}^i)\|^2_{2\mu} + q\,\|\nabla\delta p^i\|^2_{\mathbb{K}_\tau} + \|\delta\eta^i\|^2 \leq q^2 \|\delta\eta^{i-1}\|^2, \quad q = \tfrac{L}{\beta + L}, \tag{3.7}$$

where $\delta\nabla p^i$, $\boldsymbol{\varepsilon}(\delta\boldsymbol{u}^i)$, $\delta\eta^i$ are defined in (3.6).

Remark 3. The estimates in Theorem 1, satisfying the contraction estimate (3.7), also hold for the Galerkin approximations $\{\delta\eta_h\}^i \in W_h$, where W_h is a discretization space of W. Moreover, in the Appendix, we show that a similar contraction theorem holds for the sequence $\{\delta(\eta - \eta_h)^i\} \in W_h$, where $\eta^i \in W$ is the generated by the fixed-stress split iterative scheme defined in (3.4)–(3.5) and $\eta^i_h \in W_h$ is discretization of the latter sequence. Generally, it is important to note that all theorems and lemmas below are formulated for a pair $(\boldsymbol{u}, p)^i \in \boldsymbol{V_0} \times W_0$ that forms a contraction w.r.t. to $(\boldsymbol{u}, p)^{i-1} \in \boldsymbol{V_0} \times W_0$ and its discrete approximation $(\boldsymbol{u}, p)^i_h \in \boldsymbol{V_{0h}} \times W_{0h}$ that forms a contraction relative to $(\boldsymbol{u}, p)^{i-1}_h \in \boldsymbol{V_{0h}} \times W_{0h}$.

Remark 4. There exist alternative ways to choose the tuning parameter L. In particular, the physically motivated choice $L_{cl} = \frac{\alpha^2}{\lambda + 2\mu/d}$ is considered in [60], whereas [58] suggests $L_{opt} = \frac{\alpha^2}{2\,(\lambda + 2\mu/d)}$. The recent study [64] suggests the numerical evidence on the iteration counts w.r.t. the full range of the Lamé parameters for heterogeneous media. Numerical investigation of the optimality of these parameters and their comparison with physically and mathematically motivated values from the literature was done in [65]. The authors demonstrated that their optimal value is dependent not only on mechanical material parameters but also on the boundary conditions and material parameters associated with the fluid flow problem.

Remark 5. The inequality (3.7) shows that the sequence $\{\delta\eta^i\}_{i\in\mathbb{N}}$ is generated by a contractive operator. Therefore, due to the Banach theorem, it tends to a certain fixed point. Moreover, since all terms on the left-hand side of (3.7) are positive, in practice, $\{\delta\eta^i\}_{i\in\mathbb{N}}$ might converge with an even better contraction rate than $q = \frac{L}{\beta+L}$.

Corollary 1. *From Theorem 1, it follows that $\nabla\delta p^i$ and $\boldsymbol{\varepsilon}(\delta\boldsymbol{u}^i)$ in (3.6) are also converging sequences and satisfy*

$$\|\nabla\delta p^i\|^2_{\mathbb{K}_\tau} \le q\|\delta\eta^{i-1}\|^2 \quad \text{and} \quad \|\boldsymbol{\varepsilon}(\delta\boldsymbol{u}^i)\|^2_{2\mu} \le q^2\|\delta\eta^{i-1}\|^2,$$

respectively.

We use Corollary 1 to derive the error estimate for the term $\|\!|e_p|\!\|^2_p$. In particular, it yields the following result based on the estimates for the Banach contractive mappings (see [53,54]).

Lemma 1 (*Estimates for Contractive Mapping*)**.** *Let the assumptions of Theorem 1 hold. Then, we have the estimates*

$$\|\nabla(p-p^i)\|^2_{\mathbb{K}_\tau} \le \tfrac{q}{(1-q)^2}\|\delta\eta^{i-1}\|^2, \tag{3.8}$$

$$\|\boldsymbol{\varepsilon}(\boldsymbol{u}-\boldsymbol{u}^i)\|_{2\mu} \le \tfrac{q^2}{(1-q)^2}\|\delta\eta^{i-1}\|^2. \tag{3.9}$$

Proof. Consider

$$\begin{aligned}\|\nabla(p^{i+m}-p^i)\|_{\mathbb{K}_\tau} &\le \|\nabla(p^{i+m}-p^{i+m-1})\|_{\mathbb{K}_\tau} + \ldots + \|\nabla(p^{i+1}-p^i)\|_{\mathbb{K}_\tau}\\ &\le q\,(\|\eta^{i+m-1}-\eta^{i+m-2}\| + \ldots + \|\eta^i-\eta^{i-1}\|)\\ &\le q\,(q^m+\ldots+1)\|\eta^i-\eta^{i-1}\|.\end{aligned}$$

By taking the limit $m\to\infty$ and noting that in this case $(q^m+q^{m-1}+\cdots+1)\to\frac{1}{1-q}$, we arrive at (3.8). The inequality (3.9) is proved using similar arguments. □

If in Lemma 1 we consider the iterations i and $i-m$, $i>m$ as two subsequent iterations, a more general version of the estimates (3.8) and (3.9) can be formulated.

Lemma 2 (*General Estimates for Contractive Mapping*)**.** *Let the assumptions of Theorem 1 hold. Then, we have the estimates*

$$\|\nabla(p-p^i)\|^2_{\mathbb{K}_\tau} \le \min_{1\le m\le i}\left\{\tfrac{q^m}{(1-q^m)^2}\|\eta^i-\eta^{i-m}\|^2\right\}, \tag{3.10}$$

$$\|\boldsymbol{\varepsilon}(\boldsymbol{u}-\boldsymbol{u}^i)\|_{2\mu} \le \min_{1\le m\le i}\left\{\tfrac{q^{2m}}{(1-q^m)^2}\|\eta^i-\eta^{i-m}\|^2\right\}. \tag{3.11}$$

Proof. Proof follows along the lines of the proof of Lemma 1 with $m=1,\ldots,i$. □

Remark 6. The estimates in Lemma 2 improve the value of $\frac{q^m}{(1-q^m)^2}$ and $\frac{q^{2m}}{(1-q^m)^2}$ if q is close to 1. At the same time, it might look counterintuitive, but the choice $m=i$ is not always optimal. As the quotient with q decreases, the term $\|\eta^i-\eta^0\|^2$ grows. Therefore, we should choose m carefully. Computing the majorant on each step of our iterative algorithm might be computationally expensive, therefore, in certain cases, m must be chosen a priori. Alternatively, with several extra iterations after reaching the desired convergence in p and $\boldsymbol{u}$, both $\frac{q'}{(1-q')^2}$ with $q'=q^m$ and $\|\eta^i-\eta^{i-m}\|^2$ will decrease, impacting total values of the majorant.

Remark 7. Theorem 1 also yields the so-called *a priori contractive estimates*, i.e.,

$$\|\nabla(p-p^i)\|^2_{\mathbb{K}_\tau} \le \tfrac{q^{2i-1}}{(1-q)^2}\|\eta^1-\eta^0\|^2, \tag{3.12}$$

$$\|\boldsymbol{\varepsilon}(\boldsymbol{u}-\boldsymbol{u}^i)\|_{2\mu} \le \tfrac{q^{2i}}{(1-q)^2}\|\eta^1-\eta^0\|^2, \tag{3.13}$$

which can be used as an alternative upper bound.

4. Main results

Theorem 2 presents the main result of this work, that is an upper bound of the error $\big|\big[(e_{\boldsymbol{u}}, e_p)\big]\big|$ (cf. (2.11)).

Theorem 2 (*On Functional Error Estimates*)**.** *For any $p_h^i \in W_0$ and $\boldsymbol{u}_h^i \in \boldsymbol{V_0}$, we have the estimates*

$$\sum_{n=1,\ldots,N}\big|\big[(e_{\boldsymbol{u}}^{(n)}, e_p^{(n)})\big]\big| =: \big|\big[e_p, e_{\boldsymbol{u}}\big]\big| \le \overline{\mathrm{M}} := \sum_{n=1,\ldots,N}\overline{\mathrm{M}}_p^{(n)} + \overline{\mathrm{M}}_{\boldsymbol{u}}^{(n)},$$

where $\overline{\mathrm{M}}_p^{(n)}$ *and* $\overline{\mathrm{M}}_{\boldsymbol{u}}^{(n)}$ *correspond to the error introduced by approximation schemes in each variable* p *and* $\boldsymbol{u}$*, respectively, and measured by the norms* $|||\, e_{\boldsymbol{u}}^{(n)} \,|||_{\boldsymbol{u}}^2$ *and* $|||\, e_p^{(n)} \,|||_p^2$*. Omitting the suffix* (n) *for readability and generality, we can formulate both functionals as*

$$\overline{\mathrm{M}}_p := 2\left(\overline{\mathrm{M}}_p^h(p_h^i, \boldsymbol{z}_h^i) + \min\left\{\overline{\mathrm{M}}_p^i, \overline{\mathrm{M}}_p^{i,m}, \widetilde{\mathrm{M}}_p^i\right\}\right),$$

$$\overline{\mathrm{M}}_{\boldsymbol{u}} := 2\left(\overline{\mathrm{M}}_{\boldsymbol{u}}^h\big((\boldsymbol{u}, p)_h^i, (\boldsymbol{\tau}, \boldsymbol{z})_h^i\big) + \min\left\{\overline{\mathrm{M}}_{\boldsymbol{u}}^i, \overline{\mathrm{M}}_{\boldsymbol{u}}^{i,m}, \widetilde{\mathrm{M}}_{\boldsymbol{u}}^i\right\}\right),$$

where $\overline{\mathrm{M}}_p^h$*,* $\overline{\mathrm{M}}_p^i$*,* $\overline{\mathrm{M}}_p^{i,m}$*, and* $\widetilde{\mathrm{M}}_p^i$ *are defined in Lemmas 3, 6, Corollary 4, and Lemma 7, respectively, as well as* $\overline{\mathrm{M}}_{\boldsymbol{u}}^h$*,* $\overline{\mathrm{M}}_{\boldsymbol{u}}^i$*,* $\overline{\mathrm{M}}_{\boldsymbol{u}}^{i,m}$ *and* $\widetilde{\mathrm{M}}_{\boldsymbol{u}}^i$ *are presented by Lemmas 5, 8, Corollary 5, and Lemma 9, respectively.*

The functionals $\overline{\mathrm{M}}_p^h$ and $\overline{\mathrm{M}}_{\boldsymbol{u}}^h$ are defined in Section 5 by means of functional arguments. They provide the upper bounds of errors introduced in (3.4)–(3.5) for the ith iteration, when the system is solved numerically. To be precise, these error functionals provide a bound between the exact solution $(\boldsymbol{u}, p)^i = (\boldsymbol{u}^i, p^i)$ of (3.4)–(3.5) and its approximation $(\boldsymbol{u}, p)_h^i = (\boldsymbol{u}_h^i, p_h^i)$. $\overline{\mathrm{M}}_p^h$ and $\overline{\mathrm{M}}_{\boldsymbol{u}}^h$ are reliable and dependent only on explicitly computable constants, approximations, and auxiliary functions.

Estimates $\overline{\mathrm{M}}_p^i$, $\overline{\mathrm{M}}_p^{i,m}$, and $\widetilde{\mathrm{M}}_p^i$, as well as $\overline{\mathrm{M}}_{\boldsymbol{u}}^h$, $\overline{\mathrm{M}}_{\boldsymbol{u}}^i$, and $\widetilde{\mathrm{M}}_{\boldsymbol{u}}^i$ are derived in Section 6 by means of the contraction mappings estimates [53]. Bounds $\overline{\mathrm{M}}_p^i$ and $\overline{\mathrm{M}}_{\boldsymbol{u}}^i$ follow naturally from Lemma 1, whereas $\overline{\mathrm{M}}_p^{i,m}$ and $\overline{\mathrm{M}}_{\boldsymbol{u}}^{i,m}$ are derived from a more general Lemma 2. Derivation of the functionals $\widetilde{\mathrm{M}}_{\boldsymbol{u}}^i$ and $\widetilde{\mathrm{M}}_{\boldsymbol{u}}^i$ is based on yet another basic property of the contractive operators (3.12)–(3.13) that is highlighted in Remark 7.

Generally, Theorem 2 provides a mathematical tool for reliable error control of approximate solutions of the Biot problem in the poroelastic medium. The functional $\overline{\mathrm{M}}$ provides a guaranteed bound of the error in these approximations, which is confirmed by numerical examples in Section 7. The set of computational tests is designed to provide an overview of several important properties of functional error estimates, as well as confirm the universality w.r.t. some of the parameters coming either from the mathematical model (e.g., permeability, Lame coefficients, etc.) or dictated by the iterative scheme (tuning parameters of the fixed-stress split method).

5. Estimates of errors generated by discretization

Before deriving the estimates of approximation errors that appear in the contractive iterative scheme, we need to study the discretization errors encompassed in (3.4)–(3.5) for the ith iteration. Henceforth, the pair $(\boldsymbol{u}, p)^i = (\boldsymbol{u}^i, p^i)$ is considered as the exact solution of (3.4)–(3.5), whereas $(\boldsymbol{u}, p)_h^i = (\boldsymbol{u}_h^i, p_h^i)$ denotes its approximation computed by a certain discretization method. We aim to derive computable and reliable estimates of the error measured in the terms $|||e_p^i|||_p^2$ and $|||e_{\boldsymbol{u}}^i|||_{\boldsymbol{u}}^2$.

Majorant of the error in the pressure term. For the first equation (3.4), Lemma 3 presents a computable upper bound of the difference

$$e_p^i := p^i - p_h^i$$

between the exact solution $p^i \in W_0$ and its approximation $p_h^i \in W_0$, measured in terms of the energy norm $|||\, e_p^i \,|||_p^2$.

Lemma 3. *For any* $p_h^i \in W_0$*, any auxiliary vector-valued function*

$$\boldsymbol{z}_h^i \in H_{\Sigma_N^p}(\Omega, \mathrm{div}) := \left\{\, \boldsymbol{z}_h^i \in [L(\Omega)]^d \mid \mathrm{div}\boldsymbol{z}_h^i \in L^2(\Omega),\ \boldsymbol{z}_h^i \cdot \boldsymbol{n} \in L^2(\Sigma_N^p) \,\right\}, \tag{5.1}$$

and any parameter $\zeta \geq 0$*, we have the following estimate*

$$\| \nabla e_p^i \|_{\mathbb{K}_\tau}^2 + \| e_p^i \|_\beta^2 =: |||\, e_p^i \,|||_p^2 \leq \overline{\mathrm{M}}_p^h(p_h^i, \boldsymbol{z}_h^i; \zeta),$$

where

$$\overline{\mathrm{M}}_p^h(p_h^i, \boldsymbol{z}_h^i; \zeta) := (1+\zeta)\, \|\mathbf{r}_{\mathrm{d}}(p_h^i, \boldsymbol{z}_h^i)\|_{\mathbb{K}_\tau^{-1}}^2 + (1+\tfrac{1}{\zeta})\, C_\Omega^p \left(\|\mathbf{r}_{\mathrm{eq}}(p_h^i, \boldsymbol{z}_h^i)\|_\Omega^2 + \overline{\mathrm{M}}_q^h((\boldsymbol{u}, p)_h^1) + \|\boldsymbol{z}_h^i \cdot \boldsymbol{n}\|_{\Sigma_N^p}^2\right). \tag{5.2}$$

Here,

$$\mathbf{r}_{\mathrm{d}}(p_h^i, \boldsymbol{z}_h^i) := \boldsymbol{z}_h^i - \mathbb{K}_\tau \nabla p_h^i, \quad \mathbf{r}_{\mathrm{eq}}(p_h^i, \boldsymbol{z}_h^i) := \widetilde{g} - \gamma\, \eta_h^{i-1} - (\beta + L)\, p_h^i + \mathrm{div}\boldsymbol{z}_h^i,$$

where $\widetilde{g}$ *is defined in (2.6), and*

$$\overline{\mathrm{M}}_q^h := \left(C_q \left(\frac{\alpha}{\gamma}\, \overline{\mathrm{M}}_{p,L^2}^{h,\,1/2} + \frac{L}{\gamma}\, \overline{\mathrm{M}}_{\boldsymbol{u},\mathrm{div}}^{h,\,1/2}\right) + (C_q + 1)\, \|\, \eta^0 - \eta_h^0 \,\|\right)^2, \quad C_q := \sum_{k=1}^{i-1} q^k + 1,$$

where $\overline{\mathrm{M}}^h_{p,L^2}(p^1_h, \boldsymbol{z}^1_h)$ *and* $\overline{\mathrm{M}}^h_{\boldsymbol{u},\mathrm{div}}((\boldsymbol{u}, p)^1_h, \boldsymbol{\tau}^1_h, \boldsymbol{z}^1_h)$*, defined in Corollaries 2 and 3, are dependent on the explicitly given* η^0*. The constant*

$$(C^p_\Omega)^2 := \tfrac{1}{(\beta+L)}\Big(1 + \big(C^{\mathrm{tr}}_{\Sigma^p_N}\big)^2\Big) \tag{5.3}$$

is defined via the constant in the trace-type inequality

$$\| w \|_{\Sigma^p_N} \le C^{\mathrm{tr}}_{\Sigma^p_N} \| w \|_\Omega, \quad \forall w \in W_0, \tag{5.4}$$

and the positive parameters of the Biot model, β *and L.*

Proof. The majorant $\overline{\mathrm{M}}_p(p^i_h, \boldsymbol{z}^i_h; \zeta)$ follows from [66, Section 2] and [54, Section 4.2–4.3], i.e., we consider (3.4) with a bilinear form $(\mathbb{K}_\tau \nabla p^i_h, \nabla w) + (\beta + L)(p^i{}_h, w)$ subtracted from its left- and right-hand sides

$$(\mathbb{K}_\tau \nabla e^i_p, \nabla w) + (\beta + L)(e^i_p, w) = (\widetilde{g} - \gamma\, \eta^{i-1} - (\beta + L)\, p^i{}_h, w) - (\mathbb{K}_\tau \nabla p^i_h, \nabla w).$$

Next, we set $w = e^i_p$ and introduce an auxiliary function $\boldsymbol{z}^i_h \in H_{\Sigma^p_N}(\Omega, \mathrm{div})$ (cf. (5.1)) satisfying the identity $(\mathrm{div}\boldsymbol{z}^i_h, \boldsymbol{w})_\Omega + (\boldsymbol{z}^i_h, \nabla \boldsymbol{w})_\Omega = (\boldsymbol{z}^i_h \cdot \boldsymbol{n}, \boldsymbol{w})_{\Sigma^p_N}$, such that

$$\begin{aligned}\|\nabla e^i_p\|^2_{\mathbb{K}_\tau} + \|e^i_p\|^2_{\beta+L} &= (\boldsymbol{z}^i_h - \mathbb{K}_\tau \nabla p^i_h, \nabla e^i_p) + (\widetilde{g} - \gamma\, \eta^{i-1} - (\beta + L)\, p^i{}_h + \mathrm{div}\boldsymbol{z}^i_h, e^i_p) - (\boldsymbol{z}^i_h \cdot \boldsymbol{n}, e^i_p)_{\Sigma^p_N} \\ &= (\mathbf{r}_{\mathrm{d}}(p^i_h, \boldsymbol{z}^i_h), \nabla e^i_p) + (\widetilde{\mathbf{r}}_{\mathrm{eq}}(p^i_h, \boldsymbol{z}^i_h), e^i_p) - (\boldsymbol{z}^i_h \cdot \boldsymbol{n}, e^i_p)_{\Sigma^p_N},\end{aligned} \tag{5.5}$$

where $\widetilde{\mathbf{r}}_{\mathrm{eq}}(p^i_h, \boldsymbol{z}^i_h) := \widetilde{g} - \gamma\, \eta^{i-1} - (\beta + L)\, p^i_h + \mathrm{div}\boldsymbol{z}^i_h$. Using the Hölder and Young inequalities, we can estimate the first term on the right-hand side of (5.5) as

$$(\mathbf{r}_{\mathrm{d}}(p^i_h, \boldsymbol{z}^i_h), \nabla e^i_p) \le \tfrac{1}{2}(1 + \zeta)\, \|\mathbf{r}_{\mathrm{d}}(p^i_h, \boldsymbol{z}^i_h)\|^2_{\mathbb{K}^{-1}_\tau} + \tfrac{1}{2(1+\zeta)}\, \|\nabla e^i_p\|^2_{\mathbb{K}_\tau}. \tag{5.6}$$

The second term on the right-hand side of (5.5) is bounded analogously, i.e.,

$$(\widetilde{\mathbf{r}}_{\mathrm{eq}}(p^i_h, \boldsymbol{z}^i_h), e^i_p) - (\boldsymbol{z}^i_h \cdot \boldsymbol{n}, e^i_p)_{\Sigma^p_N} \le \tfrac{1}{2}(1 + \tfrac{1}{\zeta})(C^p_\Omega)^2(\|\widetilde{\mathbf{r}}_{\mathrm{eq}}(p^i_h, \boldsymbol{z}^i_h)\|^2 + \|\boldsymbol{z}^i_h \cdot \boldsymbol{n}\|^2_{\Sigma^p_N}) + \tfrac{1}{2}\, \tfrac{\zeta}{1+\zeta}\, \|e^i_p\|^2_{\beta+L}, \tag{5.7}$$

where C^p_Ω (cf. (5.3)) is a constant in the inequality

$$\|w\|^2 + \|w\|^2_{\Sigma^p_N} \le (C^p_\Omega)^2\, \|w\|^2_{\beta+L}, \qquad \forall w \in W_0,$$

defined in (5.4). By summing up the results of (5.6) and (5.7), we obtain

$$\begin{aligned}\|\nabla e^i_p\|^2_{\mathbb{K}_\tau} + \|e^i_p\|^2_\beta &\le \|\nabla e^i_p\|^2_{\mathbb{K}_\tau} + \|e^i_p\|^2_{\beta+L} \\ &\le (1 + \zeta)\, \|\mathbf{r}_{\mathrm{d}}(p^i_h, \boldsymbol{z}^i_h)\|^2_{\mathbb{K}^{-1}_\tau} + (1 + \tfrac{1}{\zeta})(C^p_\Omega)^2(\|\widetilde{\mathbf{r}}_{\mathrm{eq}}(p^i_h, \boldsymbol{z}^i_h)\|^2 + \|\boldsymbol{z}^i_h \cdot \boldsymbol{n}\|^2_{\Sigma^p_N}).\end{aligned} \tag{5.8}$$

At this point, the term $\|\widetilde{\mathbf{r}}_{\mathrm{eq}}(p^i_h, \boldsymbol{z}^i_h)\|^2$ is not fully computable in the usual sense of functional majorants since it is defined using η_{i-1}. However, it can be estimated by

$$\begin{aligned}\|\widetilde{\mathbf{r}}_{\mathrm{eq}}(p^i_h, \boldsymbol{z}^i_h)\|^2 &\le \|\widetilde{g} - \gamma\, \eta^{i-1} - (\beta + L)\, p^i_h + \mathrm{div}\boldsymbol{z}^i_h\|^2 \\ &\le 2\|\widetilde{g} - \gamma\, \eta^{i-1}_h - (\beta + L)\, p^i_h + \mathrm{div}\boldsymbol{z}^i_h\|^2 + 2\gamma^2 \|\eta^{i-1} - \eta^{i-1}_h\|^2 \\ &\le 2\|\mathbf{r}_{\mathrm{eq}}(p^i_h, \boldsymbol{z}^i_h)\|^2 + 2\gamma^2 \|\eta^{i-1} - \eta^{i-1}_h\|^2.\end{aligned} \tag{5.9}$$

Consider the norm $\|\eta^{i-1} - \eta^{i-1}_h\|$ (without the squares) and apply an approach similar to the one that was used to prove Lemma 1

$$\begin{aligned}\|\eta^i - \eta^i_h\| \le \sum_{k=1}^{i-1} \|\delta\eta^k - \delta\eta^k_h\| + \|\eta^0 - \eta^0_h\| \overset{\text{Theorem 4}}{\le} (q^{i-1} + \ldots + 1)\, \|\delta\eta^1 - \delta\eta^1_h\| + \|\eta^0 - \eta^0_h\| \\ \le \Big(\sum_{k=1}^{i-1} q^k + 1\Big)\, \|\delta\eta^1 - \delta\eta^1_h\| + \|\eta^0 - \eta^0_h\| \\ \le \Big(\sum_{k=1}^{i-1} q^k + 1\Big)\, \big(\|\eta^1 - \eta^1_h\| + \|\eta^0 - \eta^0_h\|\big) + \|\eta^0 - \eta^0_h\| \\ \le C_q\, \|\eta^1 - \eta^1_h\| + (C_q + 1)\, \|\eta^0 - \eta^0_h\|.\end{aligned}$$

Here, $\| \eta^0 - \eta_h^0 \|$ is a computable term, whereas $\|\eta^1 - \eta_h^1\|^2$ is controlled by a combination of majorants $\overline{\mathrm{M}}^h_{p,L^2}(p_h^1, \boldsymbol{z}_h^1)$ and $\overline{\mathrm{M}}^h_{\boldsymbol{u},\mathrm{div}}((\boldsymbol{u},p)_h^1, \boldsymbol{\tau}_h^1, \boldsymbol{z}_h^1)$ defined in Corollaries 2 and 3 and containing the computable quantity $\eta^0 := \frac{\alpha}{\gamma}\mathrm{div}\boldsymbol{u}^0 - \frac{L}{\gamma}p^0$., i.e.,

$$\|\eta^1 - \eta_h^1\| \le \frac{\alpha}{\gamma}\| \mathrm{div}(\boldsymbol{u}^1 - \boldsymbol{u}_h^1)\| + \frac{L}{\gamma}\| p^1 - p_h^1\| \le \frac{\alpha}{\gamma}\left(\overline{\mathrm{M}}^h_{p,L^2}(p_h^1, \boldsymbol{z}_h^1; \zeta)\right)^{1/2} + \frac{L}{\gamma}\left(\overline{\mathrm{M}}^h_{\boldsymbol{u},\mathrm{div}}((\boldsymbol{u},p)_h^1, \boldsymbol{\tau}_h^1, \boldsymbol{z}_h^1)\right)^{1/2}. \tag{5.10}$$

This yields that

$$\|\eta^i - \eta_h^i\|^2 \le \overline{\mathrm{M}}_q^h := \left(C_q\left(\frac{\alpha}{\gamma}\overline{\mathrm{M}}^{h,\,1/2}_{p,L^2} + \frac{L}{\gamma}\overline{\mathrm{M}}^{h,\,1/2}_{\boldsymbol{u},\mathrm{div}}\right) + (C_q+1)\| \eta^0 - \eta_h^0\|\right)^2 \tag{5.11}$$

The combination of (5.9) and (5.11) yields

$$\|\nabla e_p^i\|^2_{\mathbb{K}_\tau} + \|e_p^i\|^2_\beta \le (1+\zeta)\,\|\mathbf{r}_\mathrm{d}(p_h^i, \boldsymbol{z}_h^i)\|^2_{\mathbb{K}_\tau^{-1}} + (1+\tfrac{1}{\zeta})(C_\Omega^p)^2(2\|\mathbf{r}_\mathrm{eq}(p_h^i, \boldsymbol{z}_h^i)\|^2 + \overline{\mathrm{M}}_q^h((\boldsymbol{u},p)_h^1) + \|\boldsymbol{z}_h^i\cdot\boldsymbol{n}\|^2_{\Sigma_N^p}). \quad \square$$

Remark 8. Numerical reconstruction of the majorant involves several steps. They are determined by the accuracy requirements imposed on the upper bound of the error. To generate guaranteed bounds with the realistic efficiency index $I_{\mathrm{eff}}(\overline{\mathrm{M}}_p) := \frac{\overline{\mathrm{M}}_p}{\|p^i - p_h^i\|_p^2}$, we can reconstruct $\boldsymbol{z}_h^i$ from ∇p_h^i (where p_h^i is approximated by the chosen discretization method recovering the exact solution of (3.4)). However, to obtain the sharpest estimate, the functional $\overline{\mathrm{M}}_p$ must be optimized w.r.t. $\boldsymbol{z}_h^i$ and ζ iteratively. This generates an auxiliary variational problem w.r.t. the vector-valued function $\boldsymbol{z}_h^i$.

Alternatively, one can consider a mixed formulation of (3.4) and reconstruct the pair $(p_h^i, \boldsymbol{z}_h^i)$ using one of the well-developed mixed methods [67,68], simultaneously. Then both variables required for the reconstruction of $\overline{\mathrm{M}}_p$ are directly computable, and no additional post-processing (computational overhead) is required.

The majorant in Lemma 3 yields an estimate of the e_p^i measured in terms of L^2-norm.

Corollary 2. *For any $p_h^i \in W_0$, any auxiliary functions and parameters defined in Lemma 3, the estimate*

$$\|e_p^i\|^2 \le \overline{\mathrm{M}}^h_{p,L^2}(p_h^i, \boldsymbol{z}_h^i; \zeta) := \left(\tau\,\lambda_\mathbb{K}\left(C^{\mathrm{F}}_{\Sigma_D^p}\right)^{-2} + \beta\right)^{-1}\overline{\mathrm{M}}^h_p(p_h^i, \boldsymbol{z}_h^i; \zeta) \tag{5.12}$$

holds, where $\overline{\mathrm{M}}^h_p(p_h^i, \boldsymbol{z}_h^i; \zeta)$ is defined in (5.2), $C^{\mathrm{F}}_{\Sigma_D^p}$ is a constant in the Friedrichs inequality (cf. (7.2)), and $\lambda_\mathbb{K}$ is the minimum eigenvalue of the permeability tensor (cf. (1.2)).

Proof. By means of the Friedrichs inequality and (1.2), we obtain

$$\|\!|e_p^i|\!\|_p^2 \ge \tau\,\lambda_\mathbb{K}\left(C^{\mathrm{F}}_{\Sigma_D^p}\right)^{-2}\|e_p^i\|^2 + \|e_p^i\|_\beta^2 \ge \left(\tau\,\lambda_\mathbb{K}\left(C^{\mathrm{F}}_{\Sigma_D^p}\right)^{-2} + \beta\right)\| e_p^i\|^2. \tag{5.13}$$

By combining (5.13) and (5.2), we arrive at (5.12). $\square$

Majorant of the error in the displacement term. The current section considers estimates for the error

$$e_{\boldsymbol{u}}^i := \boldsymbol{u}^i - \boldsymbol{u}_h^i \tag{5.14}$$

between the exact solution $\boldsymbol{u}^i \in \boldsymbol{V_0}$ and its respective approximation $\boldsymbol{u}_h^i \in \boldsymbol{V_0}$, measured in terms of the energy norm $|\!|\!|\cdot|\!|\!|_{\boldsymbol{u}}^2$ (cf. (2.10)). Since p_h^i is, in fact, used instead of p^i, the original problem (3.5) is replaced by

$$2\mu\left(\boldsymbol{\varepsilon}(\tilde{\boldsymbol{u}}^i), \boldsymbol{\varepsilon}(\boldsymbol{v})\right) + \lambda(\mathrm{div}\tilde{\boldsymbol{u}}^i, \mathrm{div}\boldsymbol{v}) = (\boldsymbol{f}^i - \alpha\nabla p_h^i, \boldsymbol{v}), \quad \forall\,\boldsymbol{v} \in \boldsymbol{V_0}, \tag{5.15}$$

with a perturbed right-hand side. Therefore, $\boldsymbol{u}_h^i$ is an approximation of $\tilde{\boldsymbol{u}}^i$ instead of $\boldsymbol{u}^i$. In other words, $e_{\boldsymbol{u}}^i$ is composed of the error arising due to the original problem is replaced by (5.15), i.e., $\boldsymbol{u}^i - \tilde{\boldsymbol{u}}^i$, and the error $\tilde{\boldsymbol{u}}^i - \boldsymbol{u}_h^i$ arising because (5.15) is solved approximately. By means of the triangle inequality, $e_{\boldsymbol{u}}^i$ can be estimated by the above-described errors as follows:

$$\| \boldsymbol{\varepsilon}(e_{\boldsymbol{u}}^i)\|^2_{2\mu} + \| \mathrm{div}(e_{\boldsymbol{u}}^i)\|^2_\lambda =: |\!|\!|e_{\boldsymbol{u}}^i|\!|\!|_{\boldsymbol{u}}^2 \le 2\,|\!|\!|\boldsymbol{u}^i - \tilde{\boldsymbol{u}}^i|\!|\!|_{\boldsymbol{u}}^2 + 2\,|\!|\!|\tilde{\boldsymbol{u}}^i - \boldsymbol{u}_h^i|\!|\!|_{\boldsymbol{u}}^2. \tag{5.16}$$

Here, $|\!|\!|\tilde{\boldsymbol{u}}^i - \boldsymbol{u}_h^i|\!|\!|_{\boldsymbol{u}}^2$ can be estimated by a functional majorant for a class of elasticity problems (see Lemma 4), whereas $|\!|\!|\boldsymbol{u}^i - \tilde{\boldsymbol{u}}^i|\!|\!|_{\boldsymbol{u}}^2$ is controlled by the bound following from the difference of model problems (3.5) and (5.15) (see Lemma 5).

Lemma 4. *For any $\boldsymbol{u}_h^i \in \boldsymbol{V_0}$ approximating $\tilde{\boldsymbol{u}}^i$ in (5.15), any auxiliary tensor-valued function*

$$\boldsymbol{\tau}_h^i \in [\mathcal{T}_{\mathrm{Div}}(\Omega)]^{d\times d} := \left\{\, \boldsymbol{\tau}_h^i \in [L^2(\Omega)]^{d\times d} \;\middle|\; \mathrm{Div}\boldsymbol{\tau}_h^i \in [L^2(\Omega)]^d,\ \boldsymbol{\tau}_h^i\cdot\boldsymbol{n} \in L^2(\Sigma_N^{\boldsymbol{u}}) \right\},$$

and any parameter $\xi \geq 0$, we have the estimate

$$\begin{aligned}\|\boldsymbol{\varepsilon}(\tilde{\boldsymbol{u}}^i - \boldsymbol{u}_h^i)\|_{2\mu}^2 + \|\mathrm{div}(\tilde{\boldsymbol{u}}^i - \boldsymbol{u}_h^i)\|_{\lambda}^2 =: |||\tilde{\boldsymbol{u}}^i - \boldsymbol{u}_h^i|||_{\boldsymbol{u}}^2 \leq \overline{\mathrm{M}}_{\tilde{u}}((\boldsymbol{u}, p)_h^i, \boldsymbol{\tau}_h^i) \\ := (1+\xi)\int_{\Omega} \mathbf{r}_{\mathrm{d}}(p_h^i, \boldsymbol{\tau}_h^i)\mathrm{d}x + (1+\tfrac{1}{\xi})\, C_{\Omega}^{\boldsymbol{u}}\Big(\|\mathbf{r}_{\mathrm{eq}}(p_h^i, \boldsymbol{\tau}_h^i)\|_{\Omega}^2 + \|\boldsymbol{\tau}_h^i \cdot \boldsymbol{n}\|_{\Sigma_N^{\boldsymbol{u}}}^2\Big),\end{aligned} \tag{5.17}$$

where

$$\begin{aligned}\mathbf{r}_{\mathrm{eq}}(p_h^i, \boldsymbol{\tau}_h^i) &:= \boldsymbol{f}^i - \alpha\nabla p_h^i + \mathrm{Div}\boldsymbol{\tau}_h^i, \\ \mathbf{r}_{d,\mu,\lambda}(\boldsymbol{u}_h^i, \boldsymbol{\tau}_h^i) &:= 2\,\mu\,|\boldsymbol{\varepsilon}(\boldsymbol{u}_h^i)|^2 + \lambda\,|\mathrm{div}\boldsymbol{u}_h^i|^2 + \tfrac{1}{2\mu}\,(|\boldsymbol{\tau}_h^i|^2 - \tfrac{\lambda}{3\lambda+2\mu}|\mathrm{div}\boldsymbol{\tau}_h^i|^2) - 2\,\boldsymbol{\varepsilon}(\boldsymbol{u}_h^i) : \tau^i,\end{aligned} \tag{5.18}$$

β, α, μ, λ are the characteristics of the Biot model, and

$$C_{\Omega}^{\boldsymbol{u}} := C^{\mathrm{K}}\left(1 + C_{\Sigma_N^{\boldsymbol{u}}}^{\mathrm{tr}}\right) \tag{5.19}$$

is defined through the constants $C_{\Sigma_N^{\boldsymbol{u}}}^{\mathrm{tr}}$ and C^{K} in the trace-type and the Korn first inequalities

$$\|\boldsymbol{w}\|_{\Sigma_N^{\boldsymbol{u}}} \leq C_{\Sigma_N^{\boldsymbol{u}}}^{\mathrm{tr}}\,\|\boldsymbol{w}\|_{[H^1(\Omega)]^d} \quad \textit{and} \quad \|\boldsymbol{w}\|_{[H^1(\Omega)]^d} \leq C^{\mathrm{K}}\|\boldsymbol{\varepsilon}(\boldsymbol{w})\|_{[L^2(\Omega)]^{d\times d}} \quad \forall \boldsymbol{w} \in \boldsymbol{V_0}, \tag{5.20}$$

respectively.

Proof. To simplify the exposition, let us assume the following representation of the elasticity tensor

$$\mathbb{L}\,\boldsymbol{\varepsilon}(\boldsymbol{u}) := 2\,\mu\,\boldsymbol{\varepsilon}(\boldsymbol{u}) + \lambda\,\mathrm{div}(\boldsymbol{u}). \tag{5.21}$$

Then, the derivation of an a posteriori error estimate for the problem

$$\left(\mathbb{L}\,\boldsymbol{\varepsilon}(\tilde{\boldsymbol{u}}^i), \boldsymbol{\varepsilon}(\boldsymbol{v})\right) = (\boldsymbol{f}^i - \alpha\nabla p_h^i, \boldsymbol{v}), \quad \forall\, \boldsymbol{v} \in \boldsymbol{V_0}, \tag{5.22}$$

follows the lines presented in [54, Section 5.2]. In particular, considering an approximation $\boldsymbol{u}_h^i \in \boldsymbol{V_0}$, we subtract the bilinear form $\left(\mathbb{L}\boldsymbol{\varepsilon}(\boldsymbol{u}_h^i), \boldsymbol{\varepsilon}(\boldsymbol{v})\right)$ from the left- and right-hand sides of (5.22) and set $\boldsymbol{v} = \tilde{\boldsymbol{u}}^i - \boldsymbol{u}_h^i$ to obtain

$$\left(\mathbb{L}\,\boldsymbol{\varepsilon}(\tilde{\boldsymbol{u}}^i - \boldsymbol{u}_h^i), \boldsymbol{\varepsilon}(\tilde{\boldsymbol{u}}^i - \boldsymbol{u}_h^i)\right) = (\boldsymbol{f}^i - \alpha\nabla p_h^i, \boldsymbol{v}) - \left(\mathbb{L}\,\boldsymbol{\varepsilon}(\boldsymbol{u}), \boldsymbol{\varepsilon}(\tilde{\boldsymbol{u}}^i - \boldsymbol{u}_h^i)\right). \tag{5.23}$$

Next, we set $\boldsymbol{v} = \tilde{\boldsymbol{u}}^i - \boldsymbol{u}_h^i$ and add the divergence of the tensor-valued function $\boldsymbol{\tau}_h^i \in [\mathcal{T}_{\mathrm{Div}}(\Omega)]^{d\times d}$, i.e.,

$$(\mathrm{Div}\boldsymbol{\tau}_h^i, \boldsymbol{v}) + (\boldsymbol{\tau}_h^i, \boldsymbol{\varepsilon}(\boldsymbol{v})) = (\boldsymbol{\tau}_h^i \cdot \boldsymbol{n}, \boldsymbol{v})_{\Sigma_N^{\boldsymbol{u}}}, \quad \forall \boldsymbol{v} \in \boldsymbol{V_0}, \tag{5.24}$$

into the left- and right-hand sides of (5.23), which results in the identity

$$\left(\mathbb{L}\,\boldsymbol{\varepsilon}(\tilde{\boldsymbol{u}}^i - \boldsymbol{u}_h^i), \boldsymbol{\varepsilon}(\tilde{\boldsymbol{u}}^i - \boldsymbol{u}_h^i)\right) = \left(\mathbf{r}_{\mathrm{d},\mathbb{L}}(\boldsymbol{u}_h^i, \boldsymbol{\tau}_h^i), \boldsymbol{\varepsilon}(\tilde{\boldsymbol{u}}^i - \boldsymbol{u}_h^i)\right) + (\mathbf{r}_{\mathrm{eq}}(p_h^i, \boldsymbol{\tau}_h^i), \tilde{\boldsymbol{u}}^i - \boldsymbol{u}_h^i) - (\boldsymbol{\tau}_h^i \cdot \boldsymbol{n}, \tilde{\boldsymbol{u}}^i - \boldsymbol{u}_h^i)_{\Sigma_N^{\boldsymbol{u}}}, \tag{5.25}$$

where

$$\mathbf{r}_{\mathrm{d},\mathbb{L}}(\boldsymbol{u}_h^i, \boldsymbol{\tau}_h^i) := \boldsymbol{\tau}_h^i - \mathbb{L}\,\boldsymbol{\varepsilon}(\boldsymbol{u}_h^i)$$

and $\mathbf{r}_{\mathrm{eq}}(p_h^i, \boldsymbol{\tau}_h^i)$ is defined (5.18). By means of the Hölder and Young inequalities, the first term on the right-hand side of (5.23) can be estimated as

$$\left(\mathbf{r}_{\mathrm{d},\mathbb{L}}(\boldsymbol{u}_h^i, \boldsymbol{\tau}_h^i), \boldsymbol{\varepsilon}(\tilde{\boldsymbol{u}}^i - \boldsymbol{u}_h^i)\right) \leq \|\mathbf{r}_{\mathrm{d},\mathbb{L}}(\boldsymbol{u}_h^i, \boldsymbol{\tau}_h^i)\|_{\mathbb{L}^{-1}}\|\boldsymbol{\varepsilon}(\tilde{\boldsymbol{u}}^i - \boldsymbol{u}_h^i)\|_{\mathbb{L}} \leq \tfrac{\alpha_1}{2}\,\|\mathbf{r}_{\mathrm{d}}(\boldsymbol{u}_h^i, \boldsymbol{\tau}_h^i)\|_{\mathbb{L}^{-1}}^2 + \tfrac{1}{2\,\alpha_1}\|\boldsymbol{\varepsilon}(\tilde{\boldsymbol{u}}^i - \boldsymbol{u}_h^i)\|_{\mathbb{L}}^2$$

The second and third terms are combined and estimated as follows

$$(\mathbf{r}_{\mathrm{eq}}(p_h^i, \boldsymbol{\tau}_h^i), \tilde{\boldsymbol{u}}^i - \boldsymbol{u}_h^i) - (\boldsymbol{\tau}_h^i \cdot \boldsymbol{n}, \tilde{\boldsymbol{u}}^i - \boldsymbol{u}_h^i)_{\Sigma_N^{\boldsymbol{u}}} \leq \tfrac{\alpha_2}{2}\,(C_{\Omega}^{\boldsymbol{u}})^2\,(\|\mathbf{r}_{\mathrm{eq}}(p_h^i, \boldsymbol{\tau}_h^i)\|^2 + \|\boldsymbol{\tau}_h^i \cdot \boldsymbol{n}\|_{\Sigma_N^{\boldsymbol{u}}}^2) + \tfrac{1}{2\,\alpha_2}\|\boldsymbol{\varepsilon}(\tilde{\boldsymbol{u}}^i - \boldsymbol{u}_h^i)\|_{\mathbb{L}}^2$$

where $C_{\Omega}^{\boldsymbol{u}}$ (cf. (5.19)) is a constant in

$$\|\tilde{\boldsymbol{u}}^i - \boldsymbol{u}_h^i\|^2 + \|\tilde{\boldsymbol{u}}^i - \boldsymbol{u}_h^i\|_{\Sigma_N^{\boldsymbol{u}}}^2 \leq (C_{\Omega}^{\boldsymbol{u}})^2\|\boldsymbol{\varepsilon}(\tilde{\boldsymbol{u}}^i - \boldsymbol{u}_h^i)\|_{\mathbb{L}}^2$$

defined through the constants C^{K} and $C_{\Sigma_N^{\boldsymbol{u}}}^{\mathrm{tr}}$ in the Korn and trace inequalities defined in (7.4) and (7.3), respectively. By choosing parameters $\alpha_1 = (\xi + 1)$, $\alpha_2 = (1 + \frac{1}{\xi})$, where $\xi > 0$, we arrive at

$$\|\boldsymbol{\varepsilon}(\tilde{\boldsymbol{u}}^i - \boldsymbol{u}_h^i)\|_{\mathbb{L}} \leq (1+\xi)\,\|\mathbf{r}_{\mathrm{d},\mathbb{L}}(\boldsymbol{u}_h^i, \boldsymbol{\tau}_h^i)\|_{\mathbb{L}^{-1}}^2 + (1+\tfrac{1}{\xi})\,(C_{\Omega}^{\boldsymbol{u}})^2\left(\|\mathbf{r}_{\mathrm{eq}}(p_h^i, \boldsymbol{\tau}_h^i)\|^2 + \|\boldsymbol{\tau}_h^i \cdot \boldsymbol{n}\|_{\Sigma_N^{\boldsymbol{u}}}^2\right). \tag{5.26}$$

Consider now (5.21) and the tensor $\mathbb{L}^{-1}\boldsymbol{\tau}_h^i$ representation through the Lame parameters, i.e.,

$$\mathbb{L}^{-1}\boldsymbol{\tau}_h^i := \tfrac{1}{2\mu}\left(\boldsymbol{\tau}_h^i - \tfrac{\lambda}{3\lambda+2\mu}\mathrm{div}\boldsymbol{\tau}_h^i\mathbb{I}\right).$$

Then, the first term on the right-hand side of (5.26) can be rewritten as

$$\begin{aligned}\mathbb{L}^{-1}\mathbf{r}_{\mathrm{d},\mathbb{L}}(\boldsymbol{u}_h^i, \boldsymbol{\tau}_h^i) : \mathbf{r}_{\mathrm{d},\mathbb{L}}(\boldsymbol{u}_h^i, \boldsymbol{\tau}_h^i) &= \left(\mathbb{L}^{-1}\boldsymbol{\tau}_h^i - \boldsymbol{\varepsilon}(\boldsymbol{u}_h^i)\right) : \left(\boldsymbol{\tau}_h^i - \mathbb{L}\boldsymbol{\varepsilon}(\boldsymbol{u}_h^i)\right) \\ &= 2\,\mu\,|\boldsymbol{\varepsilon}(\boldsymbol{u}_h^i)|^2 + \lambda\,|\mathrm{div}\boldsymbol{u}_h^i|^2 + \tfrac{1}{2\mu}\,(|\boldsymbol{\tau}_h^i|^2 - \tfrac{\lambda}{3\lambda+2\mu}|\mathrm{div}\boldsymbol{\tau}_h^i|^2) - 2\,\boldsymbol{\varepsilon}(\boldsymbol{u}_h^i) : \tau^i =: \mathrm{r}_{\mathrm{d},\mu,\lambda}.\end{aligned} \tag{5.27}$$

Taking the latter into account, we arrive at an alternative estimate

$$\|\boldsymbol{\varepsilon}(\tilde{\boldsymbol{u}}^i - \boldsymbol{u}_h^i)\|_{2\mu}^2 + \|\mathrm{div}(\tilde{\boldsymbol{u}}^i - \boldsymbol{u}_h^i)\|_\lambda^2 \leq (1+\xi)\int_\Omega \mathrm{r}_{\mathrm{d},\mu,\lambda}(\boldsymbol{u}_h^i, \boldsymbol{\tau}_h^i)\mathrm{d}x + (1+\tfrac{1}{\xi})(C_\Omega^u)^2\big(\|\mathbf{r}_{\mathrm{eq}}(p_h^i, \boldsymbol{\tau}_h^i)\|^2 + \|\boldsymbol{\tau}_h^i\cdot\boldsymbol{n}\|_{\Sigma_N^{\boldsymbol{u}}}^2\big), \tag{5.28}$$

where $\mathbf{r}_{\mathrm{d},\mu,\lambda}(\boldsymbol{u}_h^i, \boldsymbol{\tau}_h^i)$ in defined in (5.27) and $\boldsymbol{\tau}_h^i$ is an auxiliary stress approximating function reconstructed with respect to $\boldsymbol{u}_h^i$. □

Remark 9. We note the choice of an auxiliary tensor-function providing the optimal values of the error estimate is $\boldsymbol{\tau}_h^\star := \mathbb{L}\boldsymbol{\varepsilon}(\tilde{\boldsymbol{u}}^i) := 2\,\mu\boldsymbol{\varepsilon}(\tilde{\boldsymbol{u}}^i) + \lambda\mathrm{div}(\tilde{\boldsymbol{u}}^i)\mathbb{I}$. In this case, we can show that the equilibration residual $\mathbf{r}_{\mathrm{eq}}(p_h^i, \boldsymbol{\tau}_h^i)$ vanishes, and the dual one provides the exact representation of the error.

Lemma 5 proceeds with the estimation of $e_{\boldsymbol{u}}^i$ (cf. (5.14)), accounting for the error that arises if (3.5) is replaced by (5.15).

Lemma 5. *For any $p_h^i \in W_0$, any $\boldsymbol{u}_h^i \in \boldsymbol{V_0}$ approximating $\tilde{\boldsymbol{u}}^i$ in (5.15), and any $\boldsymbol{z}_h^i \in H_{\Sigma_N^p}(\Omega, \mathrm{div})$ and $\boldsymbol{\tau}_h^i \in [\mathcal{T}_{\mathrm{Div}}(\Omega)]^{d\times d}$, the estimate*

$$|||\, e_{\boldsymbol{u}}^i \,|||_{\boldsymbol{u}}^2 \leq \overline{\mathrm{M}}_{\boldsymbol{u}}^h((\boldsymbol{u},p)_h^i, (\boldsymbol{\tau},\boldsymbol{z})_h^i) := \tfrac{2\lambda\eta^2\alpha^2}{2\chi\lambda-1}\,\overline{\mathrm{M}}_{p,L^2}^h(p_h^i, \boldsymbol{z}_h^i) + 2\,\overline{\mathrm{M}}_{\tilde{\boldsymbol{u}}}((\boldsymbol{u},p)_h^i, \boldsymbol{\tau}_h^i) \tag{5.29}$$

holds, where $\zeta \geq 0$ and $\chi \in [\frac{1}{2\lambda}, +\infty)$. Here, $\overline{\mathrm{M}}_{p,L^2}$ and $\overline{\mathrm{M}}_{\tilde{\boldsymbol{u}}}$ are defined in (5.12) and (5.17), respectively, and α and λ are the characteristics of the Biot model.

Proof. As noted in (5.16), the error is two-folded and composed from $\|\,\boldsymbol{u}^i - \tilde{\boldsymbol{u}}^i\|_{\boldsymbol{u}}^2$ and $\|\,\tilde{\boldsymbol{u}}^i - \boldsymbol{u}_h^i\,\|_{\boldsymbol{u}}^2$, where the second term is controlled by (5.17) in Lemma 4. The estimate of the first term is derived by considering the difference of (3.5) and (5.15), i.e.,

$$2\mu\,(\boldsymbol{\varepsilon}(\boldsymbol{u}^i - \tilde{\boldsymbol{u}}^i), \boldsymbol{\varepsilon}(\boldsymbol{v})) + \lambda(\mathrm{div}(\boldsymbol{u}^i - \tilde{\boldsymbol{u}}^i), \mathrm{div}\boldsymbol{v}) = -\alpha(p^i - p_h^i, \mathrm{div}\boldsymbol{v}).$$

By choosing $\boldsymbol{v} = \boldsymbol{u}^i - \tilde{\boldsymbol{u}}^i$, we obtain the identity

$$\|\boldsymbol{\varepsilon}(\boldsymbol{u}^i - \tilde{\boldsymbol{u}}^i)\|_{2\mu}^2 + \|\,\mathrm{div}(\boldsymbol{u}^i - \tilde{\boldsymbol{u}}^i)\,\|_\lambda^2 = -\alpha(p^i - p_h^i, \mathrm{div}(\boldsymbol{u}^i - \tilde{\boldsymbol{u}}^i)).$$

The latter can be estimated from above by the Cauchy inequality, which yields

$$\|\boldsymbol{\varepsilon}(e_{\boldsymbol{u}}^i)\|_{2\mu}^2 + \|\,\mathrm{div}(e_{\boldsymbol{u}}^i)\,\|_\lambda^2 \leq \alpha\|e_p^i\|\|\mathrm{div}(e_{\boldsymbol{u}}^i)\|.$$

By using the Young inequality with $\chi \geq \frac{1}{2\lambda}$, we arrive at

$$\|\boldsymbol{\varepsilon}(\boldsymbol{u}^i - \tilde{\boldsymbol{u}}^i)\|_{2\mu}^2 + (\lambda - \tfrac{1}{2\chi})\,\|\,\mathrm{div}(\boldsymbol{u}^i - \tilde{\boldsymbol{u}}^i)\,\|^2 \leq \tfrac{\chi}{2}\alpha^2\|p^i - p_h^i\|^2. \tag{5.30}$$

According to Corollary 2, the linear combination in (5.30) can be estimated as

$$\|\boldsymbol{\varepsilon}(\boldsymbol{u}^i - \tilde{\boldsymbol{u}}^i)\|_{2\mu}^2 + (\lambda - \tfrac{1}{2\chi})\,\|\,\mathrm{div}(\boldsymbol{u}^i - \tilde{\boldsymbol{u}}^i)\,\|^2 \leq \tfrac{\chi\alpha^2}{2}\,\overline{\mathrm{M}}_{p,L^2}(p_h^i).$$

By using

$$\|\boldsymbol{\varepsilon}(\boldsymbol{u}^i - \tilde{\boldsymbol{u}}^i)\|_{2\mu}^2 + \|\,\mathrm{div}(\boldsymbol{u}^i - \tilde{\boldsymbol{u}}^i)\,\|_\lambda^2 \leq \tfrac{2\chi\lambda}{2\chi\lambda-1}\Big(\|\boldsymbol{\varepsilon}(\boldsymbol{u}^i - \tilde{\boldsymbol{u}}^i)\|_{2\mu}^2 + (\lambda - \tfrac{1}{2\chi})\,\|\,\mathrm{div}(\boldsymbol{u}^i - \tilde{\boldsymbol{u}}^i)\,\|^2\Big),$$

we obtain

$$|||\boldsymbol{u}^i - \tilde{\boldsymbol{u}}^i|||_{\boldsymbol{u}}^2 \leq \tfrac{\lambda\chi^2\alpha^2}{2\chi\lambda-1}\,\overline{\mathrm{M}}_{p,L^2}(p_h^i). \tag{5.31}$$

Combining (5.17) and (5.31), we arrive at

$$\|\,\boldsymbol{\varepsilon}(e_{\boldsymbol{u}}^i)\,\|_{2\mu}^2 + \|\,\mathrm{div}(e_{\boldsymbol{u}}^i)\,\|_\lambda^2 \leq \tfrac{2\lambda\chi^2\alpha^2}{2\chi\lambda-1}\,\overline{\mathrm{M}}_{p,L^2}(p_h^i) + 2\,\overline{\mathrm{M}}_{\tilde{u}}(\boldsymbol{u}_h^i, p_h^i). \quad \square \tag{5.32}$$

In addition to (5.17), we can obtain the estimate for the error measured in terms of $\|\mathrm{div}\cdot\|^2$-norm.

Corollary 3. *For any $p_h^i \in W_0$, any $\boldsymbol{u}_h^i \in \boldsymbol{V_0}$ approximating $\tilde{\boldsymbol{u}}^i$ in (5.15), as well as any parameters and functions defined in Lemma 5, we have*

$$\|\,\mathrm{div}(e_{\boldsymbol{u}}^i)\,\|^2 \leq \overline{\mathrm{M}}_{\boldsymbol{u},\mathrm{div}}^h((\boldsymbol{u},p)_h^i, \boldsymbol{\tau}_h^i, \boldsymbol{z}_h^i) := \tfrac{1}{(2\mu\,d+\lambda)}\Big(\tfrac{2\lambda\eta^2\alpha^2}{2\eta\lambda-1}\,\overline{\mathrm{M}}_{p,L^2}(p_h^i, \boldsymbol{z}_h^i) + \overline{\mathrm{M}}_{\tilde{u}}((\boldsymbol{u},p)_h^i, \boldsymbol{\tau}_h^i)\Big), \tag{5.33}$$

where $\overline{\mathrm{M}}_p(p_h^i, \boldsymbol{z}_h^i)$ and $\overline{\mathrm{M}}_{\tilde{u}}((\boldsymbol{u},p)_h^i, \boldsymbol{\tau}_h^i)$ are defined in (5.12) and (5.17) for any $\boldsymbol{z}_h^i \in H_{\Sigma_N^p}(\Omega, \mathrm{div})$ and $\boldsymbol{\tau}_h^i \in [\mathcal{T}_{\mathrm{Div}}(\Omega)]^{d\times d}$, respectively, and μ is a characteristic of the Biot model.

Proof. By using the inequality (7.5) and substituting it in (5.17), we arrive at

$$(2\mu\, d+\lambda)\|\operatorname{div}(e^i_{\boldsymbol{u}})\|^2 \le \overline{\mathrm{M}}_{\boldsymbol{u},\mathrm{div}}(p^i_h, \boldsymbol{z}^i_h;\zeta) = \tfrac{2\lambda\,\eta^2\,\alpha^2}{2\,\eta\,\lambda-1}\,\overline{\mathrm{M}}_{p,L^2}(p^i_h) + 2\,\overline{\mathrm{M}}_{\tilde{u}}((\boldsymbol{u},p)^i_h, \boldsymbol{\tau}^i_h). \quad \square$$

6. Estimates of the errors generated by the iterative method

Next, we consider the guaranteed bounds of errors arising in the process of contractive iterations (3.4)–(3.5) applied to the system (2.7)–(2.8).

Error estimates for the pressure term. First, we confirm the following result for the error in the flow equation, which can be done in two different ways. For Lemma 6, we consider the functions $p^i_h, p^{i-1}_h \in W_0$ as approximations of two consequent pressures associated with the iterations i and $i-1$, whereas $\boldsymbol{u}^i_h, \boldsymbol{u}^{i-1}_h \in \boldsymbol{V_0}$ are the approximations of $\tilde{\boldsymbol{u}}^i$ and $\tilde{\boldsymbol{u}}^{i-1} \in \boldsymbol{V_0}$ in (5.15), respectively. From now on, when we refer to both dual variables $\boldsymbol{z}^i_h$ and $\boldsymbol{\tau}^i_h$ corresponding to the ith iteration step, we refer to them as a pair $(\boldsymbol{\tau},\boldsymbol{z})^i_h$.

Lemma 6. *For $p^i, p^{i-1} \in W_0$ approximating $p \in W_0$ in (2.8), the estimate of the error incorporated in the pressure term at the ith iteration step has the following form*

$$\begin{aligned}\|\!|\, p-p^i \,|\!\|^2_p \le \overline{\mathrm{M}}^{\,i}_p\big((\boldsymbol{u},p)^{i-1}_h,(\boldsymbol{\tau},\boldsymbol{z})^{i-1}_h,(\boldsymbol{u},p)^i_h,(\boldsymbol{\tau},\boldsymbol{z})^i_h\big) := \tfrac{3q}{1-q^2}\left(\tfrac{\left(C^{\mathrm{F}}_{\Sigma^p_D}\right)^2\beta}{\lambda_{\mathbb{K}}\,\tau}+1\right)\Big(\|\eta^i_h-\eta^{i-1}_h\|^2 \\ + \tfrac{\lambda}{2}\left(\overline{\mathrm{M}}^h_{\boldsymbol{u},\mathrm{div}}((\boldsymbol{u},p)^i_h,(\boldsymbol{\tau},\boldsymbol{z})^i_h)+\overline{\mathrm{M}}^h_{\boldsymbol{u},\mathrm{div}}((\boldsymbol{u},p)^{i-1}_h,(\boldsymbol{\tau},\boldsymbol{z})^{i-1}_h)\right) \\ + \tfrac{L}{4}\left(\overline{\mathrm{M}}^h_{p,L^2}(p^i_h,\boldsymbol{z}^i_h)+\overline{\mathrm{M}}^h_{p,L^2}(p^{i-1}_h,\boldsymbol{z}^{i-1})\right)\Big),\end{aligned} \tag{6.1}$$

where $\overline{\mathrm{M}}^h_{\boldsymbol{u},\mathrm{div}}$ and $\overline{\mathrm{M}}^h_{p,L^2}$ are defined in Corollaries 2 and 3 with $\boldsymbol{\tau}^i_h \in [\mathcal{T}_{\mathrm{Div}}(\Omega)]^{d\times d}$ and $\boldsymbol{z}^i_h \in H_{\Sigma^p_N}(\Omega,\mathrm{div})$, respectively, $q=\frac{L}{\beta+L}$, and

$$\eta^i_h = \tfrac{\alpha}{\gamma}\mathrm{div}\boldsymbol{u}^i_h - \tfrac{L}{\gamma}\,p^i_h, \qquad L \ge \tfrac{\alpha^2}{2\lambda}, \qquad \forall p^i_h \in W_0,\ \boldsymbol{u}^i_h \in \boldsymbol{V_0}.$$

Parameters α, β, λ, μ_f, $C^{\mathrm{F}}_{\Sigma^p_D}$, $\lambda_{\mathbb{K}}$, and τ are the characteristics of the semi-discrete Biot model (3.2)–(3.1).

Proof. We begin by noting that for the error $p-p^i$ caused by the iterative scheme, we have the estimate

$$\|\!|\, p-p^i \,|\!\|^2_p = \|\, p-p^i \,\|^2_\beta + \|\,\nabla(p-p^i)\,\|^2_{\mathbb{K}_\tau} \overset{(7.2)}{\le} \left(\tfrac{\left(C^{\mathrm{F}}_{\Sigma^p_D}\right)^2\beta}{\lambda_{\mathbb{K}}\,\tau}+1\right)\|\,\nabla(p-p^i)\,\|^2_{\mathbb{K}_\tau}. \tag{6.2}$$

The estimate of $\|\,\nabla(p-p^i)\,\|^2_{\mathbb{K}_\tau}$ follows from (3.8). To proceed, we need to estimate the right-hand side of (3.8), namely $\|\eta^i-\eta^{i-1}\|^2$. By adding and extracting the discretized approximations η^{i-1}_h and η^i_h, we obtain

$$\|\eta^i-\eta^{i-1}\|^2 \le 3\left(\|\eta^i_h-\eta^{i-1}_h\|^2+\|\eta^i-\eta^i_h\|^2+\|\eta^{i-1}-\eta^{i-1}_h\|^2\right). \tag{6.3}$$

Here, the first term $\|\eta^i_h-\eta^{i-1}_h\|^2$ is fully computable, and by means of the relation

$$\eta^i = \tfrac{1}{\gamma}(\alpha\,\mathrm{div}\boldsymbol{u}^i - Lp^i),$$

we obtain the estimate for the second and third terms:

$$\|\eta^i-\eta^i_h\|^2 \le \tfrac{1}{2\gamma^2}\left(\alpha^2\|\mathrm{div}(e^i_{\boldsymbol{u}})\|^2+L^2\|e^i_p\|^2\right) \overset{(5.12),\,(5.33)}{\le} \tfrac{1}{2\gamma^2}\left(\alpha^2\,\overline{\mathrm{M}}^h_{\boldsymbol{u},\mathrm{div}}(p^i_h)+L^2\,\overline{\mathrm{M}}^h_{p,L^2}(p^i_h)\right).$$

To simplify, we exclude the parameter γ by substituting $\gamma^2=2L$:

$$\|\eta^{i-1}-\eta^{i-1}_h\|^2 \le \tfrac{1}{4L}\left(\alpha^2\,\overline{\mathrm{M}}^h_{\boldsymbol{u},\mathrm{div}}(p^{i-1}_h)+L^2\,\overline{\mathrm{M}}^h_{p,L^2}(p^{i-1}_h)\right). \tag{6.4}$$

Therefore, the estimate of $\|\!|\, p-p^i \,|\!\|^2_p$ can be represented as follows

$$\begin{aligned}\|\!|\, p-p^i \,|\!\|^2_p \le \overline{\mathrm{M}}^{\,i}_p := \left(\tfrac{\left(C^{\mathrm{F}}_{\Sigma^p_D}\right)^2\beta}{\lambda_{\mathbb{K}}\,\tau}+1\right)\tfrac{3q}{1-q^2}\Big\{\|\eta^i_h-\eta^{i-1}_h\|^2 \\ + \tfrac{1}{4L}\Big(\alpha^2\left(\overline{\mathrm{M}}^h_{\boldsymbol{u},\mathrm{div}}(p^i_h)+\overline{\mathrm{M}}^h_{\boldsymbol{u},\mathrm{div}}(p^{i-1}_h)\right)+L^2\left(\overline{\mathrm{M}}^h_{p,L^2}(p^i_h)+\overline{\mathrm{M}}^h_{p,L^2}(p^{i-1}_h)\right)\Big)\Big\}.\end{aligned} \tag{6.5}$$

Finally, by substituting $\lambda=\frac{\alpha^2}{2L}$ in (6.5), we arrive at (6.1). $\square$

Corollary 4. *Let the conditions of Lemmas 2 and 6 hold. Then, for $1 \le m \le i$, the estimate of the error incorporated in the pressure term on the ith iteration step has an alternative form*

$$\begin{aligned}\| p - p^i \|_p^2 \le \overline{\mathrm{M}}_p^{i,m}\big((\boldsymbol{u},p)_h^{i-m},(\boldsymbol{\tau},\boldsymbol{z})_h^{i-m},(\boldsymbol{u},p)_h^{i},(\boldsymbol{\tau},\boldsymbol{z})_h^{i}\big) := \tfrac{3q^m}{1-q^{2m}}\left(\tfrac{\left(C^{\mathrm{F}}_{\Sigma_D^p}\right)^2\beta}{\lambda_{\mathbb{K}}\,\tau}+1\right)\Big(\,\|\eta_h^i-\eta_h^{i-m}\|^2\\ +\tfrac{\lambda}{2}\left(\overline{\mathrm{M}}^h_{\boldsymbol{u},\mathrm{div}}((\boldsymbol{u},p)_h^i,(\boldsymbol{\tau},\boldsymbol{z})_h^i)+\overline{\mathrm{M}}^h_{\boldsymbol{u},\mathrm{div}}((\boldsymbol{u},p)_h^{i-m},(\boldsymbol{\tau},\boldsymbol{z})_h^{i-m})\right)\\ +\tfrac{L}{4}\left(\overline{\mathrm{M}}^h_{p,L^2}(p_h^i,\boldsymbol{z}_h^i)+\overline{\mathrm{M}}^h_{p,L^2}(p_h^{i-m},\boldsymbol{z}^{i-m})\right)\Big).\end{aligned} \tag{6.6}$$

Alternatively, the norm on the left-hand side of (6.3) can be estimated by the contractive estimate, which results in an alternative error bound independent of functional majorants. This result is presented below.

Lemma 7. *For any $p^i \in W_0$ approximating $p \in W_0$ in (2.8), the estimate of the error incorporated in the pressure term at the ith iteration step has the following form*

$$\begin{aligned}\| p - p^i \|_p^2 \le \widetilde{\mathrm{M}}_p^i(\eta_h^1,\eta_h^0) := \left(\tfrac{\left(C^{\mathrm{F}}_{\Sigma_D^p}\right)^2\beta}{\lambda_{\mathbb{K}}\,\tau}+1\right)\tfrac{3q^{2i-1}}{1-q^2}\\ \Big(\tfrac{\alpha^2}{\gamma^2}\overline{\mathrm{M}}^h_{p,L^2}(p_h^1)+\tfrac{L^2}{\gamma^2}\,\overline{\mathrm{M}}^h_{\boldsymbol{u},\mathrm{div}}((\boldsymbol{u},p)_h^1)+\|\eta^0-\eta_h^0\|^2+\|\eta_h^1-\eta_h^0\|^2\Big),\end{aligned} \tag{6.7}$$

where

$$q=\tfrac{L}{\beta+L},\qquad \eta_h^i=\tfrac{\alpha}{\gamma}\mathrm{div}\boldsymbol{u}_h^i-\tfrac{L}{\gamma}\,p_h^i,\qquad L\ge\tfrac{\alpha^2}{2\lambda},\qquad \forall p_h^i\in W_{0h},\ \boldsymbol{u}_h^i\in\boldsymbol{V}_{\boldsymbol{0h}},$$

and $\overline{\mathrm{M}}^h_{\boldsymbol{u},\mathrm{div}}$ and $\overline{\mathrm{M}}^h_{p,L^2}$ are defined in Corollaries 2 and 3. Parameters α, β, λ, μ_f, $C^{\mathrm{F}}_{\Sigma_D^p}$, $\lambda_{\mathbb{K}}$, and τ are the characteristics of the semi-discrete Biot model (3.1)–(3.2).

Proof. We use the inequality (6.2), to obtain

$$\| p - p^i \|_p^2 \le \left(\tfrac{(C^{\mathrm{F}}_{\Sigma_D^p})^2\beta}{\lambda_{\mathbb{K}}\,\tau}+1\right)\tfrac{q}{1-q^2}\,\|\eta^i-\eta^{i-1}\|^2. \tag{6.8}$$

However, in this proof, we use a priori estimates for the sequence $\{\delta\eta^i\}$ to obtain

$$\|\eta^i-\eta^{i-1}\|^2 \le q^{2(i-1)}\,\|\eta^1-\eta^0\|^2 \le q^{2(i-1)}\,(3\|\eta^1-\eta_h^1\|^2+3\|\eta^0-\eta^0\|^2+3\|\eta_h^1-\eta_h^0\|^2), \tag{6.9}$$

where all terms on the right-hand side except $\|\eta^1-\eta_h^1\|^2$ are computable. As in Lemma 3, $\|\eta^1-\eta_h^1\|^2$ is controlled by the combination of $\overline{\mathrm{M}}^h_{p,L^2}(p_h^1,\boldsymbol{z}_h^1;\zeta)$ and $\overline{\mathrm{M}}^h_{\boldsymbol{u},\mathrm{div}}((\boldsymbol{u},p)_h^1,\boldsymbol{\tau}_h^1,\boldsymbol{z}_h^1)$, i.e.,

$$\|\eta^1-\eta_h^1\|^2 \le \frac{\alpha^2}{\gamma^2}\,\|\,\mathrm{div}(\boldsymbol{u}^1-\boldsymbol{u}_h^1)\,\|^2+\frac{L^2}{\gamma^2}\,\|\,p^1-p_h^1\,\|^2 \le \frac{\alpha^2}{\gamma^2}\overline{\mathrm{M}}^h_{p,L^2}(p_h^1,\boldsymbol{z}_h^1;\zeta)+\frac{L^2}{\gamma^2}\,\overline{\mathrm{M}}^h_{\boldsymbol{u},\mathrm{div}}((\boldsymbol{u},p)_h^1,\boldsymbol{\tau}_h^1,\boldsymbol{z}_h^1), \tag{6.10}$$

where the right-hand side contains a computable $\eta^0 := \frac{\alpha}{\gamma}\mathrm{div}\boldsymbol{u}^0-\frac{L}{\gamma}\,p^0$. Combining (6.8), (6.9), and (6.10), we arrive at

$$\| p - p^i \|_p^2 \le \left(\tfrac{(C^{\mathrm{F}}_{\Sigma_D^p})^2\beta}{\lambda_{\mathbb{K}}\,\tau}+1\right)\tfrac{3q^{2i-1}}{1-q^2}\left(\tfrac{\alpha^2}{\gamma^2}\overline{\mathrm{M}}^h_{p,L^2}(p_h^1)+\tfrac{L^2}{\gamma^2}\,\overline{\mathrm{M}}^h_{\boldsymbol{u},\mathrm{div}}((\boldsymbol{u},p)_h^1)+\,\|\eta^0-\eta_h^0\|^2+\|\eta_h^1-\eta_h^0\|^2\right).\quad\square$$

Error estimates for the displacement term. To derive the upper bound for the error $\boldsymbol{u}-\boldsymbol{u}^i$ measured in terms of

$$\|\,\boldsymbol{u}-\boldsymbol{u}^i\,\|_{\boldsymbol{u}}^2 := \|\,\boldsymbol{\varepsilon}(\boldsymbol{u}-\boldsymbol{u}^i)\,\|_{2\mu}^2+\|\,\mathrm{div}(\boldsymbol{u}-\boldsymbol{u}^i)\,\|_{\lambda}^2, \tag{6.11}$$

we draw on the idea similar to the one used to estimate the error in the pressure term.

Lemma 8. *For any $\boldsymbol{u}^i,\boldsymbol{u}^{i-1}\in\boldsymbol{V_0}$ approximating $\boldsymbol{u}\in\boldsymbol{V_0}$ in (2.7), the error in the displacement at the ith iteration step has the following form*

$$\begin{aligned}\|\,\boldsymbol{u}-\boldsymbol{u}^i\,\|_{\boldsymbol{u}}^2 \le \overline{\mathrm{M}}^i_{\boldsymbol{u}}\big((\boldsymbol{u},p)_h^{i-1},(\boldsymbol{\tau},\boldsymbol{z})_h^{i-1},(\boldsymbol{u},p)_h^{i},(\boldsymbol{\tau},\boldsymbol{z})_h^{i}\big) := (1+\tfrac{d\,\lambda}{2\mu})\tfrac{3q^2}{1-q^2}\Big(\,\|\eta_h^i-\eta_h^{i-1}\|\\ +\tfrac{\lambda}{2}\left(\overline{\mathrm{M}}^h_{\boldsymbol{u},\mathrm{div}}((\boldsymbol{u},p)_h^i,(\boldsymbol{\tau},\boldsymbol{z})_h^i)+\overline{\mathrm{M}}^h_{\boldsymbol{u},\mathrm{div}}((\boldsymbol{u},p)_h^{i-1},(\boldsymbol{\tau},\boldsymbol{z})_h^{i-1})\right)\\ +\tfrac{L}{4}\left(\overline{\mathrm{M}}^h_{p,L^2}(p_h^i,\boldsymbol{z}_h^i)+\overline{\mathrm{M}}^h_{p,L^2}(p_h^{i-1},\boldsymbol{z}^{i-1})\right)\Big),\end{aligned} \tag{6.12}$$

where $\overline{\mathrm{M}}^h_{\boldsymbol{u},\mathrm{div}}$ *and* $\overline{\mathrm{M}}^h_{p,L^2}$ *are defined in Corollaries 2 and 3 for* $\boldsymbol{z}^i_h, \boldsymbol{z}^{i-1}_h \in H_{\Sigma^p_N}(\Omega, \mathrm{div})$ *and* $\boldsymbol{\tau}^i_h, \boldsymbol{\tau}^{i-1}_h \in [\mathcal{T}_{\mathrm{Div}}(\Omega)]^{d\times d}$*, respectively,* $q = \frac{L}{\beta+L}$*, and*

$$\eta^i_h = \tfrac{\alpha}{\gamma}\mathrm{div}\boldsymbol{u}^i_h - \tfrac{L}{\gamma}\, p^i_h, \qquad L = \tfrac{\alpha^2}{2\lambda}, \qquad \forall p^i_h \in W_0,\ \boldsymbol{u}^i_h \in \boldsymbol{V_0}.$$

Parameters λ*,* μ*,* α *are the characteristics of the Biot model.*

Proof. We consider

$$|\!|\!| \boldsymbol{u} - \boldsymbol{u}^i |\!|\!|^2_{\boldsymbol{u}} \le \big(2\mu + d\,\lambda\big)\, \|\, \boldsymbol{\varepsilon}(e_{\boldsymbol{u}})\, \|^2, \tag{6.13}$$

where the right-hand side is controlled by the contractive term $\|\eta - \eta^i\|^2$, which follows from (3.9). Therefore, we obtain

$$\begin{aligned} |\!|\!| \boldsymbol{u} - \boldsymbol{u}^i |\!|\!|^2_{\boldsymbol{u}} &\le \tfrac{2\mu+d\lambda}{2\mu}\tfrac{q^2}{1-q^2}\|\eta^i - \eta^{i-1}\|^2 \\ &\le \tfrac{2\mu+d\lambda}{2\mu}\tfrac{3q^2}{1-q^2}\big(\|\eta^i - \eta^i_h\|^2 + \|\eta^{i-1} - \eta^{i-1}_h\|^2 + \|\eta^i_h - \eta^{i-1}_h\|^2\big). \end{aligned} \tag{6.14}$$

Similar to the proof of Lemma 6 (cf. (6.4)), the estimate for the second term in (6.14) results in

$$\begin{aligned} |\!|\!| \boldsymbol{u} - \boldsymbol{u}^i |\!|\!|^2_{\boldsymbol{u}} \le \overline{\mathrm{M}}^i_{\boldsymbol{u}} := \big(1 + \tfrac{d\lambda}{2\mu}\big)\tfrac{3q^2}{1-q^2}\Big(&\|\eta^i_h - \eta^{i-1}_h\| \\ &+ \tfrac{1}{4L}\Big(\alpha^2\big(\overline{\mathrm{M}}^h_{\boldsymbol{u},\mathrm{div}}(p^i_h, \boldsymbol{z}^i_h) + \overline{\mathrm{M}}^h_{\boldsymbol{u},\mathrm{div}}(p^{i-1}_h, \boldsymbol{z}^{i-1})\big) + L^2\big(\overline{\mathrm{M}}^h_{p,L^2}(p^i_h, \boldsymbol{z}^i_h) + \overline{\mathrm{M}}^h_{p,L^2}(p^{i-1}_h, \boldsymbol{z}^{i-1})\big)\Big)\Big). \end{aligned} \tag{6.15}$$

Again, by substituting $\lambda = \frac{\alpha^2}{2L}$ in (6.15), we arrive at (6.12)). □

Corollary 5. *Let the conditions of Lemmas 2 and 8 hold. Then, for* $1 \le m \le i$*, the error in the displacement at the ith iteration step has an alternative form*

$$\begin{aligned} |\!|\!| \boldsymbol{u} - \boldsymbol{u}^i |\!|\!|^2_{\boldsymbol{u}} \le \overline{\mathrm{M}}^{i,m}_{\boldsymbol{u}}\big((\boldsymbol{u},p)^{i-m}_h, (\boldsymbol{\tau},\boldsymbol{z})^{i-m}_h, (\boldsymbol{u},p)^i_h, (\boldsymbol{\tau},\boldsymbol{z})^i_h\big) := \big(1 + \tfrac{d\lambda}{2\mu}\big)\tfrac{3q^{2m}}{1-q^{2m}}\Big(&\|\eta^i_h - \eta^{i-m}_h\| \\ &+ \tfrac{\lambda}{2}\big(\overline{\mathrm{M}}^h_{\boldsymbol{u},\mathrm{div}}((\boldsymbol{u},p)^i_h, (\boldsymbol{\tau},\boldsymbol{z})^i_h) + \overline{\mathrm{M}}^h_{\boldsymbol{u},\mathrm{div}}((\boldsymbol{u},p)^{i-m}_h, (\boldsymbol{\tau},\boldsymbol{z})^{i-m}_h)\big) \\ &+ \tfrac{L}{4}\big(\overline{\mathrm{M}}^h_{p,L^2}(p^i_h, \boldsymbol{z}^i_h) + \overline{\mathrm{M}}^h_{p,L^2}(p^{i-m}_h, \boldsymbol{z}^{i-m})\big)\Big). \end{aligned} \tag{6.16}$$

Analogously, we can use contraction properties to derive an alternative bound of the error $\boldsymbol{u} - \boldsymbol{u}^i$.

Lemma 9. *For any* $\boldsymbol{u}^i \in \boldsymbol{V_0}$ *approximating* $\boldsymbol{u} \in \boldsymbol{V_0}$ *in (2.7), the error in the displacement at the ith iteration step has the following form*

$$|\!|\!| \boldsymbol{u} - \boldsymbol{u}^i |\!|\!|^2_{\boldsymbol{u}} \le \widetilde{\mathrm{M}}^i_{\boldsymbol{u}}\big(\eta^1_h, \eta^0_h\big) := \tfrac{2\mu+d\lambda}{2\mu}\tfrac{3q^{2i}}{1-q^2}\Big(\frac{\alpha^2}{\gamma^2}\overline{\mathrm{M}}^h_{p,L^2}(p^1_h) + \frac{L^2}{\gamma^2}\,\overline{\mathrm{M}}^h_{\boldsymbol{u},\mathrm{div}}((\boldsymbol{u},p)^1_h) + \|\eta^0 - \eta^0_h\|^2 + \|\eta^1_h - \eta^0_h\|^2\Big), \tag{6.17}$$

where

$$q = \tfrac{L}{\beta+L}, \qquad \eta^i_h = \tfrac{\alpha}{\gamma}\mathrm{div}\boldsymbol{u}^i_h - \tfrac{L}{\gamma}\, p^i_h, \qquad L = \tfrac{\alpha^2}{2\lambda}, \qquad \forall p^i_h \in W_0,\ \boldsymbol{u}^i_h \in \boldsymbol{V_0},$$

and $\overline{\mathrm{M}}^h_{\boldsymbol{u},\mathrm{div}}$ *and* $\overline{\mathrm{M}}^h_{p,L^2}$ *are defined in Corollaries 2 and 3. Parameters* λ*,* μ*,* α *are the characteristics of the Biot model.*

Proof. The derivation consists of combining $|\!|\!| \boldsymbol{u} - \boldsymbol{u}^i |\!|\!|^2_{\boldsymbol{u}} \le \tfrac{2\mu+d\lambda}{2\mu}\tfrac{q^2}{1-q^2}\|\eta^i - \eta^{i-1}\|^2$, (6.9), and (6.10). □

General estimate of the error in the iterative coupling scheme. To derive a reliable estimate of the error in the pressure approximation reconstructed at the *i*th iteration, we combine two different approaches, i.e., estimates for contractive mapping used for iterative methods and functional error estimates. Theorem 3 presents an upper bound of the error in the pressure term, which combines the above-mentioned approaches.

Theorem 3. *For any* $p^i_h \in W_0$ *and* $\boldsymbol{u}^i_h \in \boldsymbol{V_0}$ *that form a contraction relative to* $p^{i-1}_h \in W_0$ *and* $\boldsymbol{u}^{i-1}_h \in \boldsymbol{V_0}$*, we have the estimates*

$$\begin{aligned} |\!|\!| e_p |\!|\!|^2_p &\le \overline{\mathrm{M}}_p := 2\left(\overline{\mathrm{M}}^h_p(p^i_h, \boldsymbol{z}^i_h) + \min\left\{\overline{\mathrm{M}}^i_p, \overline{\mathrm{M}}^{i,m}_p, \widetilde{\mathrm{M}}^i_p\right\}\right), \\ |\!|\!| e_{\boldsymbol{u}} |\!|\!|^2_{\boldsymbol{u}} &\le \overline{\mathrm{M}}_{\boldsymbol{u}} := 2\left(\overline{\mathrm{M}}^h_{\boldsymbol{u}}\big((\boldsymbol{u},p)^i_h, (\boldsymbol{\tau},\boldsymbol{z})^i_h\big) + \min\left\{\overline{\mathrm{M}}^i_{\boldsymbol{u}}, \overline{\mathrm{M}}^{i,m}_{\boldsymbol{u}}, \widetilde{\mathrm{M}}^i_{\boldsymbol{u}}\right\}\right). \end{aligned}$$

Here, $\overline{\mathrm{M}}^h_p$*,* $\overline{\mathrm{M}}^i_p$*,* $\overline{\mathrm{M}}^{i,m}_p$*, and* $\widetilde{\mathrm{M}}^i_p$ *are defined in Lemmas 3, 6, Corollary 4, and Lemma 7, whereas* $\overline{\mathrm{M}}^h_{\boldsymbol{u}}$*,* $\overline{\mathrm{M}}^i_{\boldsymbol{u}}$*,* $\overline{\mathrm{M}}^{i,m}_{\boldsymbol{u}}$*, and* $\widetilde{\mathrm{M}}^i_{\boldsymbol{u}}$ *are presented by Lemmas 5, 8, Corollary 5, and Lemma 9, respectively, where* $p^{i-1}_h \in W_0$*,* $\boldsymbol{u}^{i-1}_h \in \boldsymbol{V_0}$*,* $\boldsymbol{z}^i_h, \boldsymbol{z}^{i-1} \in H_{\Sigma^p_N}(\Omega, \mathrm{div})$*,* $\boldsymbol{\tau}^i_h, \boldsymbol{\tau}^{i-1} \in [\mathcal{T}_{\mathrm{Div}}(\Omega)]^{d\times d}$*, and the parameter* $\zeta \ge 0$*.*

Proof. To decompose the error $|||\, e_p \,|||_p^2$ into two parts, we apply the triangle inequality

$$|||\, e_p \,|||_p^2 = |||\, p - p_h^i \,|||_p^2 \leq 2\left(|||\, p - p^i \,|||_p^2 + |||\, p^i - p_h^i \,|||_p^2\right). \tag{6.18}$$

The first term on the right-hand side of (6.18) is bounded by (6.1) from Lemma 6, whereas the second term is controlled by (5.2) from Lemma 3. Analogously, using the triangle rule, we obtain

$$|||\, e_{\boldsymbol{u}} \,|||_{\boldsymbol{u}}^2 = |||\, \boldsymbol{u} - \boldsymbol{u}_h^i \,|||_{\boldsymbol{u}}^2 \leq 2\left(|||\, \boldsymbol{u} - \boldsymbol{u}^i \,|||_{\boldsymbol{u}}^2 + |||\, \boldsymbol{u}^i - \boldsymbol{u}_h^i \,|||_{\boldsymbol{u}}^2\right). \tag{6.19}$$

The first term on the right-hand side of (6.19) is controlled by (6.12), (6.16), or (6.17), whereas the estimate of the second term follows from (5.17). □

7. Numerical examples

Numerical properties of the estimates above are explained in the following series of examples. We consider three tests with manufactured solutions for pressure and displacement. First two tests correspond to different values of the contraction parameter q in the fixed-stress scheme and study the efficiency of error estimators. For both of them, we consider the material properties (permeability, the Lame coefficients, etc.) that are more academic as well as more realistic. The third test (with non-polynomial exact solutions) is considered in order to exclude the effect of the super-convergence while testing the numerical scheme. We solve the Biot model at each moment in time, using the fixed-stress scheme by choosing different mesh sizes and time steps. Moreover, we vary finite element pairs used for solving the variational problem. All these alterations, including material properties, discretization parameters, and the finite element pairs, allow us to study the performance of the estimators and show their robustness. Besides, the first and third examples include the comparison of the CPU cost needed to solve (3.4)–(3.5) for pressure and displacement and of the time effort spend on the reliable error control for each variable.

In each test below, we study the convergence of the numerical scheme applied to the solver (3.4)–(3.5) for chosen discretization time step and spatial mesh size. The errors are computed by employing different norms, the total error norm, including the pair of unknowns, as well as the individual ones in both L^2 and the energy norms. We fix the number of fixed-stress iterations to study the convergence. The majorants $\overline{\mathrm{M}}_p^h$ and $\overline{\mathrm{M}}_u^h$ are either directly computed or minimized w.r.t. to the auxiliary functions. To characterize the efficiency of all above-mentioned error estimators, we use a so-called efficiency index defined as $I_{\mathrm{eff}} := \overline{\mathrm{M}}/|||e|||^2$, where $\overline{\mathrm{M}}$ is a chosen majorant and $|||e|||^2$ is the error measured in the corresponding norm. We study individual contributions of different terms to the majorants, namely of the dual term and the reliability/equilibration term. We demonstrate that the first one provides quantitatively efficient error indicators, whereas the small contribution of the second one ensures the reliability of total error bounds. We also highlight the contributor of iterative majorants $\overline{\mathrm{M}}_p^i$ and $\overline{\mathrm{M}}_p^{i,m}$ into the total error bounds for various ranges of contraction parameter q. In particular, the second example considers a set of parameters resulting in q close to 1 and highlights the quantitative improvement of the total error bound when $\overline{\mathrm{M}}_p^{i,m}$ is used instead of $\overline{\mathrm{M}}_p^i$.

For the readers' convenience, the time steps below are stated in seconds [s], and the spatial discretization steps are measured in meters [m]. We also assume that $\Omega := (0,1)^2 \in \mathbb{R}^2$, $T = 10$ throughout all the examples.

Example 1. Verification of majorants' properties on simple manufactured solution (w.r.t. two different sets of parameters). First, we consider an example with polynomial manufactured solution, in which we clarify the process of both discretization and iterative error estimates calculation as well as highlight the most important properties of the introduced majorants. Therefore, we start with relatively simple material parameters that will be changed at the end of the example to test more realistic scenarios.

Let the exact solution of (1.1) be defined as

$$\boldsymbol{u}(x,y,t) := t\,x(1-x)\,y(1-y)\,[1,1]^{\mathrm{T}} \quad \text{and} \quad p(x,y,t) := t\,x(1-x)\,y(1-y).$$

The Lame parameters are $\mu = \lambda_{\mathrm{vol}} = 1$, which leads to $\lambda_{\mathrm{plane}} = \frac{2\,\lambda_{\mathrm{vol}}\,\mu}{\lambda_{\mathrm{vol}}+2\,\mu} = \frac{2}{3}$. We set $\alpha = \beta = 1$, $C_{\mathrm{F}} = \frac{1}{\sqrt{2}\,\pi}$, and $\mathbb{K}$ [mD/cP] is a unit tensor. From the parameters above, it follows that $L = \frac{\alpha^2}{2(\lambda+2\mu/d)} = 0.3$ and $q = \frac{L}{\beta+L} = \frac{3}{13} \approx 0.23077$. Taking into account that the error estimates depend on the term $\frac{q^2}{(1-q^2)}$, which goes to infinity as q goes to 1, the efficiency of the resulting $\overline{\mathrm{M}}_{\boldsymbol{u}}$ and $\overline{\mathrm{M}}_p$ drastically depends on the value of q. In this particular example, the ratio $\frac{q^2}{(1-q^2)} = 0.05625$ is relatively small, which prevents $\overline{\mathrm{M}}_{\boldsymbol{u}}^i$ and $\overline{\mathrm{M}}_p^i$ overestimating the errors.

We start with discretization by 10 time steps (where the total number of steps in time is denoted by N) with corresponding size of the step $\tau = 1.0$ and spatial mesh-size $h = \frac{1}{64}$ using standard $\mathbb{P}_1$ (polynomial/Lagrangian first-order) finite elements (see (7.7)). Let I denote the number of iterations to solve (3.4)–(3.5) on each time-step; we consider $I = 5$ for this discretization. Table 1 illustrates the convergence of the errors in $\boldsymbol{u}$ and p w.r.t. the iteration steps $i = 1, \ldots, I$ for the time-interval $[t_9, t_{10}] = [9.0, 10.0]$. We note here, that the study of the dependence of the iteration number on discretization parameters is beyond the scope of this paper. Therefore, in all discussed numerical tests, I is constant.

Table 1
Example 1 (Academic parameters). Errors and majorants at the time step $[t_9, t_{10}]$, $\tau = 1.0$, for $h = \frac{1}{64}$, and $I = 5$. The values are measured w.r.t. the increment in $\|p\|_p^2$ and $\|\boldsymbol{u}\|_{\boldsymbol{u}}^2$.

$i = 1, \dots, I$	$\|e_p\|^2$	$\overline{\mathrm{M}}_p^h$	$\|e_p\|_\beta^2$	$\overline{\mathrm{M}}_{p,L^2}^h$	$\|e_{\boldsymbol{u}}\|^2$	$\overline{\mathrm{M}}_{\boldsymbol{u}}^h$	$\|\mathrm{dive}_{\boldsymbol{u}}\|_\lambda^2$	$\overline{\mathrm{M}}_{\boldsymbol{u},\mathrm{div}}^h$
2	1.87e−04	1.87e−04	4.77e−09	8.90e−06	1.86e−04	4.95e−04	4.45e−05	1.06e−04
4	1.87e−04	1.87e−04	2.04e−09	8.90e−06	1.86e−04	4.95e−04	4.45e−05	1.06e−04
5	1.87e−04	1.87e−04	2.04e−09	8.90e−06	1.86e−04	4.95e−04	4.45e−05	1.06e−04

Table 2
Example 1 (Academic parameters). Decrease of the values of ζ and $\overline{\mathrm{M}}_p^h$, as well as the terms $\overline{\mathrm{m}}_{\mathrm{d}}^2$ and $\overline{\mathrm{m}}_{\mathrm{eq}}^2$ that the majorant contains, w.r.t. the number of optimization cycles.

optimization step	ζ	$\|\!\|\!\|e_p\|\!\|\!\|^2$	$\overline{\mathrm{M}}_p^h$	$\overline{\mathrm{m}}_{\mathrm{d}}^2$	$\overline{\mathrm{m}}_{\mathrm{eq}}^2$	$I_{\mathrm{eff}} := \overline{\mathrm{M}}_p^h / \|\!\|\!\|e_p\|\!\|\!\|^2$
0	0.4359	1.87e-04	4.55e-04	1.87e-04	8.06e-05	1.5589
1	0.0045	1.87e-04	2.69e-04	1.87e-04	1.53e-08	1.1983
2	0.0002	1.87e-04	1.88e-04	1.87e-04	1.67e-08	1.0023

The values of $\overline{\mathrm{M}}_p^h$ and $\overline{\mathrm{M}}_{\boldsymbol{u}}^h$ are obtained by minimizing each functional w.r.t. to the auxiliary functions. For instance, the functional estimate to control the error in the variable p

$$\overline{\mathrm{M}}_p^h(p_h^i, \boldsymbol{z}_h^i; \zeta) := (1+\zeta)\,\|\mathbf{r}_{\mathrm{d}}(p_h^i, \boldsymbol{z}_h^i)\|_{\mathbb{K}_\tau^{-1}}^2 + (1+\tfrac{1}{\zeta})\,C_\Omega^p \Big(2\,\|\mathbf{r}_{\mathrm{eq}}(p_h^i, \boldsymbol{z}_h^i)\|_\Omega^2 + 2\,\gamma^2\,q^{2(i-1)}\,\|\eta^0 - \eta_h^0\|^2 + \|\boldsymbol{z}_h^i \cdot \boldsymbol{n}\|_{\Sigma_N^p}^2\Big) \quad (7.1)$$

is minimized w.r.t. the function $\boldsymbol{z}_h^i$ and parameter ζ. The results of this optimization procedure are listed in Table 2. We see that only two iterations are enough to achieve a good efficiency $I_{\mathrm{eff}} := \overline{\mathrm{M}}_p^h / \|\!\|\!\|e_p\|\!\|\!\|^2 = 1.0023$. Table 2 illustrates the decrease of the dual term $\overline{\mathrm{m}}_{\mathrm{d}}^2 := \|\mathbf{r}_{\mathrm{d}}(p_h^i, \boldsymbol{z}_h^i)\|_{\mathbb{K}_\tau^{-1}}^2 = \|\boldsymbol{z}_h^i - \mathbb{K}_\tau \nabla p_h^i\|_{\mathbb{K}_\tau^{-1}}^2$ and the reliability/equilibration term of the majorant $\overline{\mathrm{m}}_{\mathrm{eq}}^2 := \|\mathbf{r}_{\mathrm{eq}}(p_h^i, \boldsymbol{z}_h^i)\|_\Omega^2 = \|\widetilde{g} - \gamma\,\eta_h^{i-1} - (\beta + L)\,p_h^i + \mathrm{div}\boldsymbol{z}_h^i\|_\Omega^2$. In order to achieve the desired efficiency of the error estimate, the reliability term must be several orders of magnitude smaller than the dual one, which holds in this case.

Instead of minimizing the functional $\overline{\mathrm{M}}_{\boldsymbol{u}}^h$, we apply a post-processing of the function $\bar{\boldsymbol{u}}_h^i := P(\boldsymbol{u}_h^i)$, and then substitute it to approximate the auxiliary function $\boldsymbol{\tau}_h^i = \mathbb{L}\,\boldsymbol{\varepsilon}(\bar{\boldsymbol{u}}_h^i)$. This yields a sufficiently efficiency index in the range $2-6$, while saving computational effort otherwise associated with calculating the minimizer of $\overline{\mathrm{M}}_{\boldsymbol{u}}^h$. In this example, we observe that the terms $\overline{\mathrm{m}}_{\mathrm{d},\mathbb{K}}^2$ and $\overline{\mathrm{m}}_{\mathrm{d},\lambda,\mu}^2$ become rather close to the true errors $\|\!\|\!\|e_p\|\!\|\!\|^2$ and $\|\!\|\!\|e_{\boldsymbol{u}}\|\!\|\!\|^2$, respectively, and can be used as error indicators for the local error distribution over the computational domain. To confirm that, Fig. 1 presents the distribution of errors and indicators (generated by majorants) w.r.t. numbered finite element cells. On the right side of Fig. 1, we depict $\|\!\|\!\|e_p\|\!\|\!\|^2$ and $\overline{\mathrm{m}}_{\mathrm{d},\mathbb{K}}^2 := \|\mathbf{r}_{d,\mathbb{K}}(p_h^i, \boldsymbol{z}_h^i)\|^2$ and on the left side $\|\!\|\!\|e_{\boldsymbol{u}}\|\!\|\!\|^2$ and the indicator $\overline{\mathrm{m}}_{\mathrm{d},\mu,\lambda}^2 := \|\mathbf{r}_{d,\mu,\lambda}(\boldsymbol{u}_h^i, \boldsymbol{\tau}_h^i)\|^2$ w.r.t. numbered finite element cells. Green marker depicts the error and red color represents the majorant values. We see that the indicator produces a quantitatively efficient error. First, let us assume that the error bounds $\overline{\mathrm{M}}_p^h$ and $\overline{\mathrm{M}}_{p,L^2}^h$, as well as $\overline{\mathrm{M}}_{\boldsymbol{u}}^h$ and $\overline{\mathrm{M}}_{\boldsymbol{u},\mathrm{div}}^h$ are reconstructed only at the 4th and 5th steps to calculate $\overline{\mathrm{M}}_{\boldsymbol{u}}^i$ and $\overline{\mathrm{M}}_p^i$ for $i = 5$ (using (6.1) and (6.12)). Let $\|\!\|\!\|e_p^{(n)}\|\!\|\!\|^2$ and $\|\!\|\!\|e_{\boldsymbol{u}}^{(n)}\|\!\|\!\|^2$, $n = 1, \dots, N$ correspond to the error increments at the nth time-step. The contribution of the majorants for discretization errors and the iterative majorant at the Nth time step is of the same magnitude, i.e.,

$$\overline{\mathrm{M}}_p^{h,(N)} = 1.87\mathrm{e}{-04}, \quad \overline{\mathrm{M}}_p^{i,(N)} = 3.05\mathrm{e}{-04}, \quad \overline{\mathrm{M}}_{\boldsymbol{u}}^{h,(N)} = 4.95\mathrm{e}{-04}, \quad \overline{\mathrm{M}}_{\boldsymbol{u}}^{i,(N)} = 3.20\mathrm{e}{-05}.$$

Then, the Nth increment of both total errors and the corresponding majorants for pressure and displacement, respectively, is as follows:

$$\|\!\|\!\|e_p^{(N)}\|\!\|\!\|^2 = 4.86\mathrm{e}{-05}, \quad \overline{\mathrm{M}}_p^{(N)} = 2.56\mathrm{e}{-04}, \quad I_{\mathrm{eff}}(\overline{\mathrm{M}}_p^{(N)}) = 2.29 \quad \text{and}$$
$$\|\!\|\!\|e_{\boldsymbol{u}}^{(N)}\|\!\|\!\|^2 = 4.85\mathrm{e}{-05}, \quad \overline{\mathrm{M}}_{\boldsymbol{u}}^{(N)} = 2.74\mathrm{e}{-04}, \quad I_{\mathrm{eff}}(\overline{\mathrm{M}}_{\boldsymbol{u}}^{(N)}) = 2.38.$$

This makes the general error, majorant, and the corresponding efficiency index contributions to be the following

$$[(e_{\boldsymbol{u}}^{(N)}, e_p^{(N)})]^2 = 4.85\mathrm{e}{-04}, \quad \overline{\mathrm{M}}^{(N)} = 9.99\mathrm{e}{-05}, \quad I_{\mathrm{eff}}(\overline{\mathrm{M}}^{(N)}) = 2.36.$$

If instead of the 4th and 5th iterations we use 2nd and 5th ones to compute $\overline{\mathrm{M}}_{\boldsymbol{u}}^{i,m,(N)}$ and $\overline{\mathrm{M}}_p^{i,m,(N)}$ (using $m = 3$ in (3.10) and (3.11)). Then contribution of iterative majorants is

$$\overline{\mathrm{M}}_p^{i,m,(N)} = 5.03\mathrm{e}{-06} \quad \text{and} \quad \overline{\mathrm{M}}_{\boldsymbol{u}}^{i,m,(N)} = 2.81\mathrm{e}{-08},$$

and the values of the relative errors and majorants accumulated over all time steps are

$$\|\!\|\!\|e_p\|\!\|\!\|^2 = 1.87\mathrm{e}{-04}, \quad \|\!\|\!\|e_{\boldsymbol{u}}\|\!\|\!\|^2 = 1.86\mathrm{e}{-04}, \quad \overline{\mathrm{M}}_p = 3.84\mathrm{e}{-04}, \quad \overline{\mathrm{M}}_{\boldsymbol{u}} = 9.91\mathrm{e}{-04},$$

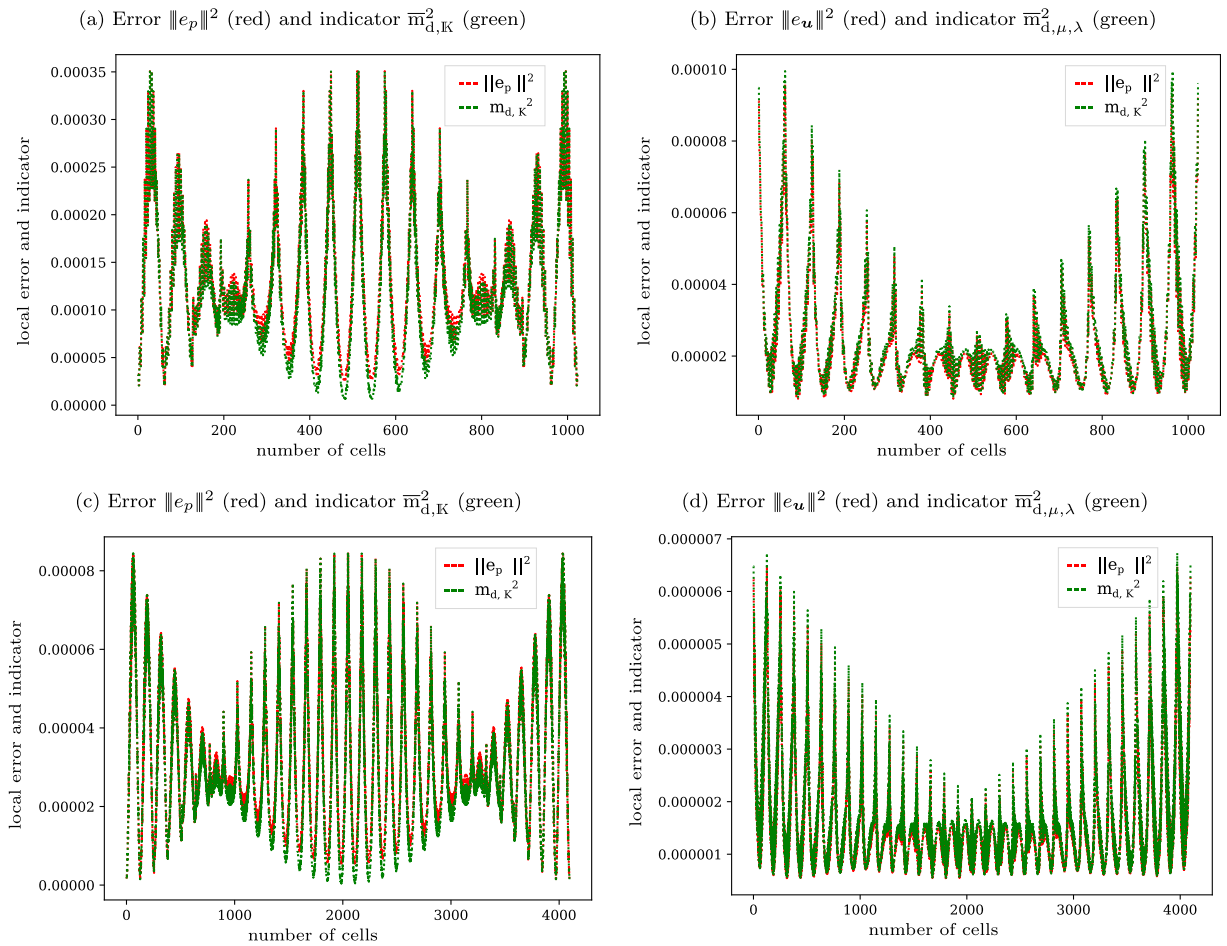

Fig. 1. *Example* 1 *(Academic parameters).* (a), (c) Local distribution of the error $\|e_p\|^2$ in red and the error indicator $\overline{\mathrm{m}}^2_{\mathrm{d},\mathbb{K}}$ generated by the majorant $\overline{\mathrm{M}}^h_p$ in green, and (b), (d) local distribution of the error $\|e_{\boldsymbol{u}}\|^2$ in red and the error indicator $\overline{\mathrm{m}}^2_{\mathrm{d},\mu,\lambda}$ generated by the majorant $\overline{\mathrm{M}}^h_{\boldsymbol{u}}$ in green. The distributions are depicted w.r.t. numbered finite element cells of the uniform meshes with (a)–(b) $h = 1/32$ and (c)–(d) $h = 1/64$. (For interpretation of the references to color in this figure legend, the reader is referred to the web version of this article.)

respectively. The corresponding efficiency indices over the entire time interval are summarized in Table 3(a). The results are presented w.r.t. meshes with two different mesh-sizes, h and τ. As the caption suggests, all these values are obtained for auxiliary functions reconstructed by the following finite elements $\boldsymbol{z}^i_h \in \mathbb{RT}_1$ and $\boldsymbol{\tau}^i_h \in [\mathrm{P}_2]^{2\times 2}$, which is an order higher than the usual choice of finite element approximation spaces for the fluxes and stresses in mixed formulations. To stress the importance of this to obtain more accurate error bounds, Table 4 lists the results obtained for cases when different finite element pairs for auxiliary functions are used, i.e., (a) $\boldsymbol{z}^i_h \in \mathbb{RT}_0$ and $\boldsymbol{\tau}^i_h \in [\mathrm{P}_2]^{2\times 2}$ or (b) $\boldsymbol{z}^i_h \in \mathbb{RT}_1$ and $\boldsymbol{\tau}^i_h \in [\mathbb{P}_1]^{2\times 2}$.

Table 5 illustrates the CPU time needed for various stages of the problem solution, i.e., first computation of both pressure and displacement, as well as a posteriori error control for each of the unknowns. For each operation, we also present the time needed as percentage of the total time spent on each time step. First, we consider Table 5(a). As expected, computing p is a much cheaper problem to solve (75–85 s on average) in comparison with the computation of $\boldsymbol{u}$ (260–270 s). Since a direct calculation of M^h_p does not involve the majorant minimization, the cost of error control for p is about 13–14 s. Reconstruction $\mathrm{M}^h_{\boldsymbol{u}}$ is more time-consuming than the one for the pressure, i.e., average time is 100–120 s. If we allow one iteration to minimize the majorant M^h_p, the cost for the error control of p increases (see Table 5(b)). The third column of the table indicates that one such iteration costs additional 200 s, and the error control for p-variable accounts for about 30%–35% of the total cost. Computational time for the case with two iterations minimizing M^h_p is illustrated in Table 5(c). Here, additional 200 s are added to the third column, making it the most costly part of the entire time step. Finally, if we allow one iteration of the $\mathrm{M}^h_{\boldsymbol{u}}$ minimization, the cost of error control increases even more. Eventually, as we improve the efficiency index of the error bounds, the computational costs to reconstruct functionals M^h_p and $\mathrm{M}^h_{\boldsymbol{u}}$ dominates over the time needed for the calculation of M^i_p and $\mathrm{M}^i_{\boldsymbol{u}}$, accounting for 95% of the total error control.

Table 3
Example 1 (Academic parameters). Convergence of errors and majorants w.r.t. the choice of spatial mesh sizes h and time steps τ (measured relatively w.r.t. $\|p\|_p^2$ and $\|\boldsymbol{u}\|_{\boldsymbol{u}}^2$). For all cases, the auxiliary functions are reconstructed by the following finite elements $\boldsymbol{z}_h^i \in \mathbb{RT}_1$ and $\boldsymbol{\tau}_h^i \in [\mathrm{P}_2]^{2\times 2}$.

h	$\|\|e_p\|\|^2$	$\overline{\mathrm{M}}_p$	$\|\|e_{\boldsymbol{u}}\|\|^2$	$\overline{\mathrm{M}}_{\boldsymbol{u}}$	$[(e_{\boldsymbol{u}}, e_p)]^2$	$\overline{\mathrm{M}}$	$I_{\mathrm{eff}}(\overline{\mathrm{M}})$
(a) $N = 10$, $\tau = 1.0$							
$1/16$	2.99e-03	6.17e-03	2.99e-03	1.58e-02	3.84e-03	1.76e-02	2.14
$1/32$	7.49e-04	1.53e-03	7.47e-04	3.96e-03	9.62e-04	4.40e-03	2.14
$1/64$	1.87e-04	3.84e-04	1.86e-04	9.91e-04	2.40e-04	1.10e-03	2.14
(b) $N = 10^2$, $\tau = 0.1$							
$1/16$	2.10e-03	4.28e-03	2.99e-04	1.58e-03	3.85e-04	1.75e-03	2.14
$1/32$	5.24e-04	1.07e-03	7.47e-05	3.94e-04	9.62e-05	4.38e-04	2.13
$1/64$	1.31e-04	2.73e-04	1.86e-05	9.85e-05	2.40e-05	1.09e-04	2.14
(c) $N = 10^3$, $\tau = 0.01$							
$1/16$	5.34e-04	2.18e-03	2.99e-05	1.57e-04	3.86e-05	1.92e-04	2.23
$1/32$	1.31e-04	5.44e-04	7.47e-06	3.92e-05	9.63e-06	4.81e-05	2.24
$1/64$	3.28e-05	1.36e-04	1.86e-06	9.80e-06	2.40e-06	1.20e-05	2.24

Table 4
Example 1 (Academic parameters). Convergence of errors and majorants w.r.t. the choice of approximation spaces for $\boldsymbol{z}_h^i$ and $\boldsymbol{\tau}_h^i$ (measured relatively w.r.t. $\|p\|_p^2$ and $\|\boldsymbol{u}\|_{\boldsymbol{u}}^2$). For all cases, simulation is performed for the discretization with $\tau = 1.0$.

h	$\|\|e_p\|\|^2$	$\overline{\mathrm{M}}_p$	$\|\|e_{\boldsymbol{u}}\|\|^2$	$\overline{\mathrm{M}}_{\boldsymbol{u}}$	$[(e_{\boldsymbol{u}}, e_p)]^2$	$\overline{\mathrm{M}}$	$I_{\mathrm{eff}}(\overline{\mathrm{M}})$
(a) $\boldsymbol{z}_h^i \in \mathbb{RT}_0$, $\boldsymbol{\tau}_h^i \in [\mathrm{P}_2]^{2\times 2}$							
$1/16$	9.45e-04	6.46e-03	8.05e-04	4.43e-03	1.75e-03	1.09e-02	2.50
$1/32$	2.36e-04	1.62e-03	2.01e-04	1.10e-03	4.37e-04	2.72e-03	2.50
$1/64$	5.90e-05	4.05e-04	5.03e-05	2.76e-04	1.09e-04	6.82e-04	2.50
(b) $\boldsymbol{z}_h^i \in \mathbb{RT}_1$, $\boldsymbol{\tau}_h^i \in [\mathbb{P}_1]^{2\times 2}$							
$1/16$	9.45e-04	1.49e-02	8.05e-04	1.93e-02	1.75e-03	3.42e-02	4.42
$1/32$	2.36e-04	3.74e-03	2.01e-04	4.83e-03	4.37e-04	8.57e-03	4.43
$1/64$	5.90e-05	9.35e-04	5.03e-05	1.21e-03	1.09e-04	2.14e-03	4.43

Now, we consider $N = 10^3$ and $h = \frac{1}{64}$, in particular, the last time-step $[t_{999}, t_{1000}]$ of a size $\tau = 0.01$. After ten iterative steps ($I = 10$), the error bounds are

$$\overline{\mathrm{M}}_p^{h,(N)} = 6.66\mathrm{e}{-05}, \quad \overline{\mathrm{M}}_p^{i,(N)} = 3.04\mathrm{e}{-02}, \quad \overline{\mathrm{M}}_{\boldsymbol{u}}^{h,(N)} = 4.90\mathrm{e}{-04}, \quad \overline{\mathrm{M}}_{\boldsymbol{u}}^{i,(N)} = 3.15\mathrm{e}{-05}.$$

We emphasize that contributions of majorant for discretization error and the iterative majorant for the pressure variable substantially differ in magnitude. These are the results obtained considering two last subsequent iteration steps with $q = 0.2307$ that correspond to $\frac{3q}{1-q^2}\left(\left(C_{\Sigma_D^p}^{\mathrm{F}}\right)^2 \beta/(\lambda_{\mathbb{K}}\tau) + 1\right) = 7.09$. Such a difference in magnitudes of majorants for p results in the efficiency index $I_{\mathrm{eff}}(\overline{\mathrm{M}}_p^{(N)}) = 43.10$. However, we can exploit the flexibility of Lemma 8 with $M = 7$ to obtain a better contraction parameter $\tilde{q} := q^7 = 3.48\mathrm{e}{-05}$, i.e.,

$$\overline{\mathrm{M}}_p^{i,m,(N)} = 1.41\mathrm{e}{-06} \quad \text{and} \quad \overline{\mathrm{M}}_{\boldsymbol{u}}^{i,m,(N)} = 2.21\mathrm{e}{-13}.$$

These values improve the efficiency index of, for example, $\overline{\mathrm{M}}_p^{(N)}$ by approximately 21.12 times, and yield

$$\|\|e_p^{(N)}\|\|^2 = 9.83\mathrm{e}{-08}, \quad \overline{\mathrm{M}}_p^{(N)} = 4.07\mathrm{e}{-07}, \quad I_{\mathrm{eff}}(\overline{\mathrm{M}}_p^{(N)}) = 2.04 \quad \text{and}$$
$$\|\|e_{\boldsymbol{u}}^{(N)}\|\|^2 = 5.59\mathrm{e}{-09}, \quad \overline{\mathrm{M}}_{\boldsymbol{u}}^{(N)} = 2.93\mathrm{e}{-08}, \quad I_{\mathrm{eff}}(\overline{\mathrm{M}}_{\boldsymbol{u}}^{(N)}) = 2.29.$$

The accumulated values over the whole time interval are as follows:

$$\|\|e_p\|\|^2 = 3.28\mathrm{e}{-05}, \quad \overline{\mathrm{M}}_p = 1.36\mathrm{e}{-04}, \quad \text{and} \quad I_{\mathrm{eff}}(\overline{\mathrm{M}}_p) = 2.04,$$

Table 5
Example 1 (Academic parameters). Comparison of the CPU time required to perform different stages of numerical calculations w.r.t. the selected time steps for the discretization parameters $N = 10$, $\tau = 1.0$, $h = \frac{1}{64}$.

n	computation of p, s (%)	computation of u, s (%)	error control for p, s (%)	error control for u, s (%)
(a) 0 iteration for M_p^h minimization				
2	76.12 (17.06 %)	258.55 (57.94 %)	13.62 (3.05 %)	97.96 (21.95 %)
4	78.23 (16.47 %)	257.60 (54.23 %)	13.26 (2.79 %)	125.91 (26.51 %)
8	76.44 (16.24 %)	258.28 (54.86 %)	12.59 (2.68 %)	123.47 (26.23 %)
(b) 1 iteration for M_p^h minimization				
2	76.09 (12.82 %)	252.59 (42.54 %)	207.68 (34.98 %)	57.39 (9.67 %)
4	80.53 (12.60 %)	261.77 (40.97 %)	217.40 (34.02 %)	79.24 (12.40 %)
8	77.85 (11.34 %)	262.77 (38.29 %)	231.08 (33.67 %)	114.54 (16.69 %)
(c) 2 iterations for M_p^h minimization				
2	79.13 (9.63 %)	252.90 (30.79 %)	422.52 (51.44 %)	66.82 (8.14 %)
4	77.39 (8.55 %)	260.41 (28.78 %)	432.71 (47.82 %)	134.29 (14.84 %)
8	82.55 (9.37 %)	262.56 (29.79 %)	437.62 (49.65 %)	98.69 (11.20 %)
(d) 2 iterations for M_p^h minimization, 1 iteration for $\mathrm{M}_{\boldsymbol{u}}^h$ minimization				
2	80.68 (9.11 %)	257.11 (29.02 %)	437.84 (49.41 %)	110.42 (12.46 %)
4	79.18 (8.98 %)	256.56 (29.10 %)	418.92 (47.51 %)	127.04 (14.41 %)
8	75.44 (7.64 %)	262.72 (26.59 %)	451.37 (45.68 %)	198.50 (20.09 %)

Table 6
Example 1 (Realistic parameters). Convergence of errors and majorants w.r.t. the choice of spatial mesh sizes (measured relatively w.r.t. $\|p_h^i\|_p^2$ and $\|\boldsymbol{u}_h^i\|_{\boldsymbol{u}}^2$) for $N = 100$ and $\tau = 0.1$.

h	$\|\!\|\!\|e_p\|\!\|\!\|^2$	$\overline{\mathrm{M}}_p$	$\|\!\|\!\|e_{\boldsymbol{u}}\|\!\|\!\|^2$	$\overline{\mathrm{M}}_{\boldsymbol{u}}$	$[(e_{\boldsymbol{u}}, e_p)]^2$	$\overline{\mathrm{M}}$	$I_{\mathrm{eff}}(\overline{\mathrm{M}})$
$1/16$	3.14e-03	2.39e-02	3.00e-04	5.25e-03	3.14e-03	2.39e-02	2.76
$1/32$	7.86e-04	5.96e-03	7.51e-05	1.31e-03	7.86e-04	5.96e-03	2.75
$1/64$	1.96e-04	1.48e-03	1.87e-04	3.28e-03	1.96e-04	1.48e-03	2.75

$$|\!|\!|e_{\boldsymbol{u}}|\!|\!|^2 = 1.86\mathrm{e}{-06}, \quad \overline{\mathrm{M}}_{\boldsymbol{u}} = 9.80\mathrm{e}{-06}, \quad \text{and} \quad I_{\mathrm{eff}}(\overline{\mathrm{M}}_{\boldsymbol{u}}) = 2.29.$$

This yields the total values $\big|\big[(e_{\boldsymbol{u}}, e_p)\big]\big| = 2.40\mathrm{e}{-06}$ and $\overline{\mathrm{M}} = 1.2029\mathrm{e}{-05}$ with the efficiency index $I_{\mathrm{eff}} = 2.24$. The latter values amount others are included in Table 3(c). We see that even with a decreasing τ, which scales the permeability tensor $\mathbb{K}$, the efficiency of total error estimates stays rather robust.

We note here that each increment of $\overline{\mathrm{M}}_p^{(N)}$ and $\overline{\mathrm{M}}_{\boldsymbol{u}}^{(N)}$ can be computed using $\widetilde{\mathrm{M}}_p^i$ and $\widetilde{\mathrm{M}}_{\boldsymbol{u}}^i$, which does not require the majorant of discretization errors $\overline{\mathrm{M}}_p^{h,(N)}$ and $\overline{\mathrm{M}}_{\boldsymbol{u}}^{h,(N)}$ on iteration steps $i-1$ or $i-m$ and, as a consequence, their minimization w.r.t. the auxiliary functions $\boldsymbol{z}_h^i$ and $\boldsymbol{\tau}_h^i$, respectively. Moreover, the values $\widetilde{\mathrm{M}}_p^i$ and $\widetilde{\mathrm{M}}_{\boldsymbol{u}}^i$ are orders of magnitude smaller than $\overline{\mathrm{M}}_p^{i,m,(N)}$ and $\overline{\mathrm{M}}_{\boldsymbol{u}}^{i,m,(N)}$, i.e., $\widetilde{\mathrm{M}}_p^i = 7.07\mathrm{e}{-10}$ and $\widetilde{\mathrm{M}}_{\boldsymbol{u}}^i = 7.33\mathrm{e}{-13}$. Such values automatically minimize the contribution of iterative estimates in both $\overline{\mathrm{M}}_p^{(N)}$ and $\overline{\mathrm{M}}_{\boldsymbol{u}}^{(N)}$, as well as further improve their efficiency.

Let us assume now more *realistic parameters* in the example above (similar to those taken from [64] and [58]). Let the exact pressure be scaled as follows: $p(x, y, t) = 10^8\, x(1-x)\, y(1-y)\, t$. The permeability tensor divided by the fluid viscosity is taken as $\mathbb{K} = 100\mathbb{I}$ [mD/cP], the fluid compressibility fixed to $4.7 \cdot 10^{-7}$ [psi^{-1}], and initial porosity ϕ_0 is assumed to be 0.2. The Biot and the bulk modulus are $M = 1.65 \cdot 10^{10}$ [Pa] and $E = 0.59 \cdot 10^9$ [Pa], respectively. That results in $\beta = \frac{1}{M} + c_f\, \phi_0 = 9.40 \cdot 10^{-8}$, which, in turn, yields a considerably small $L = \frac{\alpha^2}{2\,(\lambda + 2\mu/d)} = 1.35 \cdot 10^{-9}$. Such a tuning parameter generates instantaneous convergence of an iterative scheme with the contractive parameter $q = \frac{L}{\beta + L} = 6.73 \cdot 10^{-12}$. The resulting errors and corresponding estimates are summarized in Table 6 (for $\tau = 0.1$ and difference between spatial mesh-sizes h). For such q, even one iteration is enough for convergence. However, one can consider two/five iterations to improve the sharpness of the majorant. The efficiency indices obtained here confirm the quantitative properties of total majorants also for parameters close to those used in engineering applications.

Example 2. Dependence of the total error bound on the iterative majorants contributions (w.r.t. two different sets of parameters). In the next example, we consider another polynomial exact solution. However, the first set of material

Table 7
Example 2 (Academic parameters). Errors and majorants w.r.t. the iteration steps for $N = 10$, $\tau = 1.0$, $h = \frac{1}{64}$, and $I = 12$ (both values are measured relative to the increment in $\|p\|_p^2$ and $\|\boldsymbol{u}\|_{\boldsymbol{u}}^2$ at the Nth time step).

# it.	$\|\!\|e_p\|\!\|^2$	$\overline{\mathrm{M}}_p^h$	$\|e_p\|_\beta^2$	$\overline{\mathrm{M}}_{p,L^2}^h$	$\|\!\|e_{\boldsymbol{u}}\|\!\|^2$	$\overline{\mathrm{M}}_{\boldsymbol{u}}^h$	$\|\mathrm{dive}_{\boldsymbol{u}}\|_\lambda^2$	$\overline{\mathrm{M}}_{\boldsymbol{u},\mathrm{div}}^h$
6	1.95e-04	1.95e-04	2.60e-10	9.22e-06	8.50e-06	2.61e-05	9.81e-06	2.34e-05
...	...	...	...	...	...	...	...	...
11	1.95e-04	1.95e-04	2.61e-10	9.22e-06	8.50e-06	2.61e-05	9.81e-06	2.34e-05
12	1.95e-04	1.95e-04	2.61e-10	9.22e-06	8.50e-06	2.61e-05	9.81e-06	2.34e-05

Table 8
Example 2 (Academic parameters). Convergence of errors and majorants w.r.t. the choice of spatial mesh sizes and time steps (measured relatively w.r.t. $\|p_h^i\|_p^2$, $\|\boldsymbol{u}_h^i\|_{\boldsymbol{u}}^2$, and $[(e_{\boldsymbol{u}}, e_p)]^2$).

h	$\|\!\|e_p\|\!\|^2$	$\|\!\|e_{\boldsymbol{u}}\|\!\|^2$	$\lvert[(e_{\boldsymbol{u}}, e_p)]\rvert$	$I_{\mathrm{eff}}(\overline{\mathrm{M}}_p)$	$I_{\mathrm{eff}}(\overline{\mathrm{M}}_{\boldsymbol{u}})$	$I_{\mathrm{eff}}(\overline{\mathrm{M}})$
(a) $N = 10$, $\tau = 1.0$						
$1/16$	3.12e-03	1.36e-04	1.61e-04	$40.46 \to 4.93$	$20.58 \to 3.15$	$24.78 \to 3.49$
$1/32$	7.82e-04	3.40e-05	4.03e-05	$40.46 \to 4.93$	$20.58 \to 3.15$	$24.77 \to 3.49$
$1/64$	1.95e-04	8.50e-06	1.00e-05	$40.46 \to 4.93$	$20.58 \to 3.15$	$24.77 \to 3.49$
(b) $N = 10^2$, $\tau = 0.1$						
$1/16$	2.97e-03	1.36e-05	1.61e-05	$129.60 \to 15.27$	$20.33 \to 3.14$	$54.62 \to 6.81$
$1/32$	7.43e-04	3.40e-06	4.03e-06	$129.62 \to 16.66$	$20.33 \to 3.23$	$54.62 \to 7.21$
$1/64$	1.85e-04	8.50e-07	1.00e-06	$129.62 \to 20.45$	$20.33 \to 3.56$	$54.62 \to 8.74$

parameters (which can be regarded as more academic ones) are chosen in such a way that parameter q takes a value close 1. Such a contraction can cause the deteriorated quality of iterative error estimates, which compromises the efficiency index of total majorants. Following similar arguments made in Example 1, we highlight the improvement in the efficiency index of total error bound $\overline{\mathrm{M}}$ when the functional $\overline{\mathrm{M}}^{i,m}$ is used instead of $\overline{\mathrm{M}}^i$. In particular, it is done for different time steps and spatial mesh-sizes (see Table 7). Moreover, in the second part of this example, we choose more realistic material parameters, in particular, anisotropic permeability tensor of relatively small magnitude, which might cause a quality decrease in the discretization majorants (see, e.g., [69]). Having said that, the more realistic set of parameters often lead to rather small contraction values, making iterative component of the error bounds rather neglectable. Regardless of chosen parameters, we present the efficiency indices that confirm the robustness of total error bound.

Let the exact solution of (1.1) be defined as

$$\boldsymbol{u}(x, y, t) := \begin{bmatrix} t\,(x^2 + y^2) \\ t\,(x + y) \end{bmatrix} \quad \text{and} \quad p(x, y, t) := t\,x(1 - x)\,y(1 - y).$$

We fix the Poisson ratio to be $\nu = 0.2$ and Young modulus $E = 0.594$ [Pa], which yields the Lame parameters $\mu = 0.25$ and $\lambda = 0.12$. We set $\alpha = 1$ and $\beta = \frac{1}{M} + c_f\phi_0 = 0.11$, where $M = 1.65 \cdot 10^{-10}$ [Pa], $K_u = K + \frac{\alpha^2}{c_0} = 10.28$, $c_f = \frac{1}{c_0}\lambda_{\mathbb{K}}\frac{K+4/3\mu}{K_{\boldsymbol{u}}+4/3\mu} = 0.58$, $C_{\mathrm{F}} = \frac{1}{\sqrt{2}\pi}$, and $\mathbb{K} = I$ [mD/cP], where $\mathbb{I}$ is a unit tensor. From the parameters above, it follows that $L = \frac{\alpha^2}{2(\lambda+2\mu/d)} = 1.34$ and $q = \frac{L}{\beta+L} = 0.92$. With such q, the ratio $\frac{q^2}{(1-q)^2}$ is 133.33, which might influence the quantitative performance of the majorant.

We consider 10 time steps of the length τ = 1.0 and a spatial mesh-size $h = \frac{1}{64}$ using standard $\mathbb{P}_1$ finite elements (see (7.7)). The number of iterations to solve the problem on each time step is set to 12. For the time interval $[t_9, t_{10}]$, the convergence of errors in $\boldsymbol{u}$ and p is presented in Table 7. From one side, we can consider the iterations I and $I - 1$ as subsequent ones with a contraction parameter $q = 0.92$. From the other side, by using Lemma 2 instead, let $m = 6$ so that the 6th and 12th iterations are treated as two consecutive steps with $q' = q^6 = 0.60$. Then, the constants dependent on the ratio $\frac{q^2}{(1-q^2)} = 2.30$ attain more acceptable values. Table 8 illustrates the improved efficiency indices of error majorant as the method explained-above is employed.

Local distribution of the error in p and $\boldsymbol{u}$ on each cell of the finite-element discretization is presented for mesh sizes $h = 1/4$ and $h = 1/8$ in Fig. 2. One can see the resemblance in the local error distribution for p since the exact solutions for both examples are the same. Local values of the error and indicator in $\boldsymbol{u}$ have a more uniform distribution.

Let us consider more realistic parameters similar to those chosen in [70]. Again, let the exact pressure be $p(x, y, t) := 10^8\,x(1-x)\,y(1-y)\,t$. Mechanical parameters such as the Biot and the bulk modulus are chosen as follows: $M = 1.45 \cdot 10^4$

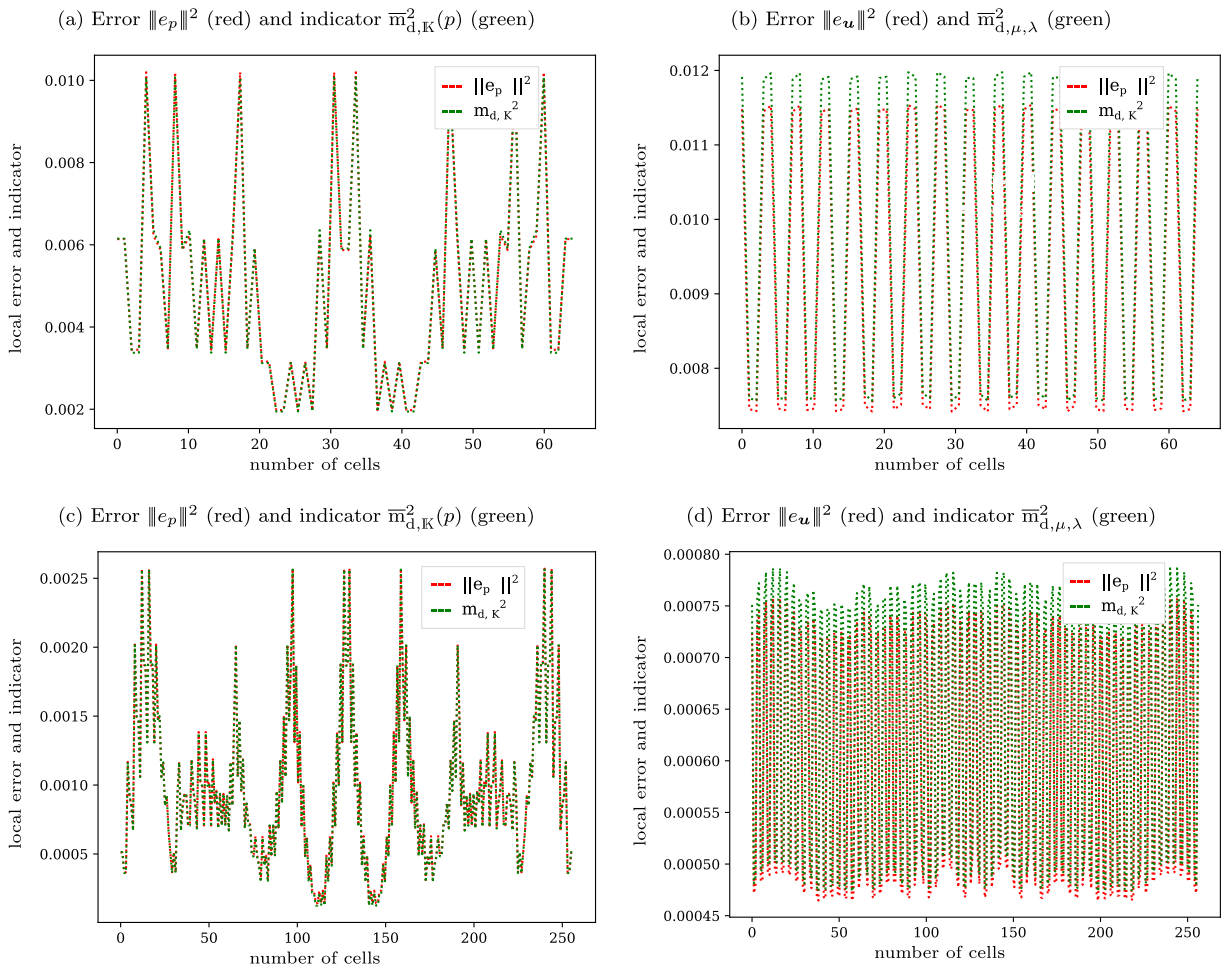

Fig. 2. *Example 2 (Academic parameters).* Errors $\|e_p\|^2$ and $\|e_{\boldsymbol{u}}\|^2$ (in red) and error indicators $\overline{\mathrm{m}}^2_{\mathrm{d},\mathbb{K}}$ and $\overline{\mathrm{m}}^2_{\mathrm{d},\mu,\lambda}$ (in green) generated by the majorants $\overline{\mathrm{M}}^h_p$ and $\overline{\mathrm{M}}^h_{\boldsymbol{u}}$, respectively, distributions w.r.t. numbered finite element cells. (For interpretation of the references to color in this figure legend, the reader is referred to the web version of this article.)

[Pa] and $E = 7 \cdot 10^7$ [Pa], respectively. The permeability tensor is $\mathbb{K} = \mathrm{diag}\{50, 200\} \cdot 10^{-10}$ [mD/cP], whereas the fluid viscosity is $\mu_f = 10^{-3}$. Thus, we obtain $\beta \approx \frac{1}{M} + c_f\phi_0 = 6.89 \cdot 10^{-5}$, which, in turn, yields a considerably small $L = \frac{\alpha^2}{2(\lambda+2\mu/\mathrm{d})} = 1.14 \cdot 10^{-8}$. Such a parameter generates contractive parameter $q = \frac{L}{\beta+L} = 1.66 \cdot 10^{-4}$. The latter means that the ratio $\frac{q^2}{(1-q)^2}$ is of order 10^{-8}, which does not degenerate the efficiency of majorant. We summarize the convergence results in Table 9. It again confirms that even in case of more realistic parameters common for engineering applications, the value of estimates remains rather efficient.

Example 3. Verification of the majorants properties w.r.t. non-polynomial manufactured solutions. To make sure that we exclude the super-convergence in testing the scheme presented above, we consider the non-polynomial manufactured solution. The chosen p and $\boldsymbol{u}$ in (1.1) are

$$\boldsymbol{u}(x, y, t) := \begin{bmatrix} x \sin \pi x (1-y) \sin \pi y\, t \\ x(1-x) y(1-y)(\sin t + 1) \end{bmatrix} \quad \text{and} \quad p(x, y, t) := \sin \pi x \sin \pi y\, (t^2 + t + 1).$$

The Lame parameters are similar to those considered in Example 1, i.e., $\mu = \lambda_{\mathrm{vol}} = 1$, $\lambda_{\mathrm{plane}} = \frac{2}{3}$. Besides, $\alpha = \beta = 1$, $C_{\mathrm{F}} = \frac{1}{\sqrt{2}\,\pi}$, and $\mathbb{K} = I$ [mD/cP]. The parameters above yield $L = 0.3$ and $q = \frac{3}{13}$.

Table 10 presents convergence results corresponding to meshes with different mesh-sizes h and time steps τ. The number of iterations is fixed to be $I = 5$ throughout all tests. Learning from the experience of first two examples, we apply Lemma 2 with $m = 3$, which yields a smaller contractive parameter $\tilde{q} := q^3 = 0.0123$. The table is divided into

Table 9
Example 2 (Realistic parameters). Convergence of errors and majorants w.r.t. the choice of spatial mesh sizes and time steps (measured relatively w.r.t. $\|p_h^i\|_p^2$, $\|\boldsymbol{u}_h^i\|_{\boldsymbol{u}}^2$, and $[(e_{\boldsymbol{u}}, e_p)]^2$).

h	$\|\!\|\!\| e_p \|\!\|\!\|^2$	$\overline{\mathrm{M}}_p$	$\|\!\|\!\| e_{\boldsymbol{u}} \|\!\|\!\|^2$	$\overline{\mathrm{M}}_{\boldsymbol{u}}$	$[(e_{\boldsymbol{u}}, e_p)]^2$	$\overline{\mathrm{M}}$	$I_{\mathrm{eff}}(\overline{\mathrm{M}})$
(a) $N = 10$, $\tau = 1.0$							
$1/16$	2.40e-03	1.23e-02	1.36e-04	8.71e-04	2.42e-03	1.24e-02	2.26
$1/32$	6.01e-04	3.07e-03	3.40e-05	2.17e-04	6.04e-04	3.09e-03	2.26
$1/64$	1.50e-04	7.66e-04	8.50e-06	5.44e-05	1.51e-04	7.71e-04	2.26
(a) $N = 100$, $\tau = 0.1$							
$1/16$	8.25e-04	3.41e-03	1.36e-05	7.80e-05	8.29e-04	3.44e-03	2.04
$1/32$	2.04e-04	8.53e-04	3.40e-06	1.95e-05	2.05e-04	8.59e-04	2.04
$1/64$	5.10e-05	2.13e-04	8.50e-07	4.87e-06	5.13e-05	2.14e-04	2.04
(a) $N = 10^3$, $\tau = 0.01$							
$1/8$	6.04e-04	1.73e-03	5.44e-06	3.05e-05	6.06e-04	1.74e-03	1.70
$1/16$	1.18e-04	4.32e-04	1.36e-06	7.63e-06	1.18e-04	4.35e-04	1.91
$1/32$	2.75e-05	1.07e-04	3.40e-07	1.90e-06	2.76e-05	1.08e-04	1.98

Table 10
Example 3. Convergence of errors and majorants w.r.t. the choice of spatial mesh sizes h and time steps τ (measured relatively w.r.t. $\|p\|_p^2$, $\|\boldsymbol{u}\|_{\boldsymbol{u}}^2$, and $[(e_{\boldsymbol{u}}, e_p)]^2$).

h	$\|\!\|\!\| e_p \|\!\|\!\|^2$	$\overline{\mathrm{M}}_p$	$\|\!\|\!\| e_{\boldsymbol{u}} \|\!\|\!\|^2$	$\overline{\mathrm{M}}_{\boldsymbol{u}}$	$[(e_{\boldsymbol{u}}, e_p)]^2$	$\overline{\mathrm{M}}$	$I_{\mathrm{eff}}(\overline{\mathrm{M}})$
(a) $\boldsymbol{z}_h^i \in \mathbb{RT}_1$ and $\boldsymbol{\tau}_h^i \in [\mathrm{P}_2]^{2\times 2}$							
	(a-1) $N = 10$, $\tau = 1.0$						
$1/16$	2.54e-03	5.29e-03	5.33e-03	6.8001e-01	2.55e-03	6.82e-03	1.63
$1/32$	6.37e-04	1.29e-03	1.33e-03	1.6861e-01	6.40e-04	1.67e-03	1.62
$1/64$	1.59e-04	3.22e-04	3.34e-04	4.2059e-02	1.60e-04	4.16e-04	1.61
	(a-2) $N = 10^2$, $\tau = 0.1$						
$1/16$	1.77e-03	3.65e-03	5.34e-04	5.2309e-02	1.78e-03	4.53e-03	1.59
$1/32$	4.44e-04	9.30e-04	1.33e-04	1.3071e-02	4.47e-04	1.15e-03	1.60
$1/64$	1.11e-04	2.53e-04	3.34e-05	3.2722e-03	1.12e-04	3.08e-04	1.66
(b) $\boldsymbol{z}_h^i \in \mathbb{RT}_0$ and $\boldsymbol{\tau}_h^i \in [\mathrm{P}_2]^{1\times 1}$							
	(b-1) $N = 10$, $\tau = 1$						
$1/16$	2.54e-03	3.05e-02	5.33e-03	2.28	2.55e-03	3.56e-02	3.73
$1/32$	6.37e-04	7.64e-03	1.33e-03	5.73e-01	6.40e-04	8.93e-03	3.73
$1/64$	1.59e-04	1.91e-03	3.34e-04	1.43e-01	1.60e-04	2.23e-03	3.73
	(b-2) $N = 100$, $\tau = 0.1$						
$1/16$	1.77e-03	1.85e-02	5.34e-04	1.33e-01	1.78e-03	2.07e-02	3.41
$1/32$	4.44e-04	4.65e-03	1.33e-04	3.34e-02	4.47e-04	5.21e-03	3.42
$1/64$	1.11e-04	1.18e-03	3.34e-05	8.36e-03	1.12e-04	1.32e-03	3.44

two parts: Table 10(a) presents the results obtained for the auxiliary functions $\boldsymbol{z}_h^i \in \mathbb{RT}_1$ and $\boldsymbol{\tau}_h^i \in [\mathrm{P}_2]^{2\times 2}$, whereas Table 10(b) uses the functions $\boldsymbol{z}_h^i \in \mathbb{RT}_0$ and $\boldsymbol{\tau}_h^i \in [\mathrm{P}_2]^{1\times 1}$. As expected, the efficiency indices in the first part of the table are slightly better than in the second one, since the auxiliary functions that minimize the majorants of discretization errors are reconstructed more accurately.

Besides the robustness of error estimates w.r.t. different discretization parameters, we address the computational time for various scenarios. We consider discretization time steps $\tau = 1$ (see Table 11(a)) and $\tau = 0.1$ (Table 11(b)). In the first part of the table, corresponding to a smaller step, we first illustrate the CPU costs for a more computationally-heavy error control, where the auxiliary function $\boldsymbol{z}_h^i \in \mathbb{RT}_1$ is used in 2 iteration steps of the majorant minimization. We see that error control for the variable p dominates in this case and takes almost half of the computational time of entire step.

Table 11
Example 3. Comparison of the CPU time required to perform several stages of the numerical calculations w.r.t. the selected time steps, $h = \frac{1}{64}$.

n	computation of p, s (%)	computation of u, s (%)	error control for p, s (%)	error control for u, s (%)
(a) $N = 100$				
	(a-1) 2 iterations for M_p^h minimization, $\boldsymbol{z}_h^i \in \mathbb{RT}_1$			
20	96.05 (8.46%)	305.87 (26.94%)	544.04 (47.91%)	189.56 (16.69%)
40	100.00 (8.38%)	305.29 (25.58%)	539.27 (45.18%)	249.01 (20.86%)
80	103.62 (8.60%)	308.15 (25.56%)	561.49 (46.58%)	232.13 (19.26%)
	(a-2) 0 it. for M_p^h minimization, $\boldsymbol{z}_h^i \in \mathbb{RT}_0$			
20	35.58 (21.62%)	118.02 (71.69%)	2.50 (1.52%)	8.51 (5.17%)
40	37.70 (22.35%)	123.79 (73.38%)	2.10 (1.25%)	5.10 (3.02%)
80	31.03 (21.24%)	106.15 (72.66%)	2.51 (1.72%)	6.40 (4.38%)
(b) $N = 10$				
	(b-1) 2 iteration for M_p^h minimization, $\boldsymbol{z}_h^i \in \mathbb{RT}_1$			
2	29.96 (12.45%)	99.34 (41.27%)	44.11 (18.33%)	67.30 (27.96%)
4	35.43 (14.19%)	113.12 (45.31%)	44.51 (17.83%)	56.58 (22.66%)
8	48.91 (13.21%)	163.18 (44.09%)	59.82 (16.16%)	98.22 (26.54%)
	(b-2) 0 iteration for M_p^h minimization, $\boldsymbol{z}_h^i \in \mathbb{RT}_0$			
2	43.41 (21.09%)	148.86 (72.30%)	2.92 (1.42%)	10.69 (5.20%)
4	36.39 (21.29%)	121.94 (71.35%)	2.36 (1.38%)	10.21 (5.98%)
8	40.92 (21.28%)	138.38 (71.96%)	2.65 (1.38%)	10.33 (5.37%)

After that, we illustrate the CPU costs for the function $\boldsymbol{z}_h^i \in \mathbb{RT}_0$ without optimization procedure. Columns four and five emphasize how inexpensive a posteriori error control can be when one only needs to calculate $\overline{\mathrm{M}}_p^h$ and $\overline{\mathrm{M}}_{\boldsymbol{u}}^h$.

8. Conclusions and future work

We analyze semi-discrete approximations of the Biot poroelastic problem and deduce guaranteed and fully computable bounds of corresponding errors. The derivation combines the estimates for contraction mappings and the functional a posteriori error majorants for elliptic problems. The obtained error bound is fully computable and independent on the discretization techniques used for the variational formulation of the Biot problem as soon as the reproduced approximations belong to admissible functional spaces. Moreover, obtained error functional does not depend on any mesh discretization constants and only contains global Poincare-type constants characterizing considered geometry.

Numerical results presented above provided the evidence of the quantitative efficiency of the majorant when it comes to the error indication. Generally, automation of the mesh adaptation procedure crucially depends on the quality of the error indicator used. It is a very important and complex topic that includes not only the question of how to reconstruct the mesh or which approximation space to use but also how to combine it with existing well-verified technologies (e.g., greedy marking, hp-refinement, etc.). Thorough investigation of these questions in the context of the error estimates introduced in this paper is an important task for future research.

CRediT authorship contribution statement

Kundan Kumar: Conceptualization, Formal analysis, Funding acquisition, Methodology, Writing - review & editing. **Svetlana Kyas:** Conceptualization, Formal analysis, Methodology, Software, Investigation, Validation, Writing - original draft, Writing - review & editing. **Jan Martin Nordbotten:** Conceptualization, Formal analysis, Methodology, Writing - review & editing. **Sergey Repin:** Conceptualization, Formal analysis, Methodology, Writing - review & editing.

Acknowledgments

The work is funded by the SIU Grant CPRU-2015/10040. The second author wants to acknowledge the Werner Siemens Foundation (Werner Siemens-Stiftung) for its support of the Geothermal Energy and Geofluids group at ETH Zurich, Switzerland. KK and JMN would like to acknowledge Norwegian Research Council project Toppforsk 250223 for funding.

Appendix

Notation and definitions of spaces. We use the standard Lebesgue space of square-measurable functions $L^2(\Omega)$ equipped with the norm $\| v \|_\Omega := \| v \|_{L^2(\Omega)} := (v, v)_\Omega^{1/2}$ for all $u, v \in L^2(\Omega)$. Let $\mathbb{M}^{d\times d}$ denote the space of real d-dimensional tensors. The products of vector-valued $\boldsymbol{v}, \boldsymbol{w} \in \mathbb{R}^{\mathrm{d}}$ and tensor-valued functions $\boldsymbol{\tau}, \boldsymbol{\sigma} \in \mathbb{M}^{d\times d}$ are defined by the relations

$$(\boldsymbol{v}, \boldsymbol{w})_\Omega := \int_\Omega \boldsymbol{v} \cdot \boldsymbol{w} \mathrm{d}x \quad \text{and} \quad (\boldsymbol{\tau}, \boldsymbol{\sigma})_\Omega := \int_\Omega \boldsymbol{\tau} : \boldsymbol{\sigma} \mathrm{d}x,$$

where $\boldsymbol{v} \cdot \boldsymbol{w} := v_i w_i$ and $\boldsymbol{\tau} : \boldsymbol{\sigma} := \tau_{ij} \boldsymbol{\sigma}_{ij}$, respectively. Next, $\mathbb{A}(x) \in \mathbb{M}^{d\times d}$, $x \in \Omega$ denotes a symmetric uniformly positive defined matrix that satisfies $0 < \underline{\lambda} \le \lambda(x) \le \overline{\lambda} \le +\infty$, $\underline{\lambda}, \overline{\lambda} \in \mathbb{R}$ with uniformly bounded eigenvalues $\lambda(x)$. Then, for the product $(\mathbf{u}, \boldsymbol{v})_{\mathbb{A}} := (\mathbb{A}\mathbf{u}, \boldsymbol{v})$, we have

$$\underline{\lambda} \| \boldsymbol{v} \| \le \| \boldsymbol{v} \|_{\mathbb{A}} \le \overline{\lambda} \| \boldsymbol{v} \| \quad \text{and} \quad (\mathbf{u}, \boldsymbol{v}) \le \| \cdot \|_{\mathbb{A}} \| \cdot \|_{\mathbb{A}^{-1}}, \quad \forall \mathbf{u}, \boldsymbol{v} \in [L^2(\Omega)]^d.$$

We use the standard notation for the Sobolev space of vector-valued functions having square-summable derivatives

$$H^1(\Omega) := \left\{ v \in L^2(\Omega) \mid \nabla v \in [L^2(\Omega)]^d \right\},$$

equipped with the norm $\| v \|_{H^1(\Omega)} := \left(\| v \|_\Omega^2 + | v |_\Omega^2 \right)^{1/2}$. Also, we use a semi-norm $| v |_\Omega := | v |_{H^1(\Omega)} := \| \nabla v \|_\Omega$, and for the vector-valued functions with square-summable divergence introduce the Hilbert space

$$H(\Omega, \mathrm{div}) := \left\{ \boldsymbol{v} \in [L^2(\Omega)]^d \mid \mathrm{div} \boldsymbol{v} \in L^2(\Omega) \right\},$$

endowed with the norm $\| \boldsymbol{v} \|_{H(\Omega,\mathrm{div})}^2 := \| \boldsymbol{v} \|_{[L^2(\Omega)]^d}^2 + \| \mathrm{div} \boldsymbol{v} \|_{L^2(\Omega)}^2$.

Let Σ be a part of the boundary such that $\mathrm{meas}_{d-1} \Sigma > 0$ (in particular, it may coincide with $\partial\Omega$). For the functions in $H^1_{0,\Sigma}(\Omega) := \left\{ v \in H^1(\Omega) \mid v |_\Sigma = 0 \right\}$, the Friedrichs-type inequality reads:

$$\| v \|_\Omega \le C_\Gamma^{\mathrm{F}} | v |_\Omega, \quad \forall v \in H^1_{0,\Sigma}(\Omega). \tag{7.2}$$

The corresponding trace operator $\gamma : H^1(\Omega) \to H^{\frac{1}{2}}(\Omega)$ is bounded and satisfies the estimate

$$v|_\Sigma := \gamma v, \quad \| v \|_\Sigma \le C_{\Sigma\Omega}^{\mathrm{tr}} \| v \|_{H^1(\Omega)}, \quad \forall v \in H^1(\Omega), \tag{7.3}$$

where $\| v \|_\Sigma$ is the norm of $L^2(\Sigma)$.

C_{K} denotes the constant in the Korn inequality

$$\| \boldsymbol{w} \|_{[H^1(\Omega)]^d} \le C_{\mathrm{K}} \| \boldsymbol{\varepsilon}(\boldsymbol{w}) \|_{[L^2(\Omega)]^{d\times d}}, \quad \forall \boldsymbol{w} \in [H^1(\Omega)]^d, \tag{7.4}$$

Also, we use the inequality

$$\| \mathrm{div}\, \boldsymbol{w} \| = \| \mathrm{tr}\, \boldsymbol{\varepsilon}(\boldsymbol{w}) \| = \| \mathbb{I} : \boldsymbol{\varepsilon}(\boldsymbol{w}) \| \le \sqrt{d} \| \boldsymbol{\varepsilon}(\boldsymbol{w}) \|, \quad \forall \boldsymbol{w} \in [H^1(\Omega)]^d, \tag{7.5}$$

where $\mathbb{I} \in \mathbb{M}^{d\times d}$ is the unit tensor of $\mathbb{M}^{d\times d}$, and $\boldsymbol{\varepsilon}(\boldsymbol{w}) \in \mathbb{M}^{d\times d}$ denotes the symmetric part of $\nabla \boldsymbol{w}$.

Next, let $Q := \Omega \times (0, T)$ denote a space–time cylinder (with given time-interval $(0, T)$, $0 < T < +\infty$), and let $\Sigma = \partial\Omega \times (0, T)$ be a lateral surface of Q, whereas $\Sigma_0 := \partial\Omega \times \{0\}$ and $\Sigma_T := \partial\Omega \times \{T\}$ define the bottom and the top part of the mantel (so that $\partial Q = \Sigma \cup \Sigma_0 \cup \Sigma_T$). Consider functions defined in $(0, T)$ with values in a functional space X (cf. [71–73]). Let $\| \cdot \|_X$ denote the norm in X, then for $r = 2$, we define the Bochner space

$$L^2(0, T; X) := \left\{ f \text{ measurable in } [\,0, T\,] \;\middle|\; \int_0^T \| f(t) \|_X^2 \mathrm{d}t < \infty \right\},$$

and respective norm $\| f \|_{L^2(0,T;X)} := \left(\int_0^T \| f(t) \|_X^2 \mathrm{d}t \right)^{1/2}$. It is a Hilbert space if X is a Hilbert space. Throughout the paper, we also use the spaces

$$H^1(0, T; X) := \left\{ f \in L^2(0, T; X) \mid \partial_t f \in L^2(0, T; X) \right\} \tag{7.6}$$

equipped with norm $\| u \|_{H^1(0,T;X)} := \left(\int_0^T \left(\| \partial_t f(t) \|_X^2 + \| f(t) \|_X^2 \right) \mathrm{d}t \right)^{1/2}$.

We assume that $\mathcal{T}_h$ is a regular mesh satisfying angle condition defined on Ω. Then, the corresponding discretization spaces with the Lagrangian finite elements of order 0 or 1 are defined as

$$\mathbb{P}_0 := \{ v_h \in L^2(\Omega) \mid \forall T \in \mathcal{T}_h,\ v_h|_T \in \mathbb{P}_0 \}, \quad \mathbb{P}_1 := \{ v_h \in H^1(\Omega) \mid \forall T \in \mathcal{T}_h,\ v_h|_T \in \mathbb{P}_1 \}, \tag{7.7}$$

where $\mathbb{P}_k$ denotes the space of polynomials of the order $k \in \mathbb{N} \cup 0$. The Raviart–Thomas elements of the lowest and first order are denoted by

$$\mathbb{RT}_0 := \{ \boldsymbol{y}_h \in H(\mathrm{div}, \Omega) : \forall T \in \mathcal{T}_h,\ \boldsymbol{y}_h|_T = \boldsymbol{a} + b\boldsymbol{x},\ \boldsymbol{a} \in \mathbb{R}^d,\ b \in \mathbb{R} \},$$

$$\mathbb{RT}_1 := \{ \boldsymbol{y}_h \in H(\mathrm{div}, \Omega) : \forall T \in \mathcal{T}_h,\ \boldsymbol{y}_h(\boldsymbol{x})|_T = \boldsymbol{q}(\boldsymbol{x}) + \boldsymbol{x}\, r(\boldsymbol{x}),\ \boldsymbol{q} \in [\mathbb{P}_1]^d,\ r \in \mathbb{P}_1 \},$$

respectively. Finally, the table below presents notation used in the paper for the physical quantities (see Table A.12).

Table A.12
Table of notation.

$\boldsymbol{\sigma}_{\text{por}}$	poroelastic Cauchy stress (total stress) tensor
$\boldsymbol{u}$	displacement of the solid
p	fluid pressure
$\boldsymbol{\sigma}$	linear elastic (effective) stress tensor
$\boldsymbol{\varepsilon}(\boldsymbol{u})$	strain tensor
λ, μ	Lamé parameters
$\boldsymbol{f}$	volumetric body force
$\boldsymbol{w}$	Darcy velocity
μ_f	fluid viscosity
$\mathbb{K}$	permeability tensor
g	gravitation constant
ρ_f	fluid phase density
α	Biot–Willis coefficient
$\beta = \frac{1}{M} + c_f\varphi_0$	storage coefficient
M	Biot constant
c_f	fluid compressibility
φ_0	initial porosity

Contraction theorem. An essential part of our analysis is based on the contraction theorem, which was proven in [57] for the poroelastic problem in question. However, Lemma 3 uses the contraction of the sequence $\{\delta(\eta - \eta_h)\}^i$, $\forall \eta \in W_h$, which is proven blow.

Theorem 4. *With $\gamma = \frac{\alpha}{\sqrt{\lambda}}$ and $L = \frac{\alpha^2}{2\lambda}$, the sequence $\{\delta(\eta - \eta_h)\}^i \in W_h$, where $\eta^i \in W$ is generated by the fixed-stress split iterative scheme defined in (3.4)–(3.5) and $\eta_h^i \in W_h$ is discretization of the latter sequence, is a contraction given by*

$$\|\boldsymbol{\varepsilon}(\delta(\boldsymbol{u} - \boldsymbol{u}_h)^i)\|_{2\mu}^2 + q\,\|\nabla\delta(p - p_h)^i\|_{\mathbb{K}_\tau}^2 + \|\delta(\eta - \eta_h)^i\|^2 \le q^2\|\delta(\eta - \eta_h)^{i-1}\|^2, \quad q = \tfrac{L}{\beta+L}. \tag{7.8}$$

Proof. Consider the difference between $(i-1)$th and ith iterations in (3.4) and (3.5). Assuming that $\delta p^i = p^i - p^{i-1}$ and $\delta\boldsymbol{u}^i = \boldsymbol{u}^i - \boldsymbol{u}^{i-1}$, as well as particular chosen $w = w_h \in W_{0h} \subset W_0$ and $\boldsymbol{v} = \boldsymbol{v}_h \in \boldsymbol{V_{0h}} \subset \boldsymbol{V_0}$ with conforming Galerkin discretization spaces W_{0h} and $\boldsymbol{V_{0h}}$ of W_0 and $\boldsymbol{V_0}$, respectively. Thus, we obtain

$$(\mathbb{K}_\tau\nabla\delta p^i, \nabla w_h) + (\beta + L)(\delta p^i, w_h) = (-\gamma\,\delta\eta^{i-1}, w_h), \qquad \forall\, w \in W_{0h}, \tag{7.9}$$

$$\big(2\,\mu\,\boldsymbol{\varepsilon}(\delta\boldsymbol{u}^i), \boldsymbol{\varepsilon}(\boldsymbol{v}_h)\big) + (\lambda\,\mathrm{div}\delta\boldsymbol{u}^i, \mathrm{div}\boldsymbol{v}_h) = (-\alpha\nabla\delta p^i, \boldsymbol{v}_h), \qquad \forall\, \boldsymbol{v}_h \in \boldsymbol{V_{0h}}, \tag{7.10}$$

For the Galerkin approximations $(\boldsymbol{u}, p)_h^i \in \boldsymbol{V_{0h}} \times W_{0h}$, the system above can be rewritten as

$$(\mathbb{K}_\tau\nabla\delta p_h^i, \nabla w_h) + (\beta + L)(\delta p_h^i, w_h) = (-\gamma\,\delta\eta_h^{i-1}, w_h), \qquad \forall\, w_h \in W_{0h}, \tag{7.11}$$

$$\big(2\,\mu\,\boldsymbol{\varepsilon}(\delta\boldsymbol{u}_h^i), \boldsymbol{\varepsilon}(\boldsymbol{v}_h)\big) + (\lambda\,\mathrm{div}\delta\boldsymbol{u}_h^i, \mathrm{div}\boldsymbol{v}_h) = (-\alpha\nabla\delta p_h^i, \boldsymbol{v}_h), \qquad \forall\, \boldsymbol{v} \in \boldsymbol{V_{0h}}. \tag{7.12}$$

The difference of (7.9)–(7.10) and (7.11)–(7.12), substitution of $w_h = \delta(p - p_h)^i$ in the flow part and $\boldsymbol{v}_h = \delta(\boldsymbol{u} - \boldsymbol{u}_h)^i$ in the corresponding mechanics part yield

$$\|\nabla\delta(p - p_h)^i\|_{\mathbb{K}_\tau}^2 + (\beta + L)\,\|\delta(p - p_h)^i\|^2 = -\gamma\,(\delta(\eta - \eta_h)^{i-1}, \delta(p - p_h)^i), \ \ \forall\, w_h \in W_{0h}, \tag{7.13}$$

$$\|\boldsymbol{\varepsilon}(\delta(\boldsymbol{u} - \boldsymbol{u}_h)^i)\|_{2\mu}^2 + \|\mathrm{div}\delta(\boldsymbol{u} - \boldsymbol{u}_h)^i\|_\lambda^2 = -\alpha\,(\delta(p - p_h)^i, \mathrm{div}\delta(\boldsymbol{u} - \boldsymbol{u}_h)^i), \ \ \forall\, \boldsymbol{v} \in \boldsymbol{V_{0h}}. \tag{7.14}$$

Application of the Young inequality in (7.13) provide the relation

$$(\beta + L)\,\|\delta(p - p_h)^i\|^2 + \|\nabla\delta(p - p_h)^i\|_{\mathbb{K}_\tau}^2 \le \tfrac{\epsilon}{2}\,\|\delta(p - p_h)^i\|^2 + \tfrac{\gamma^2}{2\epsilon}\,\|\delta(\eta - \eta_h)^{i-1}\|^2, \quad \epsilon > 0. \tag{7.15}$$

Regrouping similar terms in (7.15) implies

$$(\beta + L - \tfrac{\epsilon}{2})\,\|\delta(p - p_h)^i\|^2 + \|\nabla\delta(p - p_h)^i\|_{\mathbb{K}_\tau}^2 \le \tfrac{\gamma^2}{2\epsilon}\,\|\delta(\eta - \eta_h)^{i-1}\|^2.$$

Substitution of the optimal $\epsilon = \beta + L$, obtained from the minimization problem $\min_{\varepsilon>0}\big(2\,\epsilon\,(\beta + L - \tfrac{\epsilon}{2})\big)^{-1}$, yields

$$(\beta + L)\,\|\delta(p - p_h)^i\|^2 + 2\,\|\nabla\delta(p - p_h)^i\|_{\mathbb{K}_\tau}^2 \le \tfrac{\gamma^2}{\beta+L}\,\|\delta(\eta - \eta_h)^{i-1}\|^2. \tag{7.16}$$

By summing (7.16), multiplied by free parameter $c_0 > 0$, and (7.14), we arrive at the following inequality

$$\Big\{c_0\,(\beta + L)\,\|\delta(p - p_h)^i\|^2 + \|\mathrm{div}\delta(\boldsymbol{u} - \boldsymbol{u}_h)^i\|_\lambda^2 - \alpha\,(\delta(p - p_h)^i, \mathrm{div}\delta(\boldsymbol{u} - \boldsymbol{u}_h)^i)\Big\}$$
$$+\ \|\boldsymbol{\varepsilon}(\delta(\boldsymbol{u} - \boldsymbol{u}_h)^i)\|_{2\mu}^2 + 2c_0\,\|\nabla\delta(p - p_h)^i\|_{\mathbb{K}_\tau}^2 \le c_0\,\tfrac{\gamma^2}{\beta+L}\|\delta(\eta - \eta_h)^{i-1}\|^2. \tag{7.17}$$

Let us determine the values of parameters c_0, γ, and L such that the terms on the left-hand side of (7.17) are positive and contraction in $\|\delta(\eta-\eta_h)^{i-1}\|^2$ is achieved. It follows from $\delta(\eta-\eta_h)^i = \frac{\alpha}{\gamma}\,\mathrm{div}\delta(\boldsymbol{u}-\boldsymbol{u}_h)^i - \frac{L}{\gamma}\,\delta(p-p_h)^i$, that

$$\|\delta(\eta-\eta_h)^i\|^2 = \tfrac{\alpha^2}{\gamma^2}\,\|\mathrm{div}\delta(\boldsymbol{u}-\boldsymbol{u}_h)^i\|^2 + \tfrac{L^2}{\gamma^2}\,\|\delta(p-p_h)^i\|^2 - \tfrac{2\alpha L}{\gamma^2}\,(\mathrm{div}\delta(\boldsymbol{u}-\boldsymbol{u}_h)^i,\,\delta(p-p_h)^i). \tag{7.18}$$

Comparing (7.18) and (7.17), we arrive at the following condition for the free parameters:

$$\begin{cases} \frac{\alpha^2}{\gamma^2} \le \lambda, \\ \frac{L^2}{\gamma^2} \le c_0\,(\beta+L), \\ \frac{2\alpha L}{\gamma^2} = \alpha, \end{cases} \qquad \text{which yields} \qquad \begin{cases} L \ge \frac{\alpha^2}{2\lambda}, \\ c_0 \ge \frac{L}{2(\beta+L)}, \\ \gamma^2 = 2L. \end{cases}$$

Then, the contraction rate $q = c_0\,\frac{\gamma^2}{\beta+L}$ is monotone w.r.t. to L and attains its minimum at

$$L = \tfrac{\alpha^2}{2\lambda} \quad \text{and} \quad c_0 = \tfrac{L}{2(\beta+L)}.$$

By using the condition $\gamma^2 = 2L$, we obtain

$$\|\boldsymbol{e}(\delta(\boldsymbol{u}-\boldsymbol{u}_h)^i)\|_{2\mu}^2 + q\,\|\nabla\delta(p-p_h)^i\|_{\mathbb{K}_\tau}^2 + \|\delta(\eta-\eta_h)^i\|^2 \le q^2\|\delta(\eta-\eta_h)^{i-1}\|^2 \tag{7.19}$$

with

$$q = \tfrac{L}{\beta+L} \quad \text{and} \quad L = \tfrac{\alpha^2}{2\lambda}. \quad \square$$

References

[1] K. Terzaghi, Principle of soil mechanics, 1925, Eng. News Record, A Series of Articles.
[2] M. Biot, General theory of three-dimensional consolidation, J. Appl. Phys. 12 (1941) 155–164.
[3] M. Biot, Theory of elasticity and consolidation for a porous anisotropic solid, J. Appl. Phys. 26 (1955) 182–185.
[4] O. Coussy, Mechanics of Porous Continua, Wiley, West Sussex, 1995.
[5] R.E. Showalter, Diffusion in poro-elastic media, J. Math. Anal. Appl. 251 (2000) 310–340.
[6] R.E. Showalter, U. Stefanelli, Diffusion in poro-plastic media, Math. Methods Appl. Sci. 27 (2004) 2131–2151.
[7] M.A. Murad, A.F.D. Loula, Improved accuracy in finite element analysis of Biot's consolidation problem, Comput. Methods Appl. Mech. Engrg. 95 (1992) 359–382.
[8] A. Mikelić, M.F. Wheeler, Theory of the dynamic Biot-Allard equations and their link to the quasi-static Biot system, J. Math. Phys. 53 (2012) 123702, 15.
[9] A. Settari, F. Mourits, A coupled reservoir and geomechanical simulation system, SPE J. 3 (1998) 219–226.
[10] T. Almani, K. Kumar, M.F. Wheeler, Convergence and error analysis of fully discrete iterative coupling schemes for coupling flow with geomechanics, Comput. Geosci. 21 (2017) 1157–1172.
[11] K. Kumar, T. Almani, G. Singh, M.F. Wheeler, Multirate undrained splitting for coupled flow and geomechanics in porous media, in: Numerical Mathematics and Advanced Applications—ENUMATH 2015, in: Lect. Notes Comput. Sci. Eng., vol. 112, Springer, [Cham], 2016, pp. 431–440.
[12] T. Almani, K. Kumar, A. Dogru, G. Singh, M.F. Wheeler, Convergence analysis of multirate fixed-stress split iterative schemes for coupling flow with geomechanics, Comput. Methods Appl. Mech. Engrg. 311 (2016) 180–207.
[13] P.A. Vermeer, A. Verruijt, An accuracy condition for consolidation by finite elements, Int. J. Numer. Anal. Methods Geomech. 5 (1981) 1–14.
[14] M.B. Reed, An investigation of numerical errors in the analysis of consolidation by finite elements, Int. J. Numer. Anal. Methods Geomech. 8 (1984) 243–257.
[15] O.C. Zienkiewicz, T. Shiomi, Dynamic behaviour of saturated porous media; the generalized Biot formulation and its numerical solution, Int. J. Numer. Anal. Methods Geomech. 8 (1984) 71–96.
[16] M.A. Murad, A.F.D. Loula, On stability and convergence of finite element approximations of Biot's consolidation problem, Internat. J. Numer. Methods Engrg. 37 (1994) 645–667.
[17] M.A. Murad, V. Thomée, A.F.D. Loula, Asymptotic behavior of semidiscrete finite-element approximations of Biot's consolidation problem, SIAM J. Numer. Anal. 33 (1996) 1065–1083.
[18] J. Korsawe, G. Starke, A least-squares mixed finite element method for Biot's consolidation problem in porous media, SIAM J. Numer. Anal. 43 (2005) 318–339.
[19] J.M. Nordbotten, Stable cell-centered finite volume discretization for Biot equations, SIAM J. Numer. Anal. 54 (2016) 942–968.
[20] Y. Chen, Y. Luo, M. Feng, Analysis of a discontinuous Galerkin method for the Biot's consolidation problem, Appl. Math. Comput. 219 (2013) 9043–9056.
[21] D. Boffi, M. Botti, D.A. Di Pietro, A nonconforming high-order method for the Biot problem on general meshes, SIAM J. Sci. Comput. 38 (2016) A1508–A1537.
[22] J. Vignollet, S. May, R. de Borst, On the numerical integration of isogeometric interface elements, Internat. J. Numer. Methods Engrg. 102 (2015) 1733–1749.
[23] S.-H. Chan, K.-K. Phoon, F.H. Lee, A modified jacobi preconditioner for solving ill-conditioned Biots consolidation equations using symmetric quasi-minimal residual method, Int. J. Numer. Anal. Methods Geomech. 25 (2001) 1001–1025.
[24] K.K. Phoon, K.C. Toh, S.H. Chan, F.H. Lee, An efficient diagonal preconditioner for finite element solution of Biot consolidation equations, J. Numer. Methods Engrg. 55 (2002) 377–400.
[25] J.A. White, R.I. Borja, Block-preconditioned Newton-Krylov solvers for fully coupled flow and geomechanics, Comput. Geosci. 15 (2011) 647–659.
[26] J.B. Haga, H. Osnes, H.P. Langtangen, A parallel block preconditioner for large-scale poroelasticity with highly heterogeneous material parameters, Comput. Geosci. 16 (2012) 723–734.
[27] O. Axelsson, R. Blaheta, P. Byczanski, Stable discretization of poroelasticity problems and efficient preconditioners for arising saddle point type matrices, Comput. Vis. Sci. 15 (2012) 191–207.

[28] J.B. Haga, H. Osnes, H.P. Langtangen, A parallel block preconditioner for large-scale poroelasticity with highly heterogeneous material parameters, Comput. Geosci. 16 (2012) 723–734.
[29] N. Castelletto, J. White, H. Tchelepi, Accuracy and convergence properties of the fixed-stress iterative solution of two-way coupled poromechanics, Int. J. Numer. Anal. Methods Geomech. 39 (2015) 1593–1618.
[30] N. Castelletto, J. White, M. Ferronato, Scalable algorithms for three-field mixed finite element coupled poromechanics, J. Comput. Phys. 327 (2016) 894–918.
[31] S. Rhebergen, G.N. Wells, R.F. Katz, A.J. Wathen, Analysis of block preconditioners for models of coupled magma/mantle dynamics, SIAM J. Sci. Comput. 36 (2014) A1960–A1977.
[32] S. Rhebergen, G.N. Wells, A.J. Wathen, R.F. Katz, Three-field block preconditioners for models of coupled magma/mantle dynamics, SIAM J. Sci. Comput. 37 (2015) A2270–A2294.
[33] Q. Hong, J. Kraus, Uniformly stable discontinuous Galerkin discretization and robust iterative solution methods for the Brinkman problem, SIAM J. Numer. Anal. 54 (2016) 2750–2774.
[34] J.J. Lee, K.-A. Mardal, R. Winther, Parameter-robust discretization and preconditioning of Biot's consolidation model, SIAM J. Sci. Comput. 39 (2017) A1–A24.
[35] T. Bærland, J.J. Lee, K.-A. Mardal, R. Winther, Weakly imposed symmetry and robust preconditioners for Biot's consolidation model, Comput. Methods Appl. Math. 17 (2017) 377–396.
[36] D. Allen, Stability, accuracy, and efficiency of sequential methods for coupled flow and geomechanics, Technical Report SPE119084, The SPE Reservoir Simulation Symposium, Houston, Texas, 2009.
[37] J.A. White, N. Castelletto, H.A. Tchelepi, Block-partitioned solvers for coupled poromechanics: a unified framework, Comput. Methods Appl. Mech. Engrg. 303 (2016) 55–74.
[38] F.J. Gaspar, C. Rodrigo, On the fixed-stress split scheme as smoother in multigrid methods for coupling flow and geomechanics, Comput. Methods Appl. Mech. Engrg. 326 (2017) 526–540.
[39] Q. Hong, J. Kraus, Parameter-robust stability of classical three-field formulation of Biot consolidation model, 48, 2018, pp. 202–226,
[40] S. Meunier, Analyse d'erreur a posteriori pour les couplages hydro-Mécaniques et mise en oeuvre dans (Ph.D. thesis), École des Ponts ParisTech, 2007.
[41] A. Ern, S. Meunier, A posteriori error analysis of Euler-Galerkin approximations to coupled elliptic–parabolic problems, M2AN Math. Model. Numer. Anal. 43 (2009) 353–375.
[42] M. Vohralík, M.F. Wheeler, A posteriori error estimates, stopping criteria, and adaptivity for two-phase flows, Comput. Geosci. 17 (2013) 789–812.
[43] S. Yousef, A Posteriori Error Estimates and Adaptivity Based on Stopping Criteria and Adaptive Mesh Re Finement for Multiphase and Thermal Flows. Application to Steam-Assisted Gravity Drainage (Ph.D. thesis), Université Pierre et Marie Curie, Paris VI, 2013.
[44] D.A. Di Pietro, M. Vohralík, S. Yousef, An a posteriori-based, fully adaptive algorithm with adaptive stopping criteria and mesh refinement for thermal multiphase compositional flows in porous media, Comput. Math. Appl. 68 (2014) 2331–2347.
[45] D.A. Di Pietro, E. Flauraud, M. Vohralík, S. Yousef, A posteriori error estimates, stopping criteria, and adaptivity for multiphase compositional Darcy flows in porous media, J. Comput. Phys. 276 (2014) 163–187.
[46] E. Ahmed, S.A. Hassan, C. Japhet, M. Kern, M. Vohralík, A Posteriori Error Estimates and Stopping Criteria for Space–Time Domain Decomposition for Two-Phase Flow Between Different Rock Types, Technical Report hal-01540956, Version 1, HAL, 2017.
[47] F. Larsson, K. Runesson, A sequential-adaptive strategy in space–time with application to consolidation of porous media, Comput. Methods Appl. Mech. Engrg. 288 (2015) 146–171.
[48] R. Riedlbeck, D.A. Di Pietro, A. Ern, S. Granet, K. Kazymyrenko, Stress and flux reconstruction in Biot's poro-elasticity problem with application to a posteriori error analysis, Comput. Math. Appl. 73 (2017) 1593–1610.
[49] F. Bertrand, M. Moldenhauer, G. Starke, A Posteriori Error Estimation for Planar Linear Elasticity by Stress Reconstruction, Comput. Methods Appl. Math. 19 (3) (2019) 663–679.
[50] E. Ahmed, F.A. Radu, J.M. Nordbotten, Adaptive poromechanics computations based on a posteriori error estimates for fully mixed formulations of Biot's consolidation model, Comput. Methods Appl. Mech. Engrg. 347 (2019) 264–294.
[51] E. Ahmed, J.M. Nordbotten, F.A. Radu, Adaptive asynchronous time-stepping, stopping criteria, and a posteriori error estimates for fixed-stress iterative schemes for coupled poromechanics problems, J. Comput. Appl. Math. 364 (2020).
[52] J.M. Nordbotten, T. Rahman, S.I. Repin, J. Valdman, A posteriori error estimates for approximate solutions of the Barenblatt-Biot poroelastic model, Comput. Methods Appl. Math. 10 (2010) 302–314.
[53] S. Banach, Sur les opérations dans les ensembles abstraits et leur application aux équations intégrales, Fund. Math. 3 (1922) 133–181.
[54] S. Repin, A Posteriori Estimates for Partial Differential Equations, in: Radon Series on Computational and Applied Mathematics, vol. 4, Walter de Gruyter GmbH & Co. KG, Berlin, 2008.
[55] A. Ženíšek, The existence and uniqueness theorem in Biot's consolidation theory, Apl. Mat. 29 (1984) 194–211.
[56] R.E. Showalter, N. Su, Partially saturated flow in a poroelastic medium, Discrete Contin. Dyn. Syst. Ser. B 1 (2001) 403–420.
[57] A. Mikelić, M.F. Wheeler, Convergence of iterative coupling for coupled flow and geomechanics, Comput. Geosci. 17 (2013) 455–461.
[58] A. Mikelić, B. Wang, M.F. Wheeler, Numerical convergence study of iterative coupling for coupled flow and geomechanics, Comput. Geosci. 18 (2014) 325–341.
[59] J. Kim, H.A. Tchelepi, R. Juanes, Stability and convergence of sequential methods for coupled flow and geomechanics: drained and undrained splits, Comput. Methods Appl. Mech. Engrg. 200 (2011) 2094–2116.
[60] J. Kim, H.A. Tchelepi, R. Juanes, Stability and convergence of sequential methods for coupled flow and geomechanics: fixed-stress and fixed-strain splits, Comput. Methods Appl. Mech. Engrg. 200 (2011) 1591–1606.
[61] S. Repin, A posteriori estimates for approximate solutions of variational problems with strongly convex functionals, Probl. Math. Anal. 17 (1997) 199–226.
[62] S. Repin, A posteriori error estimation for variational problems with uniformly convex functionals, Math. Comp. 69 (2000) 481–500.
[63] P. Neittaanmäki, S. Repin, Reliable Methods for Computer Simulation, in: Studies in Mathematics and its Applications, vol. 33, Elsevier Science B.V., Amsterdam, 2004, Error control and a posteriori estimates.
[64] J.W. Both, M. Borregales, J.M. Nordbotten, K. Kumar, F.A. Radu, Robust fixed stress splitting for Biot's equations in heterogeneous media, Appl. Math. Lett. 68 (2017) 101–108.
[65] J.W. Both, U. Koecher, Numerical investigation on the fixed-stress splitting scheme for Biot's equations: Optimality of the tuning parameter, in: Numerical mathematics and advanced applications—ENUMATH 2017, in: Lect. Notes Comput. Sci. Eng., 126, 2019, pp. 789–797.
[66] S. Repin, S. Sauter, Functional a posteriori estimates for the reaction–diffusion problem, C. R. Acad. Sci., Paris 343 (2006) 349–354.
[67] D.N. Arnold, F. Brezzi, Mixed and nonconforming finite element methods: implementation, postprocessing and error estimates, RAIRO Modél. Math. Anal. Numér. 19 (1985) 7–32.
[68] D.N. Arnold, Mixed finite element methods for elliptic problems, Comput. Methods Appl. Mech. Engrg. 82 (1990) 281–300, Reliability in computational mechanics (Austin, TX, 1989).

[69] V. John, A numerical study of a posteriori error estimators for convection–diffusion equations, Comput. Methods Appl. Mech. Engrg. 190 (2000) 757–781.
[70] V. Girault, M.F. Wheeler, B. Ganis, M.E. Mear, A lubrication fracture model in a poro-elastic medium, Math. Models Methods Appl. Sci. 25 (2015) 587–645.
[71] O.A. Ladyzhenskaya, The Boundary Value Problems of Mathematical Physics, Springer, New York, 1985.
[72] O.A. Ladyzhenskaya, V.A. Solonnikov, N. Uraltseva, Linear and Quasilinear Equations of Parabolic Type, Nauka, Moscow, 1967.
[73] E. Zeidler, Nonlinear Functional Analysis and Its Applications. II/A, Springer-Verlag, New York, 1990, Linear monotone operators, Translated from the German by the author and Leo F. Boron.